Distribution Agreement

In presenting this thesis or dissertation as a partial fulfillment of the requirements for an advanced degree from Emory University, I hereby grant to Emory University and its agents the non-exclusive license to archive, make accessible, and display my thesis or dissertation in whole or in part in all forms of media, now or hereafter known, including display on the world wide web. I understand that I may select some access restrictions as part of the online submission of this thesis or dissertation. I retain all ownership rights to the copyright of the thesis or dissertation. I also retain the right to use in future works (such as articles or books) all or part of this thesis or dissertation.

Signature:

_____	_____
Jasmine Clark	Date

Real-time Visualization of Viral and Host Cell Proteins Involved In The Intracellular Transport of Mason-Pfizer Monkey Virus

By

Jasmine Clark
Doctor of Philosophy

Graduate Divisions of Biological and Biomedical Sciences
Microbiology and Molecular Genetics

_____

Eric Hunter, PhD
Advisor

_____ _____

Dave Steinhauer, PhD
Committee Member

Paul Spearman, MD
Committee Member

_____ _____

Samuel Speck, PhD
Committee Member

Daniel Kalman, PhD
Committee Member

_____ _____

Arash Grakoui, PhD
Committee Member

Gregory Melikian, PhD
Committee Member

Accepted:

_____

Lisa A. Tedesco, Ph.D. Dean of the James T. Laney School of Graduate Studies

_____

Date

Real-time Visualization of Viral and Host Cell Proteins Involved In The Intracellular Transport of Mason-Pfizer Monkey Virus

By
Jasmine Clark
BS, University of Tennessee, 2005

Advisor: Eric Hunter, PhD

An abstract of
A dissertation submitted to the Faculty of the James T. Laney School of Graduate Studies of Emory University
in partial fulfillment of the requirements for the degree of Doctor of Philosophy
in
Graduate Division of Biological and Biomedical Sciences
Microbiology and Molecular Genetics
2013

Abstract

Real-time Visualization of Viral and Host Cell Proteins Involved In The Intracellular Transport of Mason-Pfizer Monkey Virus

By Jasmine Clark

Mason-Pfizer Monkey Virus, the prototypic D-type retrovirus, co-translationally assembles immature capsids in the pericentriolar region of the cell. From here, immature capsids are transported to the plasma membrane for budding, release, and maturation into an infectious virions. Several mutational and biochemical studies have been employed to elucidate viral and host proteins important for this intracellular transport. Although these studies provided very important insight as to what proteins are involved in this portion of the viral life cycle, they have relied on population analysis of capsids. In this dissertation, we create a codon-optimized M-PMV Gag-eGFP fusion vector with an optimized Kozak consensus sequence and an alanine substitution at an internal methionine. This vector, co-expressed with untagged Gag, produces fluorescently-labeled capsids that are able to be visualized by real-time, live cell imaging. Characterization of the trafficking of these fluorescent capsids implicated a role for microtubules. This role was confirmed by employing the use of cytoskeletal inhibitors. Furthermore, using a mCherry-tagged M-PMV Env, co-transport of M-PMV Gag and Env was observed, and this co-transport as well as incorporation of Env into released virions required the presence of intact microtubules. This data provides strong support for the hypothesis that in order to produce infectious virus, M-PMV Env that has been transported to the plasma membrane from the trans Golgi network is endocytosed and recycled through the pericentriolar region, whereby these Env-containing recycling vesicles interact with assembled immature capsids, followed by co-transport, along microtubules, toward the plasma membrane for budding.

Real-time Visualization of Viral and Host Cell Proteins Involved In The Intracellular Transport of Mason-Pfizer Monkey Virus

By
Jasmine Clark
BS, University of Tennessee, 2005

Advisor: Eric Hunter, PhD

A dissertation submitted to the Faculty of the
James T. Laney School of Graduate Studies of Emory University
in partial fulfillment of the requirements for the degree of Doctor of Philosophy
in
Graduate Division of Biological and Biomedical Sciences
Microbiology and Molecular Genetics
2013

Dedication

I would like to dedicate this dissertation to my children, my little motivators, Jayda and Jacobe, who have been my biggest cheerleaders even though they don't even know what microbiology means yet. They serve as constant reminders for why I cannot and will not ever give up.

Acknowledgements

I would like to thank everyone who has been with me through this incredible journey that is graduate school. I could not have made it this far with out the unyielding support of my family and friends. I would like to specifically thank my mentor, Dr. Eric Hunter, for giving me the opportunity to realize my potential to be a virologist and being the coolest mentor a student could ask for; my mother and father for believing in me and always being a source of encouragement; my children for motivating me to be the best I could be; everyone in the Hunter and Derdeyn labs, whom have become an extension of my family; Ted Diehl, who took me under his wing when I first joined the lab and taught me all about cloning and tissue culture; Lara Pereira and Petra Grznarova for going through the trenches with me on the M-PMV projects; and all of my friends, old and new, who have laughed with me, cried with me, partied with me, babysat for me, and done anything else, no matter how small, that helped me get through this process.

Table of Contents

List of Tables and Figures

A Mason-Pfizer Monkey Virus Gag-GFP Fusion Vector Allows Visualization of Capsid Transport in Live Cells and Demonstrates a Role for Microtubules

Direct evidence for intracellular anterograde co-transport of M-PMV Gag and Env on microtubules.

Introduction

Retroviruses

History. The discovery of the first retroviruses is accredited to Vallee and Carre in 1904 of a filterable disease agent that caused an equine infectious anemia and Ellerman and Bang in 1908 for their discovery of a filterable agent capable of transmitting a chicken leukemia virus. This was followed by Peyton Rous's description of cell-free transmission of a chicken sarcoma to healthy chickens, which would later be known as Rous Sarcoma Virus (RSV) [1]. This discovery carried more weight than the previous discoveries because of the malignancy of the sarcomas, and later earned Rous the Nobel Prize in 1966. After it was discovered that RSV contained an RNA genome, RSV became the prototypical "RNA tumor virus" [2].

Several years after the discovery of the first avian retroviruses, in 1942, John Bittner identified a high molecular weight agent in the breast milk of mice that caused mammary tumor formation in mice. This virus, which was called the "milk-influence," would later be known as Mouse Mammary Tumor Virus (MMTV), the first described mammalian RNA tumor virus. In 1951, a decade after Bittner's discovery, Ludwik Gross, identified Mouse Leukemia Virus (MLV) by injecting extracts from leukemia-infected mice into the young, leukemia-free mice, which induced spontaneous leukemia formation. These examples of cancer-causing viruses in mammals led to a peaked interest in this area of study as it had implications for causes of cancers in humans. The first human RNA tumor virus

shown to cause an adult leukemia, HTLV-1, however, was not discovered until the 1980's by Robert Gallo, as well as, independently, by the Yoshida laboratory in Japan, which called it ATLV [3,4].

Pre-1970's the accepted pathway for the flow of genetic information, also described as the central dogma of molecular biology, was that DNA was transcribed into RNA, followed by translation of this RNA into proteins. However in 1970, two independent research investigators, Howard Temin and David Baltimore, discovered that the RNA tumor viruses, Rauscher Mouse Leukaemia Virus (R-MLV) and RSV contain an RNA-dependent DNA polymerase in their virions [5,6]. The discoveries of this polymerase that would later be known as "reverse transcriptase" added to support to Temin's DNA provirus hypothesis—replication of RNA tumor viruses utilize a DNA intermediate instead of an RNA intermediate like other RNA viruses—which he had described in 1964 in the National Cancer Institute Monographs. Prior to the discoveries in 1970, Temin's provirus hypothesis had been met with much resistance. After this seminal discovery, the term "retrovirus" was adopted to describe these RNA tumor viruses, and the field of retrovirology was born.

Biology. Viruses in the *Retroviridae* family, or retroviruses, are enveloped, (+) strand RNA viruses that contain the RNA-dependent DNA polymerase, reverse transcriptase. Unlike other (+) strand RNA viruses, which can be directly translated into protein by way of the host ribosomes, retroviruses must undergo an intermediate step whereby the RNA is reverse transcribed into double-stranded (ds) DNA and integrated into the host genome. This DNA intermediate

is then transcribed into viral mRNA by cellular enzymes followed by translation and production of viral proteins.

There are two subfamilies of retroviruses, *Orthroretrovirinae* and *Spumavirinae*. The orthoretroviruses can be further divided into 6 genera: *Alpharetrovirus, Betaretrovirus, Gammaretrovirus, Deltaretrovirus, Epsilonretrovirus, and Lentivirus*. Spumavirinae are compromised solely of *Spumaviruses*. Retroviruses can be further differentiated by the organization of their genomes. The alpha-, beta-, and gammaretroviruses contain a simple retroviral genome, which encodes the four retroviral genes—*gag, pro, pol,* and *env*. The other retroviral genomes are more complex, containing these four genes as well as genes that encode accessory proteins that are necessary for viral gene expression and pathogenesis.

Another method for distinguishing viruses is by morphology. In 1960, Bernhard did an extensive study using transmission electron microscopy to describe the size, shape, and characteristic of tumor virus particles[7]. He described Type A particles, intracellular precursors to Type B and D particles. These retroviral particles that are assembled intracytoplasmically are characterized by a non-enveloped electron-dense ring surrounding an empty core, and resemble a donut. The mature Type B and D retroviral particles contain a condensed core. Type C morphology is characterized by an enveloped capsid with a round, centered core. Type C viruses are usually assembled at the plasma membrane, where formation of the capsid and budding are occurring simultaneously. Examples of Type C viruses are MLV and ALV. Type B viral particles are characterized by an off-centered round core, while the Type D

particles are characterized by a bar shaped core. This morphology results upon budding, release, and maturation of the immature, Type A viral particles.

As mentioned above, every retroviral genome contains four essential genes—*gag, pro, pol, and env*. The *gag* gene encodes the major, structural polyprotein, Gag, which makes up the viral capsid. Gag is the only protein that is required to make a non-infectious virus-like particle (VLP). Each Gag protein contains three domains—the capsid domain (CA), the matrix domain (MA), and the nucleocapsid domain (NC). Each of these domains is separated by a proteolytic cleavage site. Shortly after budding of a virus from a cell, the viral protease, Pro, acts at these proteolytic cleavage sites to produce the mature virion. The retroviral *pro* gene is located downstream of *gag* and upstream of the reverse transcriptase gene. In Alpharetroviruses it is encoded as a Gag-Pro fusion protein, in Betaretroviruses this Gag-Pro fusion protein is generated through a frameshift that occurs in the 3'-end of *gag,* and in the remaining genera, the frameshift (or, in the case of Gammaretrovirus, suppression of the Gag stop-codon) results in a Gag-Pro-Pol fusion protein [8-10]. The sequence of the protease is heterogenous between virus families as well as among the same virus [11]. Despite this variability, all retroviral contain the highly conserved aspartic proteinase motif Asp-Thr/Ser-Gly [12]. The third essential gene in the retroviral genome, *pol*, encodes the RNA-dependent DNA polymerase, reverse transcriptase (RT). This protein is usually expressed as a Gag-Pro-Pol fusion protein. In retroviruses, such as HIV, RSV, MMTV, and M-PMV, *pol* lies in a different reading from that of *gag,* and the fusion protein is translated at a fixed ratio by ribosomal frameshifting [13-16]. The final gene present in all retroviral

genomes is *env*. It encodes the retroviral envelope glycoprotein (Env). This gene is located downstream of the *gag* and *pro* genes, and is expressed by mRNA splicing. The Env glycoprotein is translated on endoplasmic reticulum (ER)-bound ribosomes as a precursor protein. The precursor protein is inserted into the lumen of the rough ER by way of a signal peptide sequence at the amino-terminus. The signal peptide is removed by a cellular signal peptidase and the envelope protein is N- and/or O-glycosolated as well as oligomerized in a trimeric structure [17-20]. The protein is subsequently transported to the Golgi, where it is then proteolytically cleaved into two domains, the surface protein (SU) and the transmembrane (TM) domain, by host cell proteases [21-24]. The SU is primarily involved in receptor binding, and determines the cells that a particular retrovirus is able to infect. In contrast, the TM domain has been shown to play a major role in viral fusion.

Mason-Pfizer Monkey Virus

History. In 1970, Harish Chopra and Marcus Mason described a new virus, now known as Mason-Pfizer Monkey Virus (M-PMV), that had been isolated from a spontaneous breast carcinoma of an 8-year old female rhesus macaque [25,26]. This new virus was isolated by co-cultivation of embryo cells of several monkey species with the tumor cells and was propagated in cell culture by Jensen *et al.* [27]. The A-type intracellular viral particles were similar to previously described mouse mammary tumor-causing viruses[28] and this newly discovered virus was implicated as a possible causative agent of monkey breast cancer. Surprisingly, however, although the virus was able to transform rhesus

foreskin cells *in vitro* [29,30], when researchers tried to induce transformation *in vivo* by inoculating newborn rhesus macaques with M-PMV, the monkeys did not show any tumor-induction but instead developed several secondary infections, including pneumonia, enteritis, and rashes, characteristic of an immunosuppressive effect [31]. Several years later, M-PMV was re-isolated and its immunosuppressive effects were confirmed to be very similar to a simian-immunodeficiency disease (SAIDS) [32]. Prior to this, there were outbreaks of SAIDS at several different primate centers. Some of the outbreaks were attributed to D-type retroviruses, closely related to M-PMV, which as a group were termed Simian Retroviruses (SRV), and to-date a total of six species have been described (SRV-1-6). A 91.9 % sequence homology between M-PMV and SRV-1 provided strong evidence that the SRV-1 was very closely related to M-PMV [33]. Other outbreaks were found to be caused by a second virus, referred to as simian T-lymphotrophic virus type III (STLV-III), a lentivirus very similar to the human AIDS virus [34-36]. It became clear that although the clinical symptoms of the immunodeficiency were comparable between SRV-1 and the lentiviral SAIDS, M-PMV would not be a good model for studying human or simian AIDS caused by the lentivirus.

Biology. The 8.1 kb genome of M-PMV, flanked by an LTR region at the 5' and 3' end of the virus contains the four retroviral genes conserved across all retroviruses: *gag, pro, pol,* and *env* [33,37]. The virus encodes three *gag*-associated polyprotein precursors: Pr78 (Gag), Pr95 (Gag-Pro), and Pr180 (Gag-Pro-Pol). Upon maturation of the virion, Pr78 is cleaved into six protein products: p10, p12, p14, pp16, pp24, and p27[38]. The Pr95 polyprotein is

identified as a carboxy-terminal extension of Pr78, with a translational frameshift occurring near the carboxyl end of Gag that allows for the expression of the viral protease approximately 10% of time compared to Pr78 [33,38]. The Pr180 precursor polyprotein contains the open reading frame (ORF) for the viral polymerase, which is responsible for the reverse transcriptase, endonuclease, and integrase activity. It is expressed by way of a second translational frameshift that occurs 1% of the time compared to Pr78 [33,39]. The fourth and final ORF in the M-PMV genome encodes the 86 kD precursor for the envelope glycoprotein. Upon maturation of the virion, this precursor is cleaved at R394 to yield gp70 and gp20. The gp70 contains several glycosylation sites, while the gp20 contains the "immunosuppressive segment" of the virus [33].

Several mutational studies on M-PMV have been performed in order to elucidate and understand the role of viral proteins, as well as how the virus utilizes cellular proteins during the viral life cycle (refs).

The binding of the Env SU protein to a host cell receptor can be described as the beginning of the viral life cycle. For M-PMV and other beta- and gammaretroviruses, the retroviral envelope binds to a sodium dependent neutral-amino acid transporter, referred to as the RD-114 and D-type retrovirus receptor (RDR) [40-42]. Upon receptor-mediated binding to the cell surface, the M-PMV lipid envelope must fuse with the cellular membrane to allow entry of the capsid into the cell. Fusion activity of M-PMV Env is attributed to the TM protein, gp20. The TM protein can be divided into 3 subdomains: the extracellular domain, the membrane-spanning domain, and the cytoplasmic tail domain. In the extracellular domain, there are two heptad repeat regions. Heptad repeat (HR)

regions have been shown to play a vital role in viral infectivity and fusion for several different viruses, through their ability to form amphipathic helices, which fold into a 6-helix bundle [43-46]. Mutation of amino acids in the predicted hydrophobic face of the HR-1 helix in M-PMV gp120 by charged, polar, and nonpolar substitutions showed that the HR-1 region is very sensitive to these changes, which negatively affect the virus's ability to undergo fusion, therefore decreasing viral infectivity. Specifically, amino acids in the central portion of this region, I443 and V450, are essential for fusion and infectivity of M-PMV [47]. Along with these critical residues in the HR region of the extracellular domain, it was also demonstrated that amino acid residues in the cytoplasmic tail (CT) of M-PMV are also important for viral fusion. By performing alanine-scanning of the entire CT, Song *et al* [48] showed that while most of the mutations had no effect on surface expression of Env, these single amino acid changes could dramatically affect fusogenicity by either increasing or decreasing the virus's ability to fuse. In this study, it is hypothesized that the membrane-proximal residues in the CT create coiled-coiled interactions between the Envs, thus stabilizing the trimer and decreasing the ability for fusion to occur. Consistent with this hypothesis, mutations that would be predicted to not be able to form coiled-coil interactions cause an increase in fusogenicity, while mutations that would strengthen these interactions result in a reduction of fusogenicity [48]. In a study where the effect of making CT truncations on fusogenicity and Env incorporation into the virion were examined, it was shown that truncations made near the site of cleavage of the TM protein, gp22, into the mature form, gp20, that normally occurs upon release and maturation of the virion, resulted in increased fusion activity. These

observations provided evidence that cleavage of gp22 into gp20 during virion maturation by removing 17 amino acids from the carboxyl-terminus of the CT is necessary for M-PMV's ability to fuse [49].

Once the virus binds the receptor and fuses with the cellular membrane, it must undergo uncoating, reverse transcription, and nuclear entry and integration into the host genome. Although these processes have been studied extensively for HIV, equivalent studies of M-PMV have not been performed. Once the cell begins to make viral transcripts, the mRNA must be exported from the nucleus to cytoplasmic ribosomes for translations. For most cellular proteins, nuclear export involves the release of spliced mRNA into the cytoplasm. However, for M-PMV and other retroviruses, there is a need for the mRNA to remain unspliced in order to generate genomic RNA for packaging into virions, and for translation of the Gag, Pro, Pol protein precursors. Complex retroviruses, such as HIV-1, encode trans-acting proteins such as Rev that bind to an intronic sequence of HIV known as the Rev Response Element (RRE) in order to allow nucleocytoplasmic transport of intron-containing pre-mRNAs [50,51]. Retroviruses like M-PMV do not, however, encode these trans-acting proteins and instead contain cis-acting elements in the untranslated region (UTR) between the 3'-end of Env and the 3'-LTR known as the constitutive transport element (CTE) [52,53] Studies using CTE(-) vectors of M-PMV show that there is an absolute requirement for the CTE for virus propagation. This phenotype could be rescued by reinsertion of the CTE in to the deficient vectors [54]. The position of the CTE in the viral RNA was also shown to be vital for CTE function and M-PMV replication. When the CTE was displaced to other locations in the viral genome, such as the between the 5'-

LTR and Gag or between pol and env, the result was abrogation of or abberant production of the Gag/Pol precursor protein and nuclear export of the RNA. Both of these phenotypes could be rescued by reintroducing the CTE into the 3' UTR. The proximity of the CTE to the poly-adenylation (poly(A)) signal at the 3'-end of the transcript is critical. Increasing the distance between the poly(A) signal and the CTE results in a decrease in CTE function [55].

Following nuclear export of the intron-containing mRNA of M-PMV and translation of viral structural proteins, virion assembly occurs co-translationally in the pericentriolar region of the cell [56]. Amino acids in the MA domain of M-PMV are very important for the assembly process, as well as for post-assembly events [57]. The MA domain contains an 18-amino acid region, known as the cytoplasmic targeting/retention signal (CTRS), responsible for directing nascent polypeptides to the pericentriolar region of the cell for assembly [58]. This signal is conserved between B and D type viruses that assemble A-type particles intracytoplasmically [59], and when substituted into C-type viruses can redirect assembly from the plasma membrane to the cytoplasm. Within this CTRS, which spans from the proline at position 43 (P43) to the glycine at position 60 (G60), the arginine at position 55 (R55) is absolutely required for intracytoplasmic assembly [59]. Substituting R55 with a tryptophan or phenylalanine (R55W or R55F) results in a switch from B/D-type morphogenesis in the cytoplasm to C-type morphogenesis at the plasma membrane. The directing of nascent WT M-PMV to the pericentriolar region occurs when CTRS interacts with Tctex-1 (also known as DYNLT-1), a dynein light chain molecular motor [60]. While WT M-PMV is able to interact with this motor, R55F is not, providing evidence that this

interaction with the CTRS is critical for proper intracellular localization of M-PMV assembly.

Once the immature capsids are assembled in the pericentriolar region of the cell, they must be transported to the plasma membrane for budding. The process by which the M-PMV immature capsids are assembled and transported to the plasma membrane is an active process, requiring ATP [61]. Blocking ATP activity by treating MPMV-infected cells with sodium azide, results in a reversible block in capsid assembly and transport. Pulse-chase analysis showed that, after treating cells with ATP-blocking agents, assembled capsids were not released. Electron microscopy showed that the immature capsids in treated cells were retained in the cytoplasm, with very few localizing at the plasma membrane. This provided strong evidence that, post-assembly, intracellular transport of the virus to the plasma membrane for budding is an ATP-dependent process [61]. The MA domain of M-PMV has also been shown to be very important for intracellular transport of immature capsids from the site of assembly to the site of budding. Using sodium bisulphite mutagenesis to make random point mutations in MA, mutations at alanine 18 (A18) and alanine 79 (A79) to valines result in assembly of immature capsids and intracellular accumulation of these capsids, with little to no budding (A18V) to dramatically decreased kinetics of transport of these capsids to the plasma membrane for budding (A79V)[57]. Studies have also shown that recycling of M-PMV Env and the intracellular vesicular transport system are important for capsid transport. Expression of an Env(-) provirus results in a dramatic decrease in the kinetics of capsid maturation. Similarly, blocking the vesicular transport system of the cell by incubating cells at 20 ° C

[62], results in a near complete abrogation of capsid maturation that can be rescued by increasing the incubation temperature to 37 ° C. Stable transfection of M-PMV-expressing CMMT cells with mutants of the recycling endosomal marker, Rab11, also provided evidence for the importance of the intracellular vesicular transport system. Using the Rab11-S25N-GFP mutant which remains in a GDP-bound state, a decrease in the kinetics of capsid maturation is observed[63]. The requirement for the endocytosis of Env in efficient capsid transport can also be observed when the endocytosis signal in the CT of M-PMV Env is mutated. This mutation of the YXXL motif in the CT results in a lack of Env incorporation into virions, as well as a significant decrease in capsid release and maturation compared to wild-type [64].

As with intracellular transport, studies have shown that ATP hydrolysis and the MA domain are also important for then next step in the viral life cycle, budding and release [57,61]. Along with these factors, myristylation of glycine 2 (G2) of MA is required for intracellular transport and release. A glycine to valine substitution mutation at the myristylation signal in MA results in capsid accumulation in the perinuclear region and no release of the capsids, providing evidence of a critical role for myristylation in this process [65]. Nuclear magnetic resonance (NMR) analysis of the M-PMV MA protein and studies from MA mutants predicted that the myristate is sequestered within the MA domain prior to interacting with the plasma membrane for budding [57,66] and recent data confirm this [67]. The structure of the M-PMV MA is that of a hydrophobic core with a buried myristate surrounded by positive charges oriented on the outside of the protein. This structural conformation, coupled with an absolute requirement

for myristylation in order for budding to occcur, provided suggestive evidence that M-PMV MA undergoes a myristyl-switch mechanism in order to associate with the plasma membrane for budding. It was hypothesized that the positively-charged outer face of MA allowed charge mediated binding with the negatively charged polar head groups of the membrane and that this in turn allowed extrusion of the myristate residue into the hydrophobic interior [68]. Studies where the hydrophobicity of the MA core was increased by substitution of polar amino acids Y11, Y28, and Y67 with the more hydrophobic phenylalanine resulted in a decrease in the kinetics of virion release, and accumulation of the immature capsids under the plasma membrane [68]. Furthermore, studies substituting the positively charged amino acids in the outer domain of the MA protein with neutral amino acids also resulted in a negative effect on M-PMV capsid release. The kinetics of release were dramatically decreased for most mutants, with the exception of lysine 16 (K16) which displayed increased release kinetics. Electron microscopy analysis of the mutants showed that a majority of the mutants were stuck at or under the plasma membrane. In contrast, the K16A mutant budded into intracellular endosomes, suggesting that control of the myristyl switch was lost and that budding now occurred at the first available membrane. The studies provided further evidence that M-PMV must undergo a myrstyl switch in order for budding to occur, with the basic residues of the MA interacting with the plasma membrane, triggering the “switch” that exposes the myristic acid to be exposed and inserted into the hydrophobic region of the lipid bilayer [69].

Intracellular Vesicular Transport

For all eukaryotic cells, the targeting of proteins and organelles to the proper location is achieved by an intricate network of membranes and cytoskeletal motors. In a process known as the biosynthetic/secretory pathway, proteins that are synthesized on polysomes attached to the ER, enter the lumen of the ER where they are folded and oligomerized. This is followed by incorporation of these proteins into transport vesicles that are destined for the Golgi network, and fusion of the membranes of these vesicles with the cis-Golgi membrane [70]. The proteins then travel from the cis-Golgi membrane toward the trans-Golgi network (TGN). Proteins are then either destined for the continuous secretory pathway, whereby they are loaded into transport vesicles that fuse with the plasma membrane, or they are sequestered in the Golgi complex, awaiting a stimulus to trigger exocytosis in a regulated secretory pathway[71]. The secretory pathway involves the release of proteins into the extracellular space or the docking of proteins onto the cell surface. These latter proteins are often endocytosed as a part of the endocytic pathway. One endocytic pathway involves the envelopment of surface proteins and receptors into clathrin-coated endocytic vesicles that are then transported to a sorting endosome for the proper localization in the cell. Some of these proteins go through the recycling pathway, whereby they are endocytosed and then transported back to the plasma membrane either directly or after going through a recycling endosome[72]. This is the fate of the transferrin and the transferrin receptor as well as the low-density lipoprotein (LDL) receptor [73,74]. Other endocytosed proteins, such as TGN38, after passing through the sorting

endosome, go to the recycling endosome and are subsequently transported to the TGN. Alternatively, proteins such as furin, remain in the sorting endosome until it matures into the late endosome, and are then recycled to the TGN [75,76].

Major regulators of intracellular membrane trafficking are the Rab GTPases, also referred to as Rabs. Cycling between two states, GDP-bound and GTP-bound, Rabs function as molecular switches. They indirectly interact with components of the cell involved in vesicle budding, uncoating, motility, and tethering [77,78]. This usually occurs through effector proteins that bind to the Rabs in the GTP-bound state. For example, sorting adaptors such as TIP47 bind to Rab9, which is associated with intracellular transport between the late endosome and the TGN, as well as to the cytoplasmic domain of the mannose-6-phosphate receptor (M6PR), thus allowing this receptor to be sorted into late endosomes [79]. Another process that is important in membrane trafficking is the uncoating of vesicles. Specifically, for clathrin-coated vesicles, the clathrin coat must be removed to allow membrane fusion. Clathrin-coated vesicles contain the Rab GTPase, Rab5. With its effector protein, GTPase-activating protein and VPS9 domain-containing protein (GAPVD1), Rab5 facilitates the uncoating process of these vesicles by preventing phosphorylation of the **μ**2-subunit of the adaptor protein complex, AP-2, as well as recruitment of phosphatases and kinases that induce phosphatidylinositol-4,5-bisphosphate (PI-4,5-P_2) turnover [80-82].The ability of vesicles to bind to molecular motors associated with the cellular cytoskeleton is also a very important process that involves Rabs and their effector proteins. In melanocytes, the Rab GTPase Rab 27a and its effector protein melanophillin facilitate the interaction of

melanosomes with the actin motor, myosin Va, thereby allowing transport of these vesicles to the cell periphery [83,84]. Another well-studied Rab that associates with molecular motors of the cellular cytoskeleton is Rab11. This Rab, found in the endocytic recycling compartment associates with its effector protein, Rab11-family interacting protein 2 (Rab11-FIP2), which is recruited by another myosin motor, myosin Vb [85]. There are also several examples of microtubule-dependent motors, kinesins and dyneins directly or indirectly interacting with Rab GTPases to facilitate transport of vesicles along microtubules [86,87].

As described above, the cellular cytoskeleton and its associated molecular motors play an integral role in intracellular vesicle transport by serving as intracellular "highways." The cytoskeleton is made up microtubules, actin filaments, and intermediate filaments. Microtubules and actin filaments have motors associated with them that are important for the transport vesicular cargo through the cell. There are no known motors that associate with intermediate filaments. Microtubules are polarized tubules that originate at the microtubule-organizing center (MTOC) and radiate toward the periphery. The MTOC end of microtubules is known as the minus (-) end, and dynein motors move toward this end of the microtubule during retrograde transport of cargo from the cell periphery toward the cell center. The distal end of microtubules is referred to as the plus (+) end, and the kinesins are the motors responsible for anterograde transport of cargo from the cell center toward the periphery[88]. Actin filaments are also responsible for the transport of intracellular vesicles and their cargo and proper intracellular localization of organelles. Unlike the long-range transport attributed to microtubules, actin filaments are believed to be responsible for

localized movement of vesicular cargo and organelles [89], although recent studies have shown a microtubule-independent, actin-dependent mode of long-range transport of vesicles[90]. The motors responsible for cargo trafficking along actin filaments are the myosins. As described above, the well-studied characteristics of melanosome movement in melanocytes can be attributed to the molecular motor, mysosin Va, along actin filaments [91], and transport of recycling vesicles to the plasma membrane involves myosin Vb [85]. Myosin V has also been shown to be required for fast axonal transport in squid axons, another model system for studying the function of actin filaments in vesicle transport [92]. In order for vesicular cargo to reach their proper destination, there must be some interplay between microtubules and actin filaments. Studies on how cargoes switch from microtubules to actin are ongoing. A protein known as $p150^{glued}$ has been identified as a possible link between the two cytoskeletal elements because it is a part of the dynactin complex, which is an activator of dynein-associated vesicular transport and also has the ability to bind to the actin-related protein centractin (Arp-1) [93]. Myosin Va has also been identified as a possible linker between microtubules and actin because of its ability to move along actin as well as bind and diffuse along microtubules [94,95].

Viruses and Intracellular Transport. Since viruses are essentially obligate, intracellular "parasites," they must utilize the host cellular machinery for many steps in the viral life cycle. Studies have shown that numerous viruses utilize the cellular cytoskeleton for efficient intracellular transport toward the nucleus, post-entry. A well-studied virus that exhibits this behavior is herpes simplex virus (HSV). After fusion at the axonal membrane and release of the capsid into the

axoplasm, HSV capsids are rapidly transported in a retrograde manner toward the nucleus by way of microtubules. This trafficking occurs by binding of the HSV capsid protein to the dynein light chain motor Tctex-1 [96]. Adenovirus is another virus that has been well studied in its use of microtubules for retrograde transport. Utilizing fluorophore-tagged adenovirus (Ad) and time-lapse fluorescence microscopy, it has been shown that Ad is transported very efficiently along microtubules toward the nucleus, although this movement is bi-directional. Inhibition of dynein activity through the overexpression of p50-dynamitin, which significantly reduced the frequency of retrograde transport of Ad, also provided strong evidence that this transport toward the nucleus was mediated by capsid interactions with dynein [97]. A less well understood mechanism by which incoming viruses can traverse the cytoplasm to the nucleus in a microtubule-independent manner is by inducing the formation of "actin cables." This is the pathway utilized by the baculovirus, *Autographa californica* M nucleopolyhedrovirus (Ac-MNPV), which is able to bind to actin and induce actin polymerization, forming cables that extend toward the nucleus [98].

Once the virus enters the cell and travels toward the nucleus for replication, many viruses must also hijack the cell's cytoskeleton for egress, or anterograde transport, toward the cell periphery. There is evidence for viral use of microtubules and actin for this process. Vaccinia virus is an example of virus that utilizes both of these components. After replication in perinuclear viral factories, Vaccinia virus forms mature viruses (MV). MV are transported to the TGN where they are enveloped. This transport occurs by active transport of MV along microtubules, and envelopment is sensitive to microtubule

depolymerization [99]. These intracellular enveloped viruses (IEV) are transported to the plasma membrane where they fuse and are released and become extracellular viruses (EV). The transport of the IEV toward the plasma membrane is dependent on microtubules and the conventional kinesin, KIF5b [100,101]. Since the virus must get past a dense cortical actin layer in order to be released, there is likely association of the IEV with actin motors, although to date, no myosins, have been shown to be involved. Unlike Vaccinia virus, the lentivirus, HIV, does not transport assembled capsids to the plasma membrane, but instead must transport individual Gag proteins to the cell surface, where budding and assembly occur simultaneously. To achieve this goal, HIV Gag binds to the microtubule motor, kinesin-4 (KIF-4). Yeast-two hybrid systems, cell fractionation, and immunoprecipitation studies showed that the HIV Gag precursor, and other retroviral Gags, associate with KIF-4, consistent with the use of microtubules for transport to the plasma membrane for budding [102]. Further studies using KIF-4 knockdowns showed that HIV Gag interaction with KIF-4 is necessary for transport out of a perinuclear region of the cell, and that intracellular Gag levels as well as virus production has an absolute requirement for the presence of KIF-4 [103]. Studies have suggested that in certain cell types, particularly macrophages, HIV Gag follows a different pathway for virion release. In these cells, Gag proteins are transported to CD63-positive multivesicular bodies (MVB) where virus assembly occurs in these intracellular compartments and subsequently released by an exosomal pathway [104]. Transport to this late endosomal compartment is facilitated by HIV Gag interactions with adaptor-protein 3 (AP-3), which is found in clathrin-coated vesicular traffic from the TGN

toward late endosomes [105]. This alternate mechanism of release, however, has been met with controversy in the field, as it is contrary to studies that show the plasma membrane as the site of productive HIV budding and release in all cell types that it infects, including macrophages [106,107]. In this study, the intracellular compartments containing the HIV virions are linked to the plasma membrane by small channels, therefore implying that these compartments were not late endosomes, but instead deep invaginations of the plasma membrane. Three-dimensional image analysis of these channels showed that HIV virions were found within these channels connecting this intracellular compartment to the plasma membrane [108]. Recent studies using immunofluorescent labeling of tetraspanins and membrane-impermeable cationized-ferritin, however, provide evidence that the HIV-containing intracellular compartments in macrophages could be a heterogenous mixture of plasma membrane-connected invaginations and endosomal compartments that are inaccessible to the cell surface without membrane permeabilization [109].

This Dissertation

In this dissertation, the host factors and viral proteins involved in the intracellular transport of M-PMV immature capsids from their pericentriolar site of assembly to the plasma membrane site of budding are investigated. Although several studies have been done using deletion and substitution mutagenesis strategies, pulse-chase analyses, transmission electron microscopy, and immunofluorescence microscopy to determine what role viral proteins such as the Gag polyprotein precursor and the Env glycoprotein, play in the late stages of

the viral life cycle, after procapsid assembly has occurred, they only give a global picture of what is happening in the cell. With the recent advances in molecular biology and the availability of fluorescent protein tags such as green fluorescent protein (GFP), proteins can be visualized in real-time using live cell imaging. This offers the advantage of being able to observe individual protein behavior in a dynamic system. In virology, live-cell imaging techniques have been employed for studying the intracellular transport of HIV, HSV-1 and AAV, among other viruses [110-113].

The first study in this dissertation focuses on creating a fluorescently-tagged M-PMV Gag to be used for studying capsids in real-time to elucidate the viral and host proteins involved in different steps in the M-PMV life cycle. In order to achieve this, enhanced green fluorescent protein (eGFP) was fused to the carboxy-terminus of a codon-optimized Gag, separated by a short, flexible amino acid linker, and replacing the *pro* and *pol* genes. Electron microscopy and pulse-chase analysis of this eGFP-tagged Gag, heretofore referred to as GagGFP-M100A, created abberantly-shaped immature capsids and also had a defect in the kinetics of virus release, thus it was necessary to coexpress the GagGFP-M100A with a helper untagged proviral construct. Using intracellular localization studies comparing the tagged-Gag to untagged immunofluorescently-labeled Gag in fixed cells, it was determined that GagGFP-M100A localized similarly to WT and several mutant untagged Gag proteins, thus providing strong evidence that this GagGFP-M100A construct could be used for studying intracellular transport of capsids in live cells. Preliminary examination of the types of movement seen by individual capsids, including bi-directional long-range lateral movement through

the cell, oscillatory instantaneous velocities, and a median instantaneous velocity of approximately 7 um/s suggested that the fluorescent capsids may be trafficking along microtubules. Live cell imaging of mCherry-tagged microtubules cotransfected with GagGFP-M100A supported the hypothesis that the capsids were utilizing microtubules for long-range transport through the cell.

Preliminary results showing that the M-PMV capsids utilize microtubules for intracellular transport was further supported by treatment of M-PMV expressing CMMT cells, transfected with GagGFP-M100A, with cytoskeletal disrupting drugs. Cells were treated with nocodazole, cytochalasin-D, and acrylamide in order to depolymerize or disrupt microtubules, actin microfilaments, and intermediate filaments, respectively. Disruption of microtubules, but not actin and intermediate filaments resulted in a delay, but not complete block, in capsid release and maturation. Viruses released from nocodazole-treated cells were Env-deficient, providing evidence that microtubules are essential for Env-incorporation into virions. Employing the use of an mCherry-tagged M-PMV Env construct, and cotransfecting CMMT cells with GagGFP-M100A, co-transport of M-PMV Gag and Env were visualized for the first time. Treatment of cells with nocodazole resulted in a transient arrest in intracellular transport of M-PMV Gag, Env, and co-transporting Gag/Env at 2 hours post treatment. Interestingly at 4 hours post treatment, movement of Gag can be seen near the cell periphery, while Env and colocalized Gag/Env remained arrested. The Gag movement at 4 hours post-treatment, however was slower and less linear than in untreated cells, although mean-squared displacement analysis

suggested that this movement was by an active mode of transport and not just Brownian diffusion.

These data support a hypothesis for Gag and Env interacting intracellulary and traveling together toward the plasma membrane for budding. Specifically, the hypothesis states that M-PMV Env leaves the Golgi and is inserted into the plasma membrane by the secretory pathway. It is subsequently endocytosed and transported to the pericentriolar region of the cell in recycling vesicles where it "meets" and interacts with newly assembled immature capsids. These capsids are then trafficked to the plasma membrane, along microtubules, by interacting with the Env-containing vesicles, thus allowing the Env and Gag to be in the same location for budding.

A Mason-Pfizer Monkey Virus Gag-GFP Fusion Vector Allows Visualization of Capsid Transport in Live Cells and Demonstrates a Role for Microtubules

Jasmine Clark[1], Petra Grznarova[2], Elizabeth Stansell[1§], William Diehl[1¶], Jan Lipov[2],Paul Spearman[3], Tomas Ruml[2], Eric Hunter[1,4]

Accepted: *PLoS One,* November *2013*

Elizabeth Stansell was responsible for the preliminary work involved in the construction of the Gag-GFP fusion. William Diehl and Jasmine Clark created the final Gag-GFP constructs (Figure 1b and 1c). Jasmine Clark and Petra Grznarova did the pulse-chase experiments (Figure 1d, 1e, 3, 4b), and the fixed cell imaging (Figure 4a). Jasmine Clark did the transmission electron microscopy experiments (Figure 2) and the live-cell imaging and single particle tracking experiments (Figure 5 and Figure 6).

Abstract

Immature capsids of the Betaretrovirus, Mason-Pfizer Monkey virus (M-PMV), are assembled in the pericentriolar region of the cell, and are then transported to the plasma membrane for budding. Although several studies, utilizing mutagenesis, biochemistry, and immunofluorescence, have defined the role of some viral and host cells factors involved in these processes, they have the disadvantage of population analysis, rather than analyzing individual capsid movement in real time. In this study, we created an M-PMV vector in which the enhanced green fluorescent protein, eGFP, was fused to the carboxyl-terminus of the M-PMV Gag polyprotein, to create a Gag-GFP fusion that could be visualized in live cells. In order to express this fusion protein in the context of an M-PMV proviral backbone, it was necessary to codon-optimize *gag*, optimize the Kozak sequence preceding the initiating methionine, and mutate an internal methionine codon to one for alanine (M100A) to prevent internal initiation of translation. Co-expression of this pSARM-Gag-GFP-M100A vector with a WT M-PMV provirus resulted in efficient assembly and release of capsids. Results from fixed-cell immunofluorescence and pulse-chase analyses of wild type and mutant Gag-GFP constructs demonstrated comparable intracellular localization and release of capsids to untagged counterparts. Real-time, live-cell visualization and analysis of the GFP-tagged capsids provided strong evidence for a role for microtubules in the intracellular transport of M-PMV capsids. Thus, this M-PMV Gag-GFP vector is a useful tool for identifying novel virus-cell interactions involved in intracellular M-PMV capsid transport in a dynamic, real-time system.

Introduction

In studying the role of viral and host cell factors involved in retroviral assembly, trafficking, and budding, the mechanism by which capsids are transported through the cytoplasm is still an poorly understood process. It has been shown previously that for Mason-Pfizer Monkey Virus (M-PMV), capsids are assembled intracellularly at the pericentriolar region by way of a cytoplasmic targeting-retention signal (CTRS), and are subsequently trafficked to the plasma membrane for budding [1,2]. This process is unique when compared to a virus such as HIV, which exhibits C-type retrovirus morphogenesis, in that assembly and budding are spatially and temporally separated. This separation thus allows for studying these processes individually in order to elucidate the role of viral and cellular factors necessary for assembly and intracellular transport.

Like most simple retroviruses, M-PMV encodes a Gag polyprotein, Pr78, that assembles to form the immature capsid and expression of this gene alone results in the assembly and release of immature virus particles [3]. Pr78 is modified by an N-terminal myristic acid residue that is mostly buried within the folded protein [4]. Following interaction of Gag with the plasma membrane the exposure of this myristic acid moiety appears to be critical for envelopment and budding of the virus [5]. These previous studies with M-PMV have employed the use of genetic, biochemical and fixed-cell immunofluorescent methodologies for elucidating the role of viral and cellular components in viral assembly, transport, and budding [2,6-9]. Prior data has shown that blocking vesicular trafficking by shifting the temperature of the cell to 20°C causes a significant delay in M-PMV Gag release kinetics and maturation, indicating a role for the cellular vesicular

transport system in capsid transport [10,11]. It has also been shown that Env glycoprotein expression is necessary for efficient capsid release and maturation [7,10,12]. Several capsid mutations have provided key insights into the processes involved in M-PMV assembly and transport. Specifically, a single amino acid change from arginine to tryptophan (R55W) in the CTRS causes a switch from B/D type capsid assembly to C-type assembly [3] by preventing nascent Gag molecules from interacting with the dynein light chain Tc-tex and their subsequent transport on microtubules to the pericentriolar region of the cell. Another mutation in the matrix (MA) protein of Gag, R22A, displays a transport defect in which assembled immature capsids are unable to reach the plasma membrane resulting in their aggregation under the cortical actin layer. This dominant negative mutation, which appears to block transit through the actin layer, causes a complete block in viral release from the cell [5]. Further, a double mutation, K16A/K20A, in a basic region of MA, results in the budding of immature capsids into intracellular vesicles, suggesting that these residues play an important role in regulating myristic acid exposure . These data and mutants, while providing insights into the dynamics of Gag assembly, intracellular trafficking, and interactions with cellular membranes, have not allowed studies of individual capsid movement within the cell.

Recent advances in molecular virology have allowed for the use of fluorescently tagged proteins for studying intracellular viral processes. In these studies, a fluorescent protein, usually enhanced green fluorescent protein (eGFP), is fused to the viral protein of interest followed by utilization of real-time live cell imaging techniques for visualizing its behavior. In fusing GFP to the protein of

interest, however, several controls are required in order to make sure that the fusion does not disrupt the normal biological processes of the protein. For HIV, Muller et al., were able to successfully tag HIV Gag by inserting GFP near the C-terminus of the matrix (MA) domain of Gag, which had previously been shown to accept short epitope tags without disrupting replication [13]. Successful fusion of GFP to viral capsid proteins, has been used for the study of virus intracellular localization, assembly, and trafficking for other viruses such as herpes simplex virus (HSV) and adeno-associated virus (AAV) [14,15]. Therefore, construction of a GFP-tagged protein that functions similarly to the wild-type counterpart, can be an integral tool in studying viral-host cell interactions in a dynamic system.

In this study, we set out to create an M-PMV Gag-GFP fusion construct that could be used to investigate capsid assembly and the role of the cytoskeleton in intracellular trafficking in a dynamic system. In order to achieve this, it was necessary to codon-optimize the M-PMV *gag*, strengthen the Kozak consensus sequence for the initiating methionine of Gag, mutate an internal initiating methionine codon of *gag* and replace the M-PMV *pro* and *pol* genes with the gene for eGFP. Cotransfection of this Gag-GFP vector with a helper provirus resulted in capsid assembly and release with an efficiency similar to WT M-PMV. The intracellular localization of eGFP-tagged WT and mutant constructs was compared to untagged proteins labeled by immunofluorescent staining in fixed cells and shown to be equivalent. Fluorescently-labeled, mobile capsids were visualized in live cells, and both the kinetics and co-localization of capsids show a key role for microtubules in their intracellular transport from the pericentriolar region to the plasma membrane.

Materials and Methods

Cell Lines

Infectious M-PMV-producing CMMT cells, were originally derived by co-culturing rhesus mammary tumor cells with rhesus monkey embryo cells [16-18]. COS-1 cells, derived from the African green monkey kidney cell line, CV-1, by transformation with an origin-defective mutant of SV40 [19] and 293T cells, derivatives of the 293 cell line containing an insertion of the temperature sensitive gene for the SV40 T-antigen [20], were obtained from the American Type Culture Collection. All cells were cultured in Dulbecco's modified Eagle's medium (DMEM) supplemented with 10% fetal bovine serum (Gibco). Cell lines were maintained at 37°C with 5% CO_2.

Plasmids

The plasmids used in this study are depicted in Figure 1. The plasmid pSARM-X is an M-PMV proviral vector that expresses the M-PMV genome under the control of the viral LTRs (Figure 1A). The plasmid pSARM-GagGFP was constructed by inserting a codon-optimized *gag* gene and linked e*gfp* gene between the EagI and XhoI sites of pSARM-X, replacing the *gag, pro,* and *pol* genes. Briefly, the codon-optimized *gag* gene was amplified with primers containing an EagI site in the forward primer and an AgeI site in the reverse primer. The eGFP was amplified from a pEGFP-N1 vector using primers with an AgeI site in the forward primer and a PspXI site and putative splice acceptor site in the reverse primer. The amplified *gag* was digested with EagI and AgeI; the amplified *eGFP* was digested with AgeI and XhoI (and isoschizomer of PspXI);

and the pSARM-X provirus was digested with EagI and XhoI. Fragments were ligated by three-way ligation to create pSARM-GagGFP (Figure 1B). The vector was confirmed using both diagnostic digestion with BlpI and sequencing of the complete insert.

To enhance the Kozak consensus sequence of the Gag-GFP construct and to prevent internal ribosomal initiation, the plasmid was mutated using four overlapping ultramers spanning from the EagI site to the SbfI site of codon-optimized *gag*. The ultramers contained a strengthened Kozak consensus sequence at the initiating methionine as well as a methionine to alanine substitution at the second methionine (M100A) (Figure 1C). All four ultramers were annealed using temperature-gradient PCR (50-65 °C) with Taq polymerase. The subsequent 500 bp fragment was digested with EagI and SbfI and inserted back into pSARM-GagGFP to create pSARM-GagGFP-M100A.

The M-PMV proviruses encoding the R55W, -R22A, -K16A/K20A mutations have been described previously [3,5]. The GagGFP-M100A-R55W, -R22A, -K16A/K20A mutants were derived using the QuikChange Lightning Site-directed Mutagenesis Kit (Agilent Technologies, La Jolla, CA), using pSARM-GagGFP-M100A as the template and respective mutagenic primers (Table 1). Mutants were confirmed by sequencing.

Metabolic Labeling and Immunoprecipitation

A total of 4 μg of the various pSARM-derived constructs were transfected into COS-1 or 293T cells using Lipofectamine 2000 (Invitrogen, Carlsbad, CA). At 18-24 hours after transfection, cells were starved in DMEM lacking methionine and cysteine (Gibco) for 15 minutes. Cells were subsequently labeled with 100 μCi ^{35}S-methionine (Perkin-Elmer NEN, Boston, MA) per well for 30 minutes. Following labeling (Pulse), the labeling media was replaced with complete DMEM (Gibco) and cultured for the indicated times (Chase). Cell-associated and cell-free viral proteins were then analyzed. Cell supernatants were collected from each well and cellular debris was removed by low-speed centrifugation and virus particles lysed by the addition of Triton X-100 to 1%. Cells in each well were subsequently gently lysed with 1% Triton X-100 lysis buffer [1% Triton X-100, 50mM NaCl, 25mM Tris, pH 8.0]. Cell lysates were pre-cleared with fixed *Staphylococcus aureus* (*Staph. A.*) overnight at 4°C, then M-PMV proteins were immunoprecipitated using either polyclonal goat-anti-M-PMV or rabbit-anti-Pr78 anti-sera. Immune complexes were isolated by addition of fixed *Staph. A.* and washed with lysis buffer containing 0.1% SDS (0.1% SDS, 1% Triton X-100, 50mM NaCl, 25mM Tris, pH 8.0; lysis buffer B) [21]. The immunoprecipitated proteins were resolved by electrophoresis on 12% SDS-polyacrylamide gels (SDS-PAGE) (BioRad).

Quantifying Gag Release

SDS-PAGE gels were fixed in Coomassie Blue solution [0.05 % Coomassie Brilliant Blue, 10% glacial acetic acid, 50% methanol, 40% H_2O], dried and then exposed to phosphor screens and the radiolabeled protein bands were digitally acquired using the Packard Cyclone™ system. Optiquant imaging analysis software (Perkin Elmer, Shelton, CT) was used to quantify the amount of viral proteins based on the number of digitized light units (DLU) for each band. To measure the percentage of M-PMV GagGFP released, the ratio of GagGFP in the supernatant versus total cell-associated and released GagGFP was determined. Conversely, to measure the percentage of cell-associated M-PMV Gag, the ratio of total cell-associated Gag versus total cell-associated and released Gag was determined. For the positive control, the total cell-associated and released Gag (Pr78, Pr95, and Pr180) was measured.

Electron Microscopy

COS-1 cells were transfected with the indicated plasmids using Fugene 6 (Promega) transfection reagent. At 24 hours post-transfection, cells were fixed in a 2.5% glutaraldehyde fixative (10%- 25% EM grade glutaraldehyde, 50% 0.2M cacodylate buffer, 40% distilled H_20) for at least two hours at 4°C. The cells were washed and subsequently fixed in 1% osmium fixative (2 parts 0.2M cacodylate buffer, 1 part 6% potassium ferrocyanide, 1 part 4% osmium tetroxide). The cells were then dehydrated with ethanol, followed by infiltration with a 1:1 ratio of 100% ethanol and Epon resin for at least one hour. Cells were embedded in fresh Epon resin at 60°C for 48 hours, and then cut into ultrathin sections and picked

up on a copper grid. Virus particles were viewed using a JEOL-JEM 1210 transmission electron microscope.

Virus Purification

293T cells seeded onto a 10 cm culture plate were transfected with 15 μg of total DNA with Lipofectamine 2000. For co-transfected cells, a ratio of approximately 4:1 (11.5 μg and 3.5 μg of pSARM-GagGFP-M100A and pSARM-D26N, respectively) was used. Proteins in transfected cells were radiolabeled with ^{35}S for 48 hours by incubating cells in 90% Met-/Cys- DMEM (Gibco) in complete DMEM complemented with 100 μCi/mL ^{35}S. Cellular supernatants were filtered through a 0.45 um filter (Thermo-Scientific, Waltman, MA) then overlaid on a 20%-50% sucrose (w/w), with 10% steps, discontinuous gradient. Samples were spun at 35,000 rpm at 4°**C** for 3 hours in the Beckman-Coulter Optima L-80 XP Ultracentrifuge using the SW41-Ti swinging bucket rotor. Using upward displacement, 1 mL fractions were isolated. 200 μl of Lysis Buffer A and 6 μl of 20% SDS were added to each fraction, and virions were immunoprecipated with a polyclonal goat-anti-M-PMV antisera. Immune complexes were isolated by addition of fixed *Staph. A*. and washed with lysis buffer B. Immunoprecipitated proteins were resolved on 12 % SDS-PAGE gels. The density of each fraction was calculated using refractive indices.

Western Blot

Supernatants from 10cm culture dishes of 293T cells transfected with 4μg of pSARM-GagGFP-M100A or 1.6 μg and 3.2 μg pSARM-GagGFP-M100A and pSARM-X, respectively, were collected 48h post transfection. Virions were isolated by ultracentrifugation through a 25% sucrose cushion and the pellet was resuspended in 100 μl protein loading buffer. 25 μl of each sample was resolved in a 12% SDS-PAGE gel. Samples were transferred to a nitrocellulose membrane, blocked with 5% non-fat dry milk, and blotted with a mixture of two monoclonal mouse-anti-GFP antibodies (Roche, Germany). Immune complexes were subsequently bound by a horseradish peroxidase (HRP)-conjugated donkey-anti-mouse IgG antibody (Santa Cruz Biotechnology, Dallas, Texas). Pierce SuperSignal West Femto Chemiluminescent HRP substrate (ThermoScientific, Rockford, IL) was applied to blot followed by exposure to film.

Fixed Cell Microscopy

For imaging GFP-tagged as well as untagged Gag, COS-1 cells were plated at 80-90% confluency on coverslips (Fisher Scientific). Cells were co-transfected at a ratio of 4:1 with 3.2 μg WT or mutant M-PMV provirus and 0.8 μg WT or mutant pSARM-GagGFP-M100A, or were transfected with the untagged WT or mutant provirus only. 24 hours post transfection, cells were fixed with cold methanol:acetone (1:1). Coverslips containing cells transfected with GFP-tagged virus were then placed on glass slides with Prolong Antifade Gold (Invitrogen). Coverslips containing the fixed cells transfected with untagged provirus were

reacted with polyclonal rabbit-anti-p27 antisera (1:500 dilution), and after washing 3X in PBS, bound antibodies were tagged with 1:10,000 diluted Alexa-488-conjugated Goat-anti-Rabbit IgG (Invitrogen) and subsequently placed on glass slides with Prolong Antifade Gold. Cells were then imaged on the Deltavision Core Imaging System (Applied Precision, Issaquah, Washington) with a CoolSnap camera at 60X magnification.

Live Cell Microscopy

CMMT cells, which constitutively produce WT M-PMV proteins, were plated to 70-80% confluency on 35-mm coverslip-bottom dishes (Matek, Ashland, MA), then transfected with 4 μg pSARM-GagGFP-M100A construct using the Lipofectamine 2000 transfection reagent. For co-localization studies with microtubules, cells were co-transfected with pSARM-GagGFP-M100A and p-mCherry-tubulin (A gift from Roger Tsien to Paul Spearman). Images were acquired using the Deltavision Core Imaging System with a CoolSnap camera. All experiments were done in a 37°C chamber with CO_2 infusion at 60X magnification.

Time-lapse Image Analysis

Deltavison (.dv) files were imported into FIJI, an NIH open-source image analysis software distribution, using the Bio-Formats Importer (LOCI) plugin [22,23]. Particles were detected and tracked in two- and three dimensions using the Particle Tracker (MOSAIC) plugin. This plugin allowed for automated tracking of single particles based on an algorithm described by Sbalzarini *et al.*

[24]. To calculate maximum instantaneous velocity, the instantaneous velocity at each time point was calculated using the x- and y- position of a 2D image and the following formula:

$$v_n = \frac{\sqrt{(x_{n+1}-x_n)^2 + (y_{n+1}-y_n)^2}}{t} \times pixel\ size$$

v_n - instaneous velocity at time n

x_n - x-position at time n

y_n - y position at time n

t - time lapse between successive frames

pixel size - representative size/pixel

To calculate the total displacement of a trajectory, the distance between the beginning and end of a trajectory was calculated using the x- and y- position of the 2D image and the following formula:

$$d_{total} = \sqrt{(x_{last}-x_{first})^2 + (y_{last}-y_{first})^2}$$

d_{total}- total displacement

x_{first}- x-position at beginning of trajectory

x_{last}- x-position at end of trajectory

y_{first}- y-position at beginning of trajectory

y_{last}- y-position at end of trajectory

For tracking along microtubules, single particles were manually tracked by following the particle in successive frames until the particle was no longer visible or no longer able to be discriminated by eye. To define trajectory types,

trajectories were categorized by visual examination of the trajectories made using the ImageJ Particle Tracker (MOSAIC) plugin. Trajectories with less than (<) 10 frames were filtered out. For quality control, the total displacement of the trajectories was calculated.

Results

Construction of an M-PMV provirus expressing a Gag-eGFP fusion protein

Initial experiments to construct a GFP-tagged M-PMV Gag protein, in which the *pro-pol* region of the genome was replaced with the gene for eGFP, resulted in the synthesis of a ~70kD protein consistent with the product of aberrant splicing (Data not shown). We therefore codon-optimized the *gag* gene and created a *gag-egfp* gene fusion as described in Methods. In order to express the codon-optimized Gag-GFP fusion protein from an M-PMV provirus, the chimeric gene was inserted into pSARM-X to replace the *gag, pro* and *pol* genes as described in Methods (Figure 1A, B). Since the *pro* and *pol* genes were removed from this construct and cleavage could not occur upon release, a pSARM-X construct containing a mutation in the active site of *pro*, D26N, was used as the positive control in the experiments described below.

In order to investigate whether the Gag-GFP construct was synthesized, assembled, and transported with similar kinetics to WT Gag, pulse-chase experiments were carried out. Immunoprecipitation of pulse-labeled cells transfected 24 hours previously with the pSARM-D26N plasmid showed major bands at 78, 95, and 180 kD (Figure 1D, Lane 1 Pulse), consistent with the Gag, Gag-Pro, and Gag-Pro-Pol precursors. Pulse-chase analysis of the new construct, pSARM-GagGFP showed two major bands at approximately 95 and 105 kD (Figure 1D, Lane 2 Pulse). Both of the bands were inefficiently released into the supernatant after a 4h chase in complete medium (Figure 1D, Lane 2 4h Sup).

An analysis of the sequence of the codon-optimized *gag* gene showed a weak Kozak-consensus sequence preceding the initiating methionine, as well as a second in-frame methionine at amino acid 100 (M100), raising the possibility that ribosomes, were traversing the primary initiating methionine of *gag* and initiating translation at M100. We therefore optimized the Kozak consensus sequence at the initiating methionine, and substituted an alanine codon for that of M100 (M100A) (Figure 1C and Supplementary Figure S1). M-PMV M100A had previously been shown to have no effect on Gag processing or release kinetics [9]. The Kozak-optimization and the M100A mutation in this pSARM-GagGFP-M100A construct resulted in efficient initiation from the first methionine, eliminated expression of the truncated protein, and showed Gag-GFP expression at comparable levels to D26N (Figure 1D, Lane 3 Pulse). Moreover, these modifications resulted in more efficient transport and release of the Gag-GFP fusion protein (Figure 1D, Lane 3 4h sup.).

A pulse-chase analysis also revealed that the Env glycoprotein was inefficiently expressed in the Gag-GFP fusion construct even though the *env* gene was present. In wild-type M-PMV Env is expressed from a spliced mRNA, and all putative *env* splice acceptor sites (Supplementary Figure S1) are present in the region flanking the 3' end of GFP in the pSARM-GagGFP-M100A fusion, but this construct still yielded background levels of Env expression (Figure 1E). Analysis of the nucleotide sequence of non-codon-optimized versus codon-optimized M-PMV Gag showed that a majority of the potential splice branch points were

removed during codon-optimization (data not shown). The possibility that the branch point for Env splicing was in the *pro* or *pol* genes, which have been completely removed from this construct, also cannot be ruled out**.**

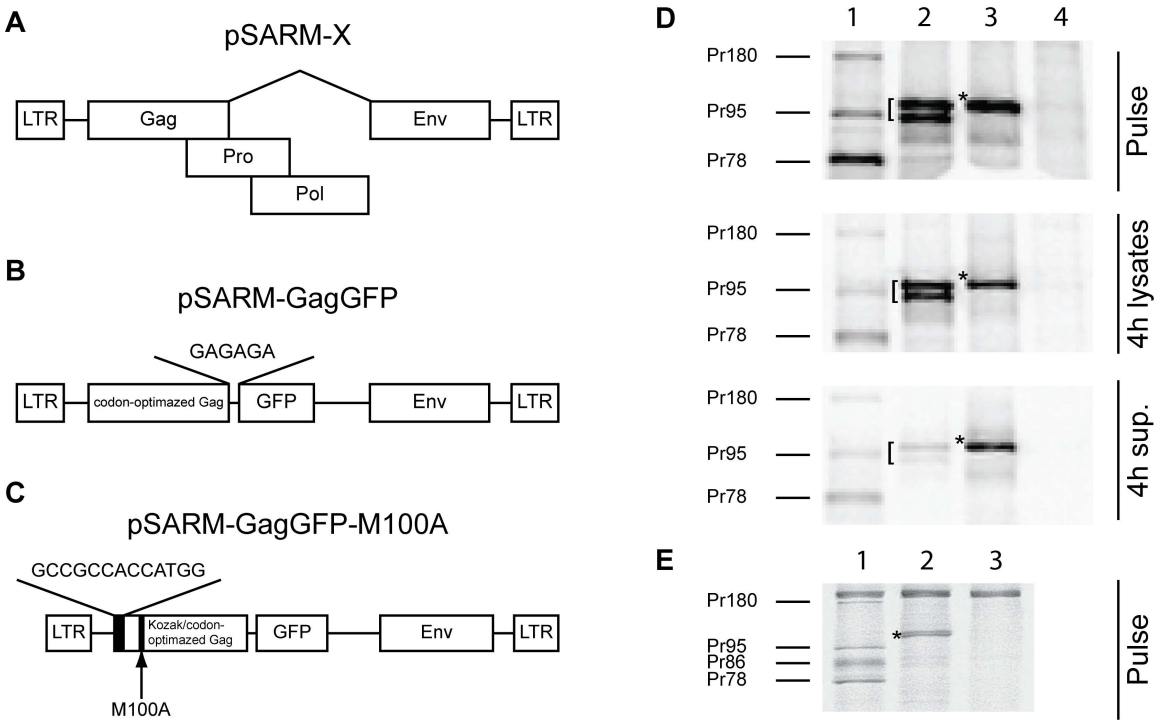

Figure 1 Construction of GagGFP pSARM-X.
Genetic organization of construct pSARM-X (A), pSARM-GagGFP (B), pSARM-GagGFP-M100A (C). (D) 293T cells (untransfected, Lane 4) were transfected with pSARM-D26N (Lane 1), pSARM-GagGFP (lane 2) and pSARM-GagGFP-M100A (Lane 3). Viral proteins were metabolically labeled with [^{35}S]-methionine followed by a 4-hour chase in unlabeled media. Lysates from the pulse and chase (4h lysates) as well as culture medium from the chase (4h sup.) were then immunoprecipitated with rabbit anti-p27^{CA} antibody and resolved on SDS-PAGE. (E) 293T cells were transfected with pSARM-D26N (Lane 1) and pSARM-GagGFP-M100A (Lane 2). Viral proteins were metabolically labeled with [^{35}S]-methionine and lysates were then immunoprecipitated with goat anti-MPMV antibody and resolved on SDS-PAGE. Positions of the viral precursor proteins Pr180 (Gag-Pro-Pol), Pr95 (Gag-Pro), Pr86 (Envelope) and Pr78 (Gag) are shown. Products of pSARM-GagGFP ([) and pSARM-GagGFP-M100A (*) are shown.

Expression of eGFP-fused Gag alone causes aberrant capsid formation

To determine if the fusion of a 27 kD eGFP protein to the carboxyl terminus of Gag impacted the shape and size of the resulting immature capsids, capsid structure was visualized using transmission electron microscopy (TEM). 293T cells were transfected with pSARM-GagGFP-M100A or pSARM-X, and prepared for TEM. The results from analysis of thin section electron-micrographs showed that capsids from cells transfected with pSARM-GagGFP-M100A were aberrantly shaped in comparison to capsids from cells transfected with the WT provirus (Figure 2B), although they were distributed similarly throughout the cytoplasm (Supplementary Figure S2A and B). The immature capsids in cells transfected with pSARM-GagGFP-M100A were larger in diameter, were not uniform in shape, and had a “beads-on-a-string” morphology compared to the more compact, homogenously-shaped immature capsids of the WT (Figure 2B versus 2A).

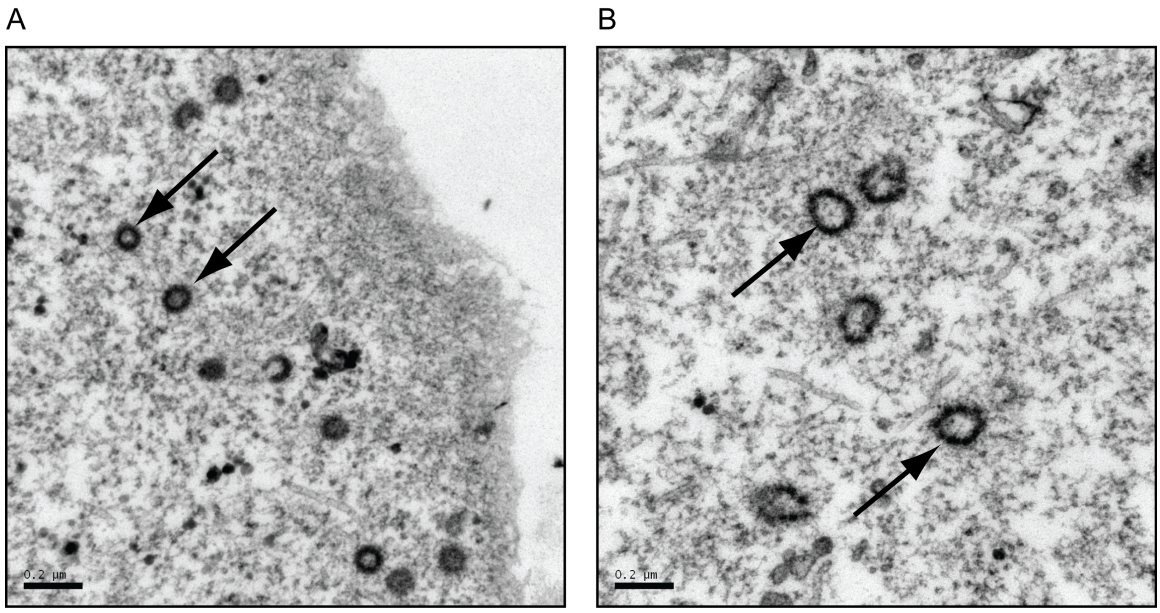

Figure 2 Verification of viral particles shapes by transmission electron microscopy.
COS-1 cells were transfected with pSARM-X wild type provirus (A) or pSARM-GagGFP-M100A (B). 24 hours after transfection were cells fixed in a 2.5% glutaraldehyde fixative for 2 hours at 4 °C. The cells were washed and subsequently fixed in 1% osmium fixative. The cells were then dehydrated with ethanol, followed by infiltration with 100% ethanol and Epon resin for at least one hour. Cells were then embedded in fresh Epon resin at 60°C for 48 hours then cut into ultrathin sections and picked up on a copper grid. The arrows in (A) point to WT intracellular capsids of homogenous shape, with a diameter of approximately 100 nm. The arrows in (B) point to GagGFP-containing intracellular capsids having a beads-on-a-string shape and varying diameters greater than 100 nm. Bar = 200 nm.

Release kinetics of capsid is delayed in the absence of WT virus and rescued during cotransfection with WT

Since previous reports have shown that Env expression is necessary for efficient virion release and capsid maturation [2,7,10,12], and the TEM data showed improper capsid morphology when cells were transfected with pSARM-GagGFP-M100A alone, a pulse-chase experiment was carried out to determine whether cotransfection with WT pSARM-X changed the kinetics and efficiency of Gag-GFP release from cells. Proteins were pulse-labeled with ^{35}S methionine for 30min and chased with unlabeled media for 2 or 4 hours. Cell lysates from the pulse and each chase time-point, as well as cell culture medium (supernatants) from the chase plates were immunoprecipitated with rabbit anti-p27^{CA} antibody (Figure 3A). The mutant pSARM-D26N was used as the positive control (Lane 1). Radioactivity corresponding to the immunoprecipitated proteins were quantitated as described in Methods. Consistent with previous reports, approximately 2 hours after the pulse, 50% of the cell-associated precursors (Pr78, Pr95, and Pr180) had been released into the culture medium (Figure 3B, Supplementary Figure S3). Cells transfected with pSARM-GagGFP-M100A alone showed a large delay in release kinetics, and even after a 4 hour chase, only 45% had been released. For cells cotransfected at a ratio of 4:1 D26N to pSARM-GagGFP-M100A, which mimics WT protein expression, in which Pr95 and Pr180 are translated 15% and 5% of the time respectively through ribosomal slippage [25,26], there was an increase kinetics of Gag-GFP release, with 50% of Gag

released approximately 3 hours after the pulse (Figure 3A, lane 3; Figure 3B). TEM microscopy of these co-transfected cells revealed capsids with WT morphology (Supplementary Figure S2C)

In order to confirm that co-assembly of Gag-GFP and untagged Gag was occurring in co-transfected cells, two different experiments were performed. In the first cells were either singly transfected with pSARM-GagGFP-M100A, or co-transfected with this vector and WT pSARM-X , which expresses a functional viral protease. A Western blot analysis, using a mouse anti-GFP antibody, of virions pelleted through a 25% sucrose cushion showed that, in contrast to the 110 kD Gag-GFP released from singly transfected cells, the Gag-GFP in virions from co-transfected cells was efficiently cleaved to the expected p4-GFP (Supplementary Figure S4, pSARM-GagGFP + WT).

In the second approach, supernatants from cells transfected with pSARM-GagGFP-M100A or co-transfected with pSARM-D26N, and radiolabeled with ^{35}S methionine, were analyzed on discontinuous sucrose gradients. As can be observed in Supplementary Figure S5, Pr78 and Gag-GFP from co-transfected cells were observed primarily in fractions 4 and 5 (density 1.12 g/mL and 1.17 g/mL). Similar results were obtained for virus released from cells singly transfected by pSARM-D26N (Pr78) and pSARM-X (p27 and gp70). In contrast, virions released from pSARM-GagGFP-M100A transfected cells exhibited a more heterogeneous density and were observed in fractions 3-6 (density 1.08 g/mL – 1.20 g/mL).

Because of these results, further experiments with the pSARM-Gag-GFP-M100A vector included co-transfection with WT pSARM-X at a ratio of 4:1 (WT: GagGFP), or transfection into CMMT cells, a rhesus macaque mammary tumor fibroblast cell line that constitutively expresses WT M-PMV.

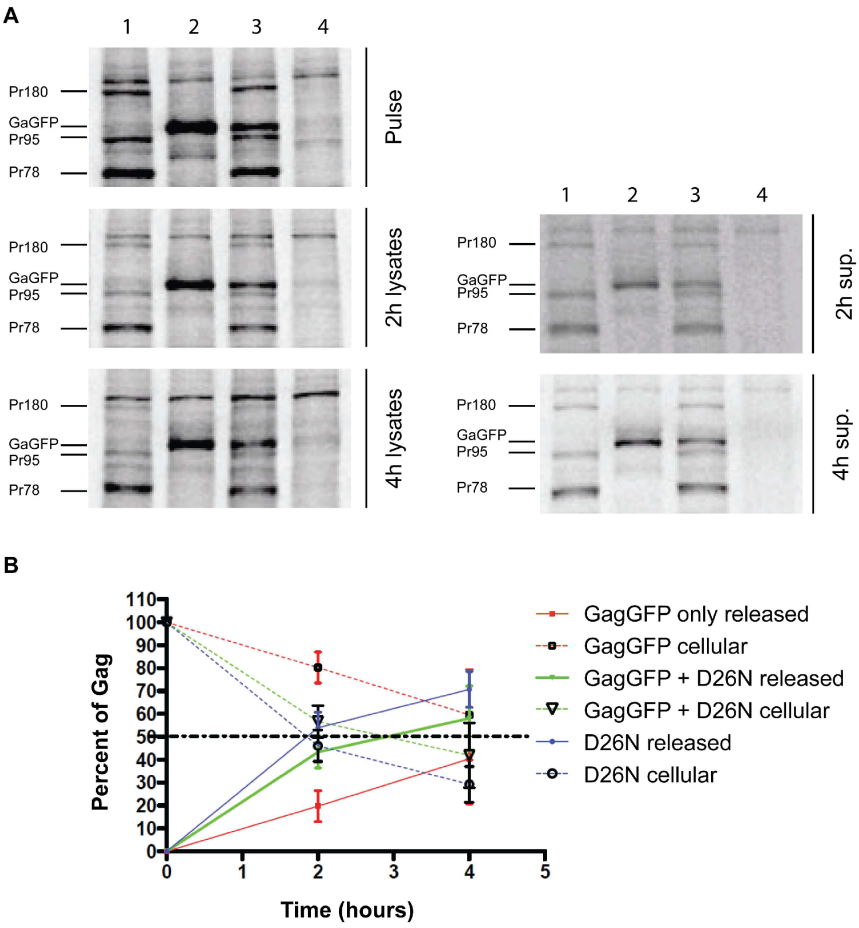

Figure 3 Analysis of release kinetics of the GagGFP fusion protein.
(A) 293T cells (untransfected, Lane 4) were transfected with pSARM-D26N (Lane 1), pSARM-GagGFP-M100A (Lane 2) and co-transfected (Lane 3) with pSARM-D26N and pSARM-GagGFP-M100A at a 4:1 ratio. Viral proteins were metabolically labeled with ^{35}S methionine and then immunoprecipitated with rabbit anti-$p27^{CA}$ antibody from lysates of pulse-labeled cells (pulse), pulse-labeled and 2h and 4h chased cells (2h lysates and 4h lysates) and from the culture media collected after 2h or 4h chase respectively (2h and 4h sup.). Positions of the viral precursor proteins Pr180 (Gag-Pro-Pol), Pr95 (Gag-Pro) and Pr78 (Gag) and product of pSARM-GagGFP-M100A are shown. (B) The percentage of cell associated viral protein was measured by calculating the ratio of protein from the lysates versus the total protein (lysates and sup.). Conversely, the percentage of released viral protein was measured by calculating the ratio of protein from the supernatants versus the total protein. For D26N, the total amount of cell-associated and released Gag is calculated by adding the amounts of each of the precursors (Pr180, Pr95, and Pr78). For GG and GG co-transfections, the amount of Gag cellular and released Gag corresponds to the amount of Gag-GFP.

M-PMV GagGFP subcellular localization is similar to untagged M-PMV provirus.

To verify that the GFP fusion was not affecting cellular localization of Gag, COS-1 cells were transfected with untagged forms of wild type provirus or previously described M-PMV Gag mutants (R55W, R22A, K16A/K20A) and following fixation were stained with a rabbit anti-Gag antibody. The staining pattern was compared to COS-1 cells co-transfected with pSARM-GagGFP-M100A or the same vector into which the R55W, R22A, or K16A/K20A mutations were introduced, along with the respective pSARM provirus at a 1:4 ratio.
The COS-1 cells producing untagged forms of Gag were fixed 24 h after transfection and immunostained; the cells producing GFP fused forms of Gag were fixed 24h after transfection.

Previous work with immunostained wild-type Gag reported a dispersed distribution of Gag in the cytoplasm, with a higher concentration of signal in pericentriolar region, which is the site of particle assembly and Env recruitment [2,10,19]. Similar subcellular localization was observed here in COS-1 cells expressing both untagged (Figure 4A, WT untagged) and WT GagGFP (Figure 4A, WT GFP-tagged). However, the WT GagGFP displayed a somewhat denser staining pattern, likely owing to enhanced protein production resulting from the codon optimization of gag.

Stansell *et al.* showed that a double mutation in the matrix domain, K16A/K20A results accumulation of capsids on and efficient budding into intracellular vesicles, with a concomitant 50 to 70% reduction in the efficiency of viral particle

release [5]. In both the native and GFP-tagged systems, this mutation resulted in fewer discrete fluorescent capsids in the cytoplasm and the presence of large brightly fluorescent bodies, consistent with the previously described phenotype of budding into intracellular vesicles (Figure 4A, K16A/K20A Untagged and GFP-tagged). Co-staining with the red membrane dye, DiI, supports the conclusion of budding into vesicles (data not shown).

The R55W mutation within the matrix domain of M-PMV Gag, is known to significantly reduce intracellular assembly and redirect it to the plasma membrane of the cell [3]. In the immunostained cells, the dispersed intracytoplasmic staining of capsids was drastically reduced and was replaced by an intense fluorescent signal along the plasma membrane (Figure 4A, R55W Untagged). A similar, but more intense staining pattern was observed in the Gag-GFP expressing cells (Figure 4A, R55W, GFP-tagged).

Stansell *et al* also showed that an R22A mutation in the matrix protein of Gag results in a complete block to virus particle release from infected cells [5]. The particle release defect of the GFP-tagged and untagged form of R22A Gag was verified in a pulse-chase experiment. The cells were pulsed for 30min with ^{35}S-methionine and then chased for 4h. M-PMV proteins were immunoprecipitated, using a goat anti-MPMV antibody, then analyzed on an SDS-PAGE gel, from both the pulse (Figure 4B, Pulse gels) and pulse-chase cell lysates (Figure 4B, 4h lysates), as well as from the cell culture medium of the 4h chased cells (Figure 4B, 4h sup). Control wells were transfected with WT-D26N (Figure 4B, lane 2),

pSARM-GagGFP-M100A (Figure 4B, lane 3), and pSARM-X (Figure 4B, lane 4), and detectable amounts of Pr78, Gag-GFP, and p27 respectively were observed in the 4h supernatants. In contrast, while pSARM-R22A (Figure 4B, lane 5) and pSARM-GagGFP-M100A-R22A (Figure 4B, lane 6) transfected cells exhibited similar precursor protein patterns in the pulse and pulse-chase cell lysates to their WT counterparts, no released proteins (p27 or Gag-GFP) were detectable in the 4h-supernantants.

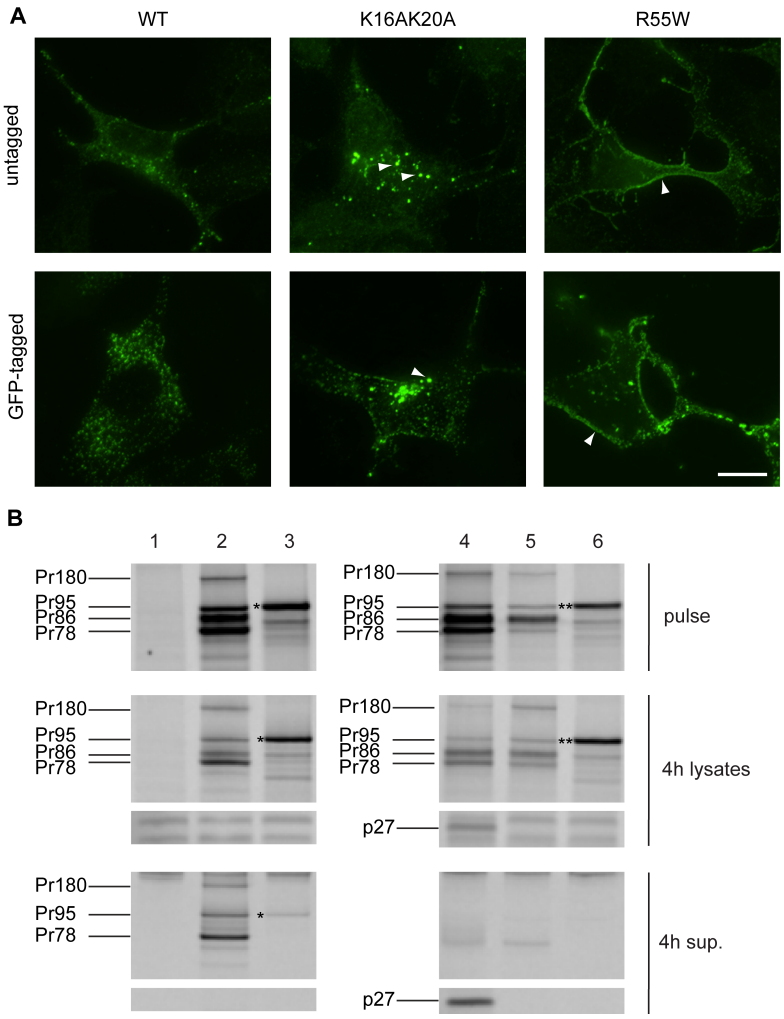

Figure 4 Comparison of untagged and GFP-tagged M-PMV Gag wild-type and mutants in COS-1 cells.

(A) COS-1 cells were cotransfected at the ratio of 4:1 with pSARM-WT and pSARM-GagGFP-M100A, pSARM-R55W and pSARM-GagGFP-M100A-R55W, or pSARM-K16A/K20A and pSARM-GagGFP-M100A-K16A/K20A (**tagged**) or transfected with the untagged pSARM-WT, pSARM-R55W or pSARM-K16A/K20A mutants (**untagged**). Cells were fixed 24 h post-transfection with cold methanol:acetone (1:1). Cells transfected with untagged provirus were stained by primary rabbit antibody against M-PMV p27 and secondary FITC-conjugated anti-rabbit antibody. Localization of K16A/K20A mutant into intracellular vesicles and localization of R55W on plasma membrane is shown. Scale bar, 20 μm. (B) COS-1 cells (untransfected, Lane 1) were transfected with pSARM-D26N (Lane 2), pSARM-GagGFP-M100A (Lane 3), pSARM-X (Lane 4), pSARM-R22A (Lane 5) and pSARM-GagGFP-M100A-R22A (Lane 6). Viral proteins were metabolically labeled with [^{35}S] and then immunoprecipitated with goat anti-MPMV antibody from lysates of pulse-labeled cells (pulse), pulse-labeled and 4h chased cells (4h lysates) and from the culture medium collected after the 4h chase (4h sup.). Positions of the viral precursor proteins Pr180 (Gag-Pro-Pol), Pr95 (Gag-Pro), Pr86 (Envelope) and Pr78 (Gag) are shown. Products of pSARM-GagGFP-M100A (*) and pSARM-GagGFP-M100A-R22A (**) are shown.

Real-time imaging of the Gag-GFP fusion construct shows lateral movement throughout the cell.

M-PMV-expressing CMMT cells were transfected with pSARM-GagGFP-M100A and visualized in real-time with exposures every 5 seconds for 2 minutes. Using the Particle Tracker plugin on the FIJI software package, particles were detected and then automatically tracked [24].Trajectory data showed three different populations of fluorescent particles (Figure 5A, Movie S1, Supplementary Figure S6). Population 1 showed trajectories with restricted movement and little to no displacement from the beginning to the end of the trajectory path (Figure 5B.1). The median displacement for trajectories that are seen in this population is 1.6 pixels, and occurred approximately 15% of the time for trajectories containing at least 10 time points (Supplementary S6A and B). Population 2 showed particles moving in an erratic, Brownian manner, with very little displacement (Figure 5B.2). The trajectories in this population appear larger than those of the first population, although there is very little long-range movement within the trajectory. The median total displacement of particles in this population is significantly higher (6.9 pixels) than in Population 1. Tracks in this population made up approximately 41% of the trajectories that had at least 10 times points (Supplementary Figure S6A and B). Population 3, occurring 44% of the time, displayed long, linear tracks with, in most cases, significant displacement from the beginning of the track to the end (Figure 5B.3). The median displacement in this population was 15.5 pixels (Supplementary Figure S6B). This lateral movement across the cell was bidirectional in nature at times, and the

instantaneous velocities oscillated between periods of complete cessation of movement followed by periods of long-range movement. The median, maximum instantaneous velocity of tracks in Population 3 was approximately 700nm/s (Figure 5C).

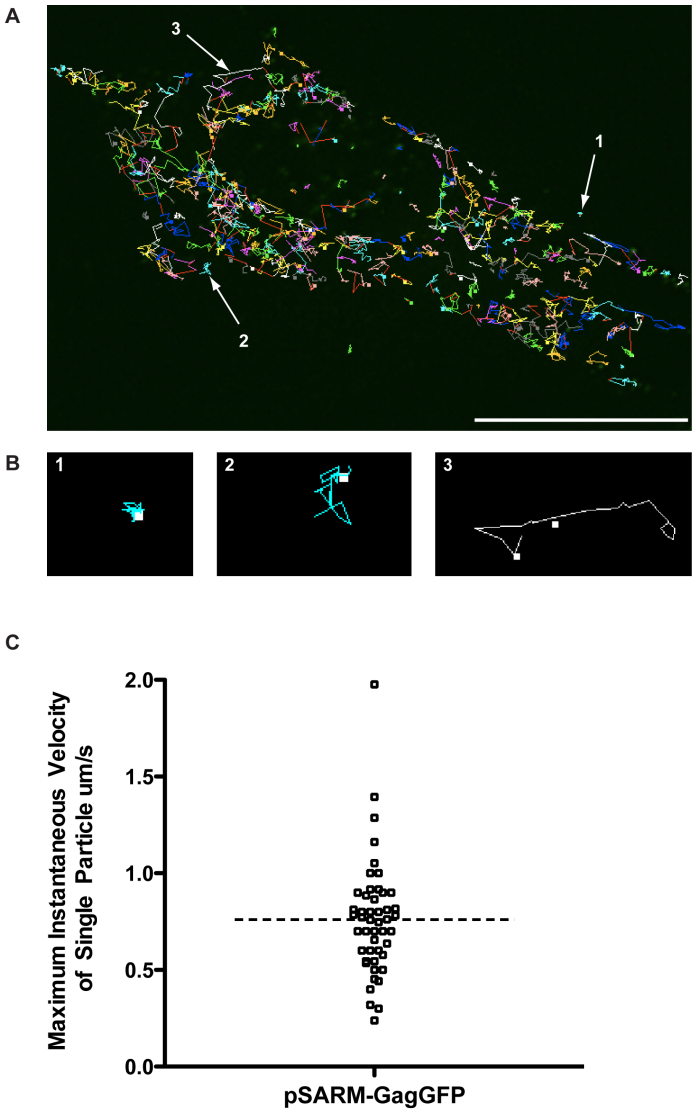

Figure 5 Real-time imaging of GagGFP fusion protein in live cells.
(A) M-PMV expressing CMMT cells were transfected with pSARM-GagGFP-M100A and visualized 24 hours later in real-time every 5 seconds for 2 minutes. Using the Particle Tracker plug-in on FIJI, particles were detected and then tracked. Scale bar = 20 μm. Real time imaging of these frames is shown in movie S1. (B) Trajectory data showed trajectories with restricted movement and little to no displacement from the beginning to the end of the trajectory path (1), trajectories where the particle moved in an erratic, Brownian manner, and displayed very little displacement (2) and long tracks with significant displacement from the beginning of the track to the end (3). (C) To calculate the instantaneous velocity for a trajectory in population 3, the distance traveled between each time point was calculated and divided by the time interval (5s). Maximum instantaneous velocity refers to the maximum instantaneous velocity for an individual trajectory.

Fluorescently-labeled capsids associate and transport along microtubules.

The results from the live cell imaging of capsid transport suggested a possible role for microtubules in their intracellular transport. Specifically, the bidirectional movement and the oscillating velocities of capsid movement have been previously described for endosomal movement as well as viral movement along microtubules [27-30]. To test whether the capsids were associated with and were transported along microtubules, CMMT cells were co-transfected with pSARM-GagGFP-M100A and mCherry-labeled tubulin and then imaged 24 hours post-transfection. Images were captured every second for one minute in one z-stack. Time-lapse data of these cells shows a majority of the capsids are not moving, but nevertheless colocalize with a tubule (Movie S2). When a smaller section of the cell is examined at higher effective magnification, capsids that display rapid, lateral movement with significant displacement appear to traffic along the path of the microtubules (Figure 6). Examples of retrograde and anterograde movement along tubules can be seen, as well as examples of capsid that appear to switch from one tubule to another (data not shown).

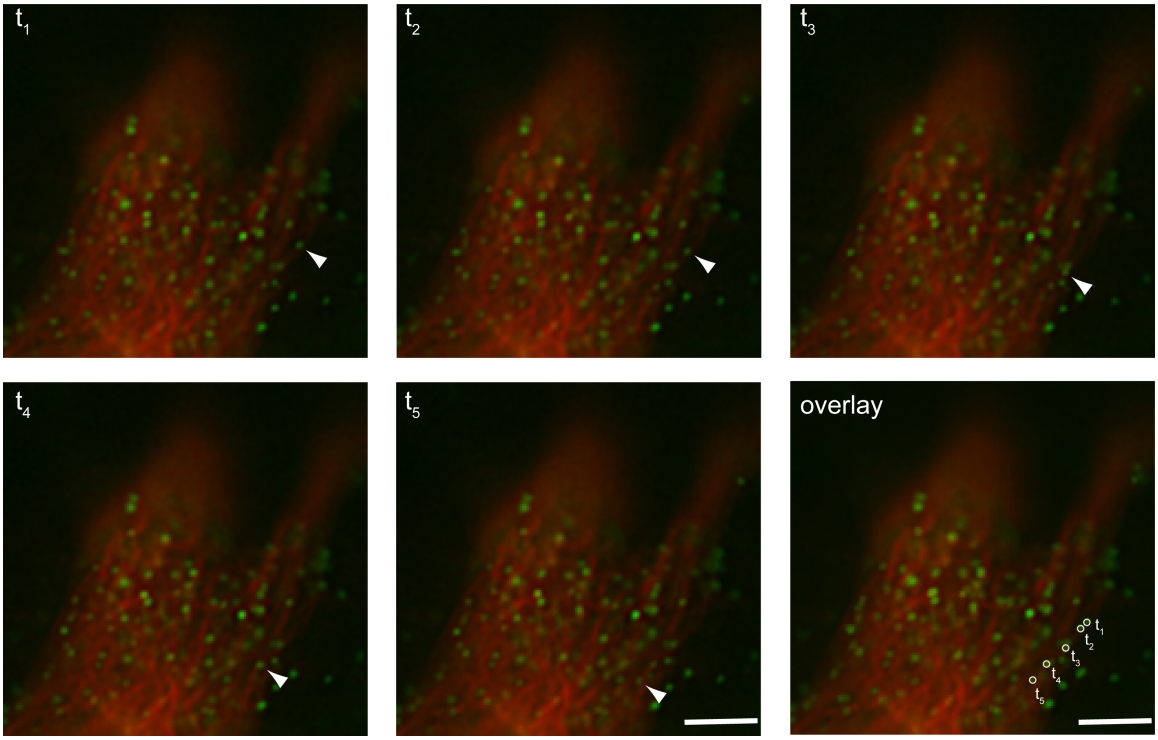

Figure 6 Real-time imaging of GFP labeled virus-like particles along the microtubule.
M-PMV expressing CMMT cells were cotransfected with pSARM-GagGFP-M100A and mCherry-tubulin and imaged 24 hours later in real-time. Images were captured at consecutive intervals of 1 second for one minute in one focal plane. Scale bar= 1 μm. Real time imaging of these frames is shown in movie S2.

Discussion

To date, the host cell factors involved in the assembly and intracellular trafficking of retroviral proteins remain poorly understood. For M-PMV, much work has been done to elucidate the cellular factors involved in assembly of premature capsids in the pericentriolar region of the cell. Factors such as the microtubule organizing center and dynein motors have previously been described to interact with the Gag assembling on polysomes through an interaction with the cytoplasmic targeting and retention signal in the matrix domain of Gag. It has also been shown that the cellular vesicular trafficking system has a role in intracellular capsid transport, since a temperature block of 20°C, which reversibly inhibits vesicle trafficking, causes an accumulation of capsid particles at the pericentriolar site of assembly [2,7,10,12]. In addition, several mutations in the cytoplasmic domain of the Env glycoproteins [2,7,10,12], and others in the Gag polyprotein has suggested that endocytic recycling pathways are critical for Env's involvement in efficient capsid intracellular transport [7,10]. However, most of these studies utilized population-based pulse-chase experiments and fixed cell immunofluorescence. The availability of fluorescently labeled M-PMV proteins that can be visualized in a living cellular system clearly has the potential to provide more insight into the roles of cellular factors in the intracellular transport of M-PMV capsids from their site of assembly to the plasma membrane site of egress.

Constructing and optimizing an M-PMV Gag-GFP fusion.

The goal of this study was to construct an M-PMV Gag-GFP fusion protein that could be visualized in live cells and to use this construct to investigate intracellular trafficking of M-PMV capsids. First, the *gag*-gene of M-PMV was codon optimized to prevent aberrant splicing observed with the native coding region. Despite this, fusion of *gfp* to the 3' end of the codon-optimized *gag* resulted in the production of a truncated GFP-tagged protein, in addition to the full-length product. This shorter product was shown to result from ribosomal initiation from an internal, in-frame methionine 100 amino acids from the primary initiation codon for *gag*. Although this methionine is present in the WT M-PMV *gag*, only background levels of protein are initiated from this methionine. However, previous work had shown that even single nucleotide changes to the second codon of Gag could result in ribosomes skipping the initiating methionine (M1) and initiating translation of a truncated Gag more than 50% of the time [31]. It is therefore probable that initiation from this second methionine in the GFP fusion construct was due to codon optimization, which allowed the ribosome to recognize this second methionine at a higher rate than it would in the non-codon optimized *gag*. Introduction of the M100A mutation, previously shown to have no effect on virus infectivity, and optimization of the Kozak sequence before M1, resulted primarily in full-length translation products.

Another caveat to constructing a Gag-GFP fusion protein that is biologically relevant is the fact that fusion of a 27-kD GFP protein to the carboxyl-terminus of Gag could interfere with capsid morphogenesis. Indeed in a previous study, only

incomplete and aberrant particles were assembled when the frame-shifting signal at the end of *gag* was mutated to generate only Gag-Pro and Gag-Pro-Pol precursors [32]. When 293T cells were transfected with the pSARM-Gag-GFP-M100A construct alone, transmission electron microscopy showed the assembly of larger, non-spherical capsids that had an unusual "beads-on-a-string" external surface. Additionally, when virus was subjected to density centrifiguation through a 20%-50% sucrose gradient, GagGFP-containing virions appear in fractions 3-6, while WT virions and virions from co-transfected cells were primarily present in the 4^{th} and 5^{th} fractions, confirming that virions from cells transfected with pSARM-GagGFP-M100A alone have a more diverse and in some cases lower density than WT virions. Moreover, pulse-chase analyses showed that the kinetics of release for these aberrant capsids was also greatly reduced. In order to assemble a GFP-tagged capsid that is transported with kinetics similar to a WT capsid, co-assembly of Gag and Gag-GFP proteins in ratios resembling Gag and Gag-Pro must occur. Because of this, all experiments involving the Gag-GFP fusion protein were performed in the context of WT virus, either by cotransfection or by transfection of Gag-GFP into the CMMT cell line that constitutively expresses WT M-PMV.

To confirm further that that the Gag-GFP fusion protein behaved similarly to untagged, WT Gag, a comparison was made of the subcellular localization of both WT and several well-characterized Gag mutants. Immunofluorescent staining showed that GFP-tagged Gag localized similarly to the untagged Gag. WT forms of both exhibited a dispersed distribution of fluorescent puncta, with a

concentration in the pericentriolar region. This pattern was dramatically altered in pSARM-GFP-M100 vectors encoding the R55W and K16A/K20A mutants. In the former, Gag staining outlined the periphery of the cells with predominantly diffuse staining in the cytoplasm, consistent with capsid assembly now occurring on the plasma-membrane [3]. And for the latter, brightly staining vesicular structures were observed, consistent with budding into a variety of intracellular vesicles [5]. Along with this visual evidence that the Gag-GFP fusion protein behaves similarly to untagged Gag, a pulse-chase analysis of the tagged and untagged R22A mutant showed that, like the untagged mutant, pSARM-GagGFP-M100A-R22A also failed to be released from cells. This provides compelling evidence that the Gag-GFP fusion protein utilizes virus-cell interactions comparable to the untagged Gag, and can be used for characterizing the nature of M-PMV Gag intracellular transport in dynamic, real time applications.

Evidence for M-PMV capsid use of the cellular cytoskeleton for transport.

Particle tracking of GFP-tagged capsids in transfected CMMT cells and COS-1 cells provided evidence for three types of capsid movement. In the first, the particles exhibited very little lateral movement, consistent with them being anchored to a subcellular structure. In the second, capsid movement was consistent with Brownian movement – presumably representing capsids free in the cytoplasm. Finally, a subset of capsids exhibited long-range oscillatory movement, with kinetics that are consistent with movement on microtubules. Characterization of endosomal intracellular transport, as well as the interaction

of several different viruses with the microtubular network of the cell, shows that microtubular cargo have instantaneous velocities that are oscillatory in nature and movement is bidirectional [27-30,33]. The microtubule motors involved in anterograde transport toward the plasma membrane, kinesins, have been shown to propel cargo as fast as 4 □m/s, as well as to stall cargo during "pauses" [27-29,33,34]. Microtubule-dependent transport of viruses has been extensively studied in Vaccinia virus [30,35]. In these studies, intracellular enveloped viruses (IEV) have been shown to require the use of microtubule motor, kinesin-1, for saltatory transport from their intracellular site of replication and assembly to the cortical actin layer. These studies have shown a wide range of instantaneous velocities, with an average of approximately 8 μm/s. Live cell imaging analysis from these studies also describe bidirectional movement of IEVs and movement consistent with switching of IEVs from one microtubule to another.

In this current study, a subset of capsids was observed to be associated with microtubules, but not moving. Since these kinetic studies capture only a very small fraction of time (1-2 minutes), it is possible that the microtubule-associated capsids are stalled along the microtubule at this time. The capsids that appear to be transporting along the microtubules have instantaneous maximum velocities up to 2 μm/s with a median of 700 nm/s, when images were captured every 5 seconds. The capsid movement observed in our system also displays bidirectional transport, and evidence of jumping from one microtubule to another microtubule can also be seen. These observations provide strong support for the hypothesis that the capsids are utilizing microtubules for intracellular transport.

A major caveat to this study is that the real-time imaging only captures approximately 4% of the time necessary for 50% of capsids to be released from the cell. This means the imaging is limited to characterizing localized movement of individual capsids in a small window of time. Further experimentation must be performed to characterize the collective nature of capsid movement over longer periods of time.

Conclusion

The current study shows that employing the use a fluorescently-tagged M-PMV Gag protein can be useful in characterizing the nature of M-PMV Gag assembly and transport in a real-time imaging system. In order to utilize this system, however, it is necessary to use a codon-optimized Gag with an M100A mutation in the MA protein to prevent internal initiation. Codon-optimization results in a dysfunction in splicing necessary for Env expression, and Env expression has been shown to be critical in efficient capsid release kinetics. TEM results also show that transfection of 293T cells with the Gag-GFP fusion protein results in aberrantly shaped capsids. Both of these phenotypes amplify the importance of co-expression of the Gag-GFP fusion protein with the WT or D26N Gag from a proviral vector, which both express Env at WT levels and allows for co-assembly for tag and untagged Gag proteins. Following optimization of these conditions, Gag-GFP expressing cells display intracellular movement of assembled capsids that is consistent with transport along microtubules.

Tables and Supporting Information

Table 1. List of primers

Plasmid	Primer Name	Primer Sequence
pSARM-GagGFP	GagGFP F-EagI	5'-TGCGTCTCAACCTCGGCCG
	GagGFP R-AgeI	5'-CGACCGGTCCCGCACCTTCATACTGTGTTGGAGG
	GFP F-AgeI	5'-TGCCTCCTCCAACACAGTATTGAGTGCGGGACCGGT
	GFP R-PspXI + SA	5'-ACTCTCCTCGAGGAGAGAATCACTTGTACAGCTCGTCCATGCCGA
PSARM-GagGFP-M100A	Kozak F-EagI ultramer	5'-CAACCTCGGCCGGCGATTAAAAGTGAAAGTAAACTCTCTTGGCCGCCGCGGGAACCTGCCGCGTTGGACCTGAAAGTAAGTGTTGGCCGCCACCATGGGACAGGAGCTGTCACAGCATGAGAGGTATGTGGAGCAGCTGAAGCAG
	Kozak R ultramer	5'-GAAAGCAATCTCCCACTCTTCTCCAGCGCTTAATGTCGATGGTTCCCTCTTGGGGAAACCAAGGACAGGTGTCTTTTACGAAATCAAAAAATTTCAGAAGGTCGGCGTATTTGACCTTCACTCCCCTGGTTTTAAGGGCCTGCTTCAGCTGCTCCACATA
	M100A F ultramer	5'-GCTGGAGAAGAGTGGGAGATTGCTTTCAGGACTACTATAACACATTTGGCCCCGAAAAAGTTCCCGTTACTGCATTTAGCTACTGGAATCTCATTAAAGAGCTGATTGATAAAAAGGAAGTGAACCCACAGGTCGCTGCCGCAGTCGCGCAGACTGAG
	M100A R-SbfI ultramer	5'-CTTTGTCCTGCAGGGAAGAAGACTTGGCTCCTTCGTCGTCACTATCCAGAGAAATAAGGTCCAAGTCGGGATTCTGTGATGTCTTCGTCAGGTCCGTCTGACTATTGCTTTTAAGAATTTCCTCAGTCTGCGCGACTGCGG
pSARM-GagGFP-R55W	R55W F	5'-GGAACCATCGACATTAAGTGGTGGAGAAGAGTGGGAGA
	R55W R	5'-TCTCCCACTCTTCTCCACCACTTAATGTCGATGGTTCC
pSARM-GagGFP-K16A/K20A	K16A/K20A F	5'-CATGAGAGGTATGTGGAGCAGCTGGCGCAGGCCCTTGCGACCAGGGGAGTGAAGGTCAAATAC
	K16A/K20A R	5'-GTATTTGACCTTCACTCCCCTGGTCGCAAGGGCCTGCGCCAGCTGCTCCACATACCTCTCATG
pSARM-GagGFP-R22A	R22A F	5'-GCCCTTAAAACCGCGGGAGTGAAGGTC
	R22A R	5'-GACCTTCACTCCCGCGGTTTTAAGGGC

Available in electronic version of this dissertation

Movie 1 (Movie S1) Real-time imaging of GagGFP fusion in CMMT cells.
M-PMV expressing CMMT cells were transfected with pSARM-GagGFP-M100A and visualized on the Deltavision Core Imaging System 24 hours later. 3D images (with 10 z-sections spaced 200 nm apart) were in captured every 5 seconds for a total of 2 minutes. The video is a projection of all z-sections in one plane.

Available in electronic version of this dissertation.

Movie 2 (Movie S2) Real-time imaging of GFP labeled virus-like particles along the microtubule.
M-PMV expressing CMMT cells were cotransfected with pSARM-GagGFP-M100A and mCherry-tubulin and imaged 24 hours later in real-time. Images were captured at consecutive intervals of 1s for one minute in one focal plane.

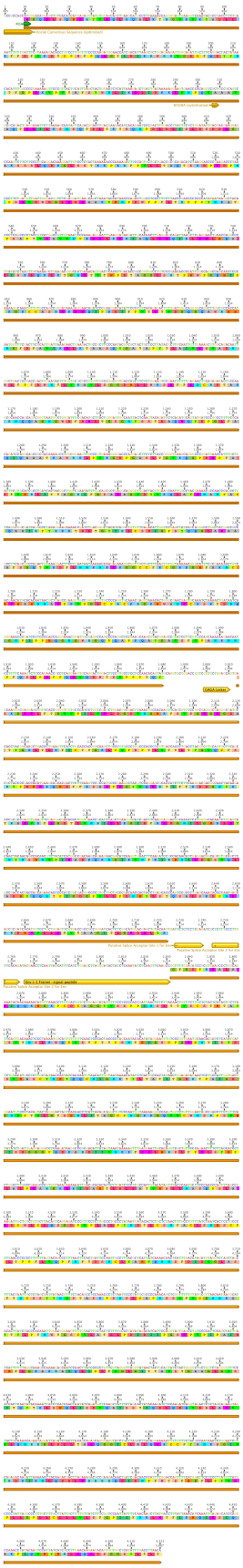

Supplemental Figure 1 (Figure S1) Annotated nucleotide and amino acid sequence of pSARM-GagGFP-M100A.
The nucleotide sequence for pSARM-GagGFP-M100A was imported into the bioinformatics software Geneious™ version 5.5.5 (Biomatters, www.geneious.com). With this software, the nucleotide sequence was translated in the correct frame. The position of the optimized Kozak consensus sequence, the initiating methionine (M1), the methionine to alanine substitution (M100A), GA-linker used to separate Gag and eGFP, and two putative splice acceptor sites for Env were annotated.

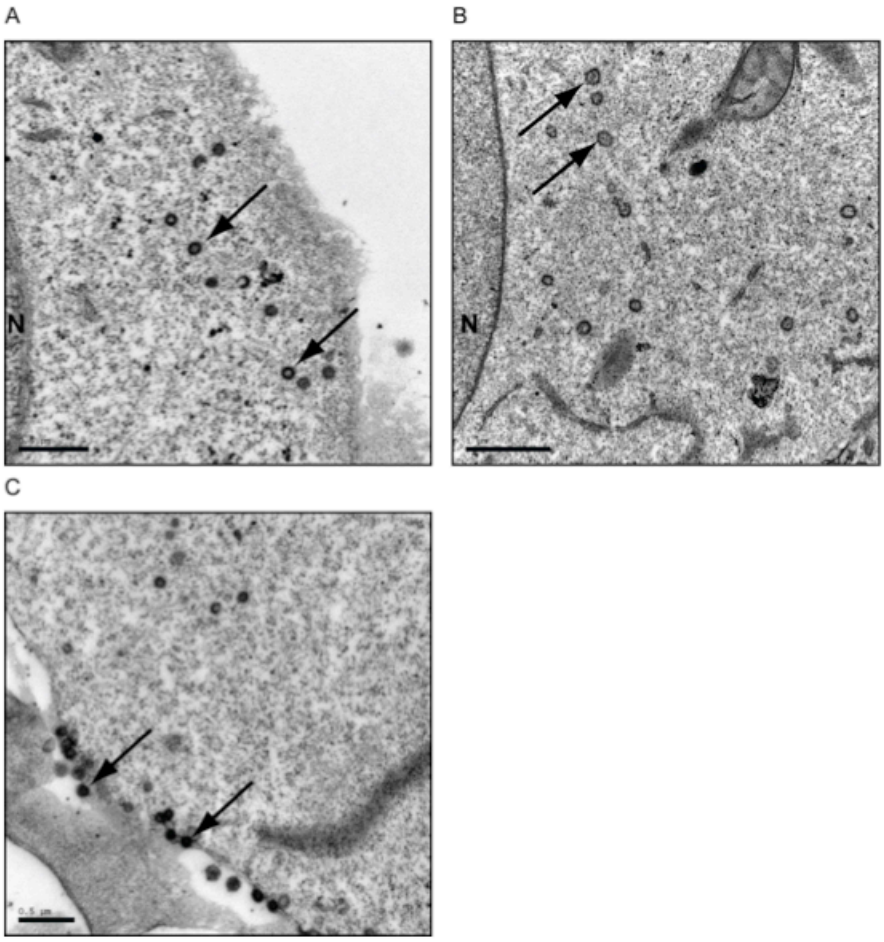

Supplementary Figure 2 (Figure S2) Transmission electron microscopic imaging of the intracellular localization of immature capsids

Transmission electron microscopy (TEM) images of COS cells transfected with pSARM-X (A), pSARM-GagGFP-M100A (B), and cotransfected with pSARM-X and pSARM-GagGFP (C). Arrowheads point to representative immature M-PMV capsids.

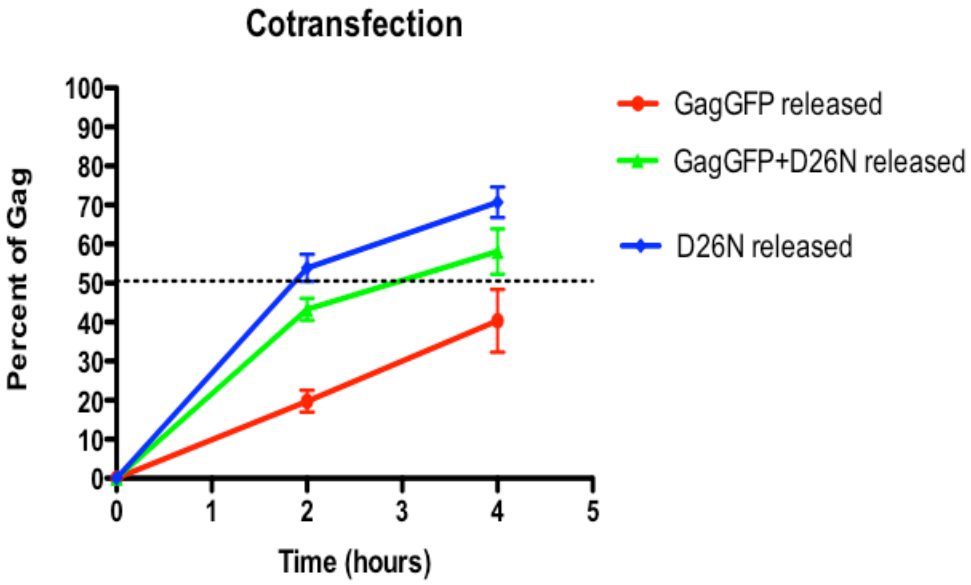

Supplementary Figure 3 (Figure S3) Percent GagGFP released from cells

Quantitation of the % GagGFP released from the cell at each time point from pulse-chase analysis of 293T cells transfected with pSARM-GagGFP-M100A only (red), a 4:1 ratio of pSARM-D26N and pSARM-GagGFP-M100A as compared to the total amount of Gag released from cells transfected with pSARM-D26N (blue).

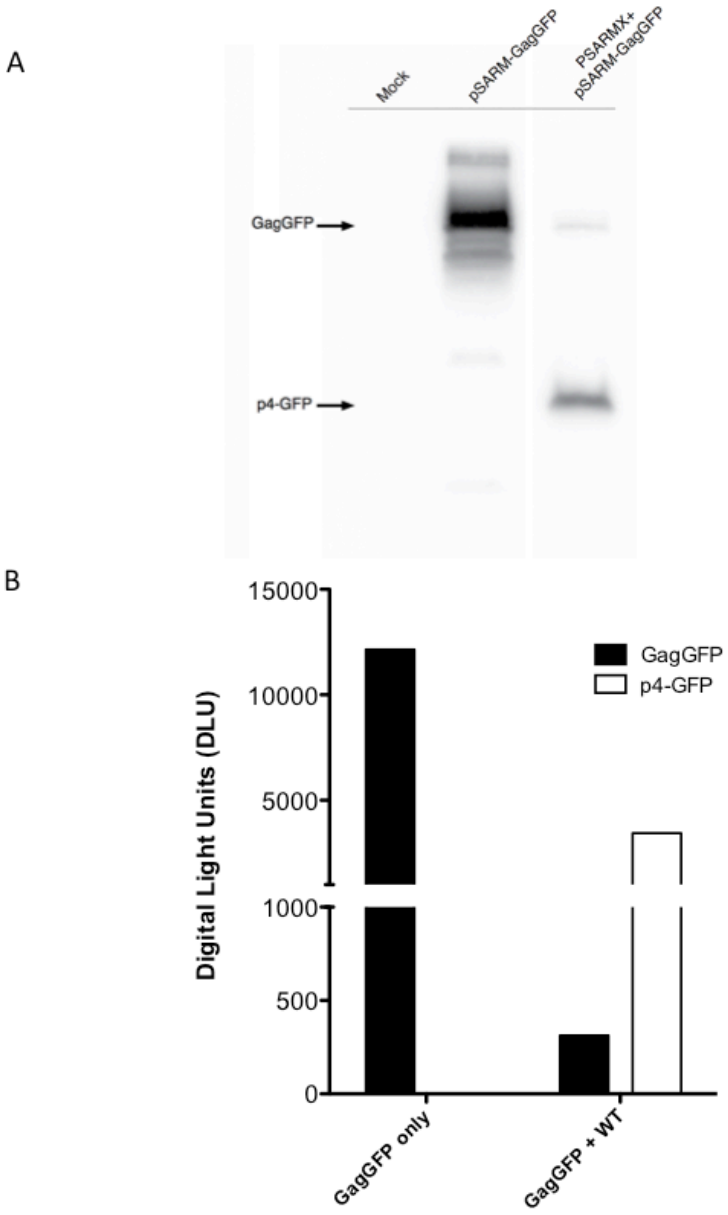

Supplemental Figure 4 (Figure S4) Western blot analysis of virus released from cotransfected cells

(A) Western blot of supernatants from 293T cells, untransfected (lane 1), or transfected with pSARM-GagGFP-M100A only (lane 2) or a 4:1 ratio of pSARM-X and pSARM-GagGFP-M100A (lane 3). Supernatants were resolved on 12% SDS-PAGE, and blotted with antibody against GFP. (B) Quantitation of band intensity of western blot. Black bars represent the band corresponding to the uncleaved Gag-GFP fusion and white bars represent the cleaved p4-GFP found in 293T cells transfected with pSARM-GagGFP-M100A, or cotransfected with pSARM-GagGFP-M100A and pSARM-X.

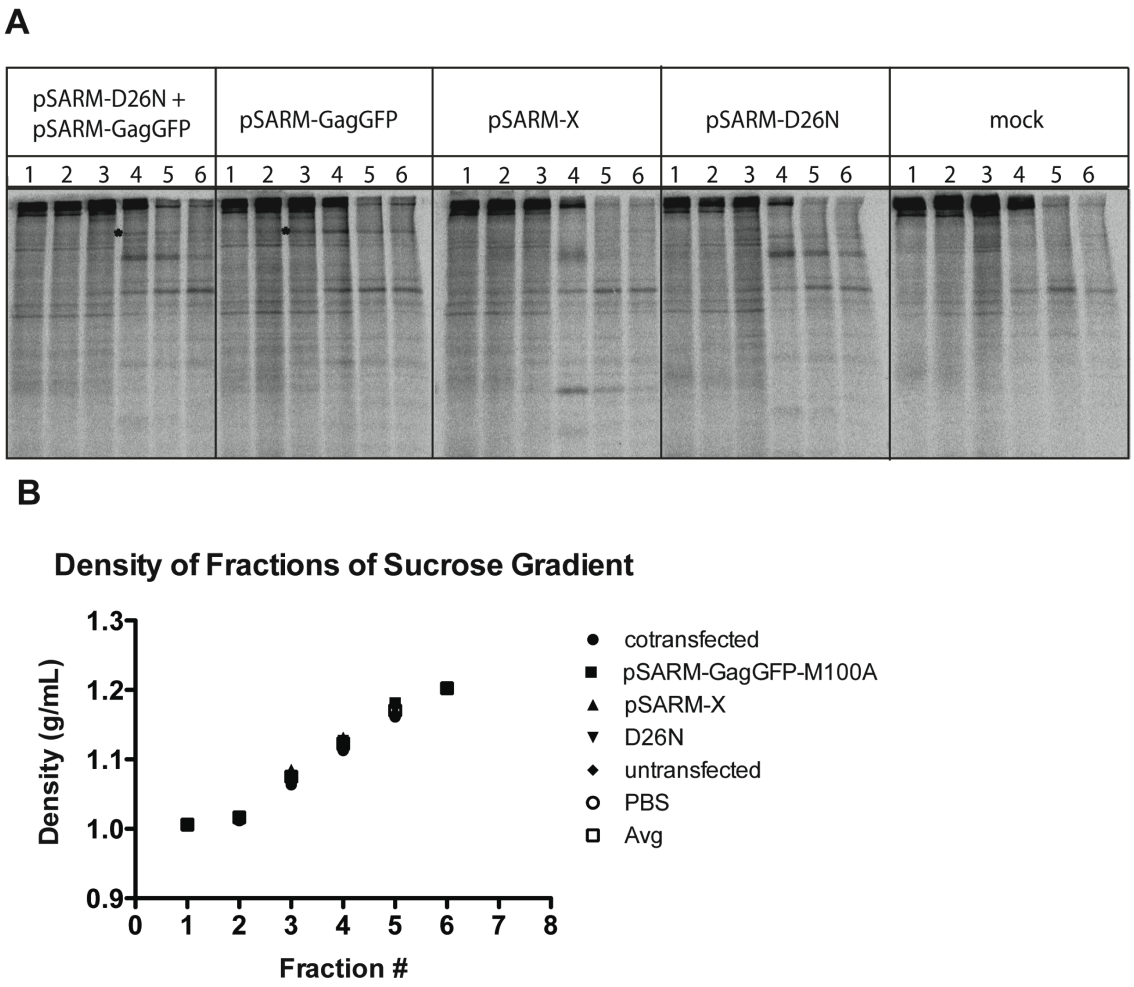

Supplemental Figure 5 (Figure S5) Density fractionation of virions released into the cell supernatant

(A) Sucrose gradient density fractionation of supernatants from 293T cells cotransfected with pSARM-D26N and pSARM-GagGFP, pSARM-GagGFP alone, pSARM-X, pSARM-D26N, or untransfected (mock). Culture supernatants were collected 48 hours after transfection and overlayed on a 20%-50% (w/w) sucrose gradient, followed by ultra-centrifugation in at 35,000 rpm for 3 hours in a SWTi-41 rotor. Fractions were collected by upward displacement and immunoprecipitated with an antibody against whole M-PMV. Samples were resolved on 12% SDS-PAGE gel. (*) represents the band corresponding to Gag-GFP fusion protein. (B) The refractive index of each fraction was measured using a refractometer. The density was determined by comparing the refractive indices to a standard conversion table for the density and refractive index in sucrose.

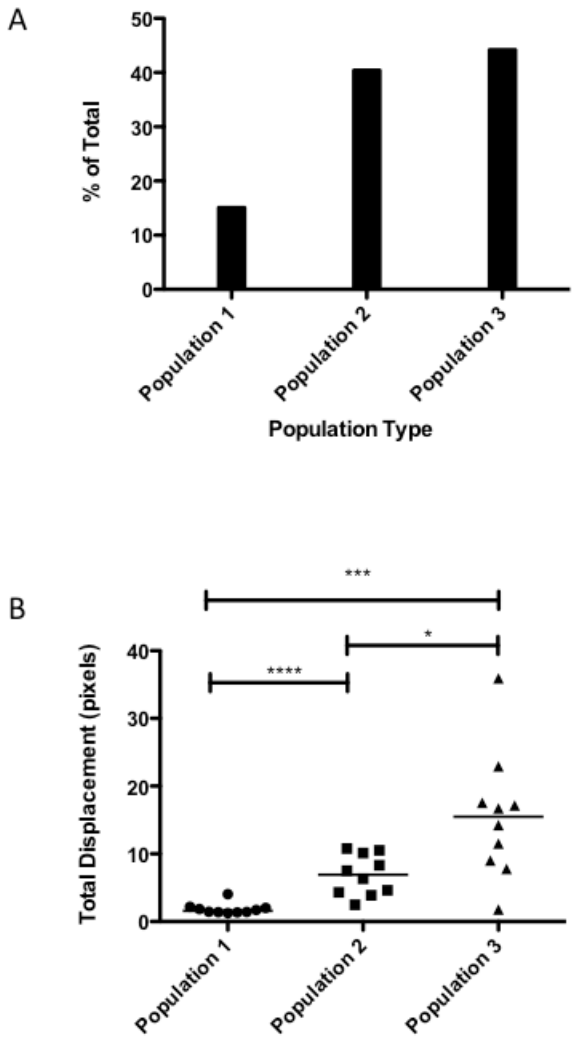

Supplementary Figure 6 (Figure S6)
(A) Percentage of each type of trajectory found in Figure 5A. Analysis is based on categorizing 20 different trajectories from 4 subsections of the cell (left of nucleus, above nucleus, below nucleus, and right of nucleus). (B) The total displacement of 10 separate trajectories from each population type was calculated. The line represents the median for each population. Statistical analysis was based on the non-parametric Mann-Whitney t-test.

Acknowledgements

We acknowledge and thank the James B. Pendleton Charitable Trust for the contribution of advanced imaging equipment utilized in the experiments in this manuscript. We also thank the Robert P. Apkarian Integrated Electron Microscopy Core of Emory University for transmission electron microscopy sample preparation. As well, we thank Dr. Konrad Bradley, Dr. Lisa McLay, Dr. Aaron Reeve, Dr. Pablo Pendaloza of Emory University, as well as Dr. Sarka Haubova and Dr. Marcela Wildova of The Institute of Chemical Technology in Prague, Czech Republic for their exploratory and preliminary work on this project.

Literature Cited

1. Choi G, Park S, Choi B, Hong S, Lee J, et al. (1999) Identification of a cytoplasmic targeting/retention signal in a retroviral Gag polyprotein. J Virol 73: 5431-5437.

2. Sfakianos JN, LaCasse RA, Hunter E (2003) The M-PMV cytoplasmic targeting-retention signal directs nascent Gag polypeptides to a pericentriolar region of the cell. Traffic 4: 660-670.

3. Rhee SS, Hunter E (1990) A single amino acid substitution within the matrix protein of a type D retrovirus converts its morphogenesis to that of a type C retrovirus. Cell 63: 77-86.

4. Prchal J, Junkova P, Strmiskova M, Lipov J, Hynek R, et al. (2011) Expression and purification of myristoylated matrix protein of Mason-Pfizer monkey virus for NMR and MS measurements. Protein Expr Purif 79: 122-127.

5. Stansell E, Apkarian R, Haubova S, Diehl WE, Tytler EM, et al. (2007) Basic residues in the Mason-Pfizer monkey virus gag matrix domain regulate intracellular trafficking and capsid-membrane interactions. J Virol 81: 8977-8988.

6. Stansell E, Tytler E, Walter MR, Hunter E (2004) An early stage of Mason-Pfizer monkey virus budding is regulated by the hydrophobicity of the Gag matrix domain core. J Virol 78: 5023-5031.

7. Song C, Dubay SR, Hunter E (2003) A tyrosine motif in the cytoplasmic domain of mason-pfizer monkey virus is essential for the incorporation of glycoprotein into virions. J Virol 77: 5192-5200.

8. Chung HY, Morita E, von Schwedler U, Muller B, Krausslich HG, et al. (2008) NEDD4L overexpression rescues the release and infectivity of human immunodeficiency virus type 1 constructs lacking PTAP and YPXL late domains. J Virol 82: 4884-4897.

9. Sakalian M, Hunter E (1999) Separate assembly and transport domains within the Gag precursor of Mason-Pfizer monkey virus. J Virol 73: 8073-8082.

10. Sfakianos JN, Hunter E (2003) M-PMV capsid transport is mediated by Env/Gag interactions at the pericentriolar recycling endosome. Traffic 4: 671-680.

11. Punnonen EL, Ryhanen K, Marjomaki VS (1998) At reduced temperature, endocytic membrane traffic is blocked in multivesicular carrier endosomes in rat cardiac myocytes. Eur J Cell Biol 75: 344-352.

12. Song C, Micoli K, Bauerova H, Pichova I, Hunter E (2005) Amino acid residues in the cytoplasmic domain of the Mason-Pfizer monkey virus glycoprotein critical for its incorporation into virions. J Virol 79: 11559-11568.

13. Muller B, Daecke J, Fackler OT, Dittmar MT, Zentgraf H, et al. (2004) Construction and characterization of a fluorescently labeled infectious human immunodeficiency virus type 1 derivative. J Virol 78: 10803-10813.

14. Lux K, Goerlitz N, Schlemminger S, Perabo L, Goldnau D, et al. (2005) Green fluorescent protein-tagged adeno-associated virus particles allow the study of cytosolic and nuclear trafficking. J Virol 79: 11776-11787.

15. Desai P, Person S (1998) Incorporation of the green fluorescent protein into the herpes simplex virus type 1 capsid. J Virol 72: 7563-7568.

16. Chopra HC, Mason MM (1970) A new virus in a spontaneous mammary tumor of a rhesus monkey. Cancer Res 30: 2081-2086.

17. Jensen EM, Zelljadt I, Chopra HC, Mason MM (1970) Isolation and propagation of a virus from a spontaneous mammary carcinoma of a rhesus monkey. Cancer Res 30: 2388-2393.

18. Mason MM, Bogden AE, Ilievski V, Esber HJ, Baker JR, et al. (1972) History of a rhesus monkey adenocarcinoma containing virus particles resembling oncogenic RNA viruses. J Natl Cancer Inst 48: 1323-1331.

19. Gluzman Y (1981) SV40-transformed simian cells support the replication of early SV40 mutants. Cell 23: 175-182.

20. Graham FL, Smiley J, Russell WC, Nairn R (1977) Characteristics of a human cell line transformed by DNA from human adenovirus type 5. J Gen Virol 36: 59-74.

21. Kessler SW (1975) Rapid isolation of antigens from cells with a staphylococcal protein A-antibody adsorbent: parameters of the interaction of antibody-antigen complexes with protein A. J Immunol 115: 1617-1624.

22. Linkert M, Rueden CT, Allan C, Burel JM, Moore W, et al. (2010) Metadata matters: access to image data in the real world. J Cell Biol 189: 777-782.

23. Schindelin J, Arganda-Carreras I, Frise E, Kaynig V, Longair M, et al. (2012) Fiji: an open-source platform for biological-image analysis. Nat Methods 9: 676-682.

24. Sbalzarini IF, Koumoutsakos P (2005) Feature point tracking and trajectory analysis for video imaging in cell biology. J Struct Biol 151: 182-195.

25. Bradac J, Hunter E (1984) Polypeptides of Mason-Pfizer monkey virus. I. Synthesis and processing of the gag-gene products. Virology 138: 260-275.

26. Chatterjee S, Bradac J, Hunter E (1985) A rapid screening procedure for the isolation of nonconditional replication mutants of Mason-Pfizer monkey virus: identification of a mutant defective in pol. Virology 141: 65-76.

27. Amorim MJ, Bruce EA, Read EK, Foeglein A, Mahen R, et al. (2011) A Rab11- and microtubule-dependent mechanism for cytoplasmic transport of influenza A virus viral RNA. J Virol 85: 4143-4156.

28. Chambers R, Takimoto T (2010) Trafficking of Sendai virus nucleocapsids is mediated by intracellular vesicles. PLoS ONE 5: e10994.

29. Dohner K, Nagel CH, Sodeik B (2005) Viral stop-and-go along microtubules: taking a ride with dynein and kinesins. Trends Microbiol 13: 320-327.

30. Hollinshead M, Rodger G, Van Eijl H, Law M, Hollinshead R, et al. (2001) Vaccinia virus utilizes microtubules for movement to the cell surface. J Cell Biol 154: 389-402.

31. Rhee SS, Hunter E (1987) Myristylation is required for intracellular transport but not for assembly of D-type retrovirus capsids. J Virol 61: 1045-1053.

32. Kohoutova Z, Rumlova M, Andreansky M, Sakalian M, Hunter E, et al. (2009) The impact of altered polyprotein ratios on the assembly and infectivity of Mason-Pfizer monkey virus. Virology 384: 59-68.

33. Murray JW, Bananis E, Wolkoff AW (2000) Reconstitution of ATP-dependent movement of endocytic vesicles along microtubules in vitro: an oscillatory bidirectional process. Mol Biol Cell 11: 419-433.

34. Penfold ME, Armati P, Cunningham AL (1994) Axonal transport of herpes simplex virions to epidermal cells: evidence for a specialized mode of virus transport and assembly. Proc Natl Acad Sci U S A 91: 6529-6533.

35. Rietdorf J, Ploubidou A, Reckmann I, Holmstrom A, Frischknecht F, et al. (2001) Kinesin-dependent movement on microtubules precedes actin-based motility of vaccinia virus. Nat Cell Biol 3: 992-1000.

Direct evidence for intracellular anterograde co-transport of M-PMV Gag and Env on microtubules.

Lara E. Pereira[1*], Jasmine Clark[1*], Petra Grznarova[2], Xiaoyun Wen[3], Rachel LaCasse[4] Tomas Ruml[2], Paul Spearman[3], and Eric Hunter[1**].

*Authors contributed equally to this work

Accepted: *Virology,* November 2013

Rachel LaCasse did the preliminary work for this project. Lara Pereira tested the effects of the cytoskeletal inhibitors on the different cytoskeletal elements (Figure 1) as well as performed the pulse-chase analysis using the cytoskeletal inhibitors and quantitated the kinetics of release of capsids and the amount of capsid release (Figure 2). Lara Pereira also performed the pulse chase analysis on virions released from the cell in nocodazole versus untreated cells (Figure 3). Jasmine Clark did the live-cell imaging and velocity quantitation of nocodazole-treated cells (Figure 4) and the mean-squared displacement analysis (Figure 5). Petra Grznarova and Xiaoyun Wen created the Env-Cherry construct used in Figure 4. Lara Pereira drew the model for anterograde co-transport of M-PMV Env and Gag in Figure 6.

Abstract

The intracellular transport of Mason-Pfizer monkey virus (M-PMV) assembled capsids from the pericentriolar region to the plasma membrane (PM) requires trafficking of envelope glycoprotein (Env) to the assembly site via the recycling endosome. However, it is unclear if Env-containing vesicles play a direct role in trafficking capsids to the PM. Using live cell microscopy, we demonstrate, for the first time, anterograde co-transport of Gag and Env. Nocodazole disruption of microtubules had differential effects on Gag and Env trafficking, with pulse-chase assays showing a delayed release of Env-deficient virions. Particle tracking demonstrated an initial loss of linear movement of GFP-tagged capsids and mCherry-tagged Env, followed by renewed movement of Gag but not Env at 4h post-treatment. Thus, while delayed capsid trafficking can occur in the absence of microtubules, efficient anterograde transport of capsids appears to be mediated by microtubule-associated Env-containing vesicles. .

Key words: M-PMV, envelope, Gag, anterograde transport, cytoskeleton, live cell-imaging

Introduction

Intracellular targeting and transport of virus structural components is critical to efficient retrovirus replication. In most retroviruses, the nascent Gag polyproteins are transported directly to the plasma membrane where assembly of the capsid shell and membrane extrusion occurs simultaneously. Viruses that undergo this form of type-C morphogenesis include the pathogenic human viruses, human immunodeficiency virus and human T-cell leukemia virus (HIV and HTLV-I, respectively). In contrast to type-C morphogenesis, M-PMV, the prototypic type-D retrovirus, exhibits spatial and temporal separation of capsid assembly, intracellular transport and budding. The Gag polyprotein is first targeted to an intracytoplasmic pericentriolar site where capsid assembly occurs [1-3]. An 18 amino acid sequence in the matrix domain (MA) of Gag polyprotein, termed the cytoplasmic targeting/retention signal (CTRS), is critical for directing intracytoplasmic assembly of the MPMV immature capsids to the pericentriolar region, through its interaction with the dynein light chain Tctex-1 [4]. A single amino acid change of arginine to tryptophan (R55W) within the CTRS results in loss of this interaction and the switch of type-D morphogenesis to type-C morphogenesis [4-7]. Additional mutagenesis studies in this laboratory have also shown that certain single or multiple amino acid changes within MA can abrogate transport from the assembly site, redirect budding to intracellular vesicles, block later stages of transport or prevent capsid interactions with the plasma membrane [7-9].

While functional domains within the Gag polyprotein precursor have been found to play important roles in capsid assembly and intracellular transport, they invariably involve interactions with multiple host cell components. Indeed, the site of M-PMV capsid assembly, the microtubule organizing center (MTOC), anchors a number of cellular components, such as the chaperonin TRiC, that are involved in capsid assembly [10,11]. The MTOC also serves as a focal point of interaction between M-PMV capsids and envelope glycoprotein (Env), which along with components of the pericentriolar recycling endosome, are required for efficient export of preassembled Gag to the plasma membrane [3,12]. In these previous studies, we demonstrated that expression of a provirus lacking the *env* gene resulted in accumulation of Gag in the pericentriolar region and a 7-fold decrease in the kinetics of capsid release when compared to wild-type. Furthermore, temperature block experiments that inhibit vesicular trafficking have suggested that Env-containing vesicles may be required for transport of assembled capsids from the pericentriolar region, and that this is dependent on a functional recycling endosome. Mutations in Rab11 GTPase, an enzyme that regulates recycling trafficking, and the inhibition of membrane tubule formation with the phospholipase A2 enzymes inhibitor ONO-RS-082 both result in decrease in virion release [3,12,13].

Thus, while experimental studies to-date argue that passage of Env through the recycling endosome is critical for efficient M-PMV virion release, details of intracellular capsid transport that occur prior to release remain unclear. Although co-localization between Gag and Env vesicles has been demonstrated in

the pericentriolar cytoplasmic region in fixed cells, questions remain as to whether these interactions are sustained to yield anterograde co-transport of Gag and Env, or if Env facilitates the transfer of pre-assembled capsids to an anterograde trafficking network. Studies involving protein structural analyses, yeast two-hybrid and GST pull-down experiments have demonstrated that M-PMV Gag interacts in a CTRS-dependent manner with cellular Tctex-1 [4], a light chain of the dynein motor complex, suggesting a microtubule-dependent mode of retrograde transport of Gag to the pericentriolar region for capsid assembly. In addition, utilizing a green fluorescent protein (GFP)-tagged Gag construct we have obtained preliminary evidence that microtubules are involved in intracellular transport of assembled capsids. Studies that have explored the function of microtubules and plus-ended motors in anterograde transport of various virus proteins [14-20] have demonstrated an absolute dependence on this cytoskeletal network for virus trafficking. Microtubule-independent transport of viruses has, thus far, been reported primarily for adenovirus proteins, and this movement is mostly directed towards the cell nucleus [21,22]. In the current study, live cell imaging analysis provides, for the first time, direct evidence for intracellular anterograde co-transport of M-PMV Gag and Env. Furthermore, a comprehensive analysis of microtubules, actin and intermediate filaments by live cell microscopy and/or pulse-chase biochemical experiments demonstrate that Gag-Env co-transport and release is essentially microtubule-dependent. However, novel and striking differences in trafficking and release patterns were observed for Gag and Env following microtubule depolymerization, shedding light on the nature of their interactions with host cell trafficking components.

Materials and Methods

Cell lines and reagents. CMMT cells, originally established by co-cultivating rhesus mammary tumor cells with rhesus monkey embryo cells, actively produce infectious M-PMV. COS-1 cells, derived from the African green monkey kidney cell line, CV-1, by transformation with an origin-defective mutant of SV40 [36] were obtained from the American Type Culture Collection. These cells were cultured in Dulbecco's modified Eagle's medium (DMEM) supplemented with 10% fetal bovine serum, 2mM L-glutamine, 100 U penicillin G/ml and 100μg/ml streptomycin sulfate (all from Gibco). The cell line was maintained at 37°C in a 5% CO_2 incubator. Stock solutions of the cytoskeletal disrupting agents (Sigma) were prepared in dimethyl sulfoxide (DMSO) and diluted >1000-fold in culture medium for experiments. Cytochalasin D was used at a final concentration of 2.5 μM to depolymerize actin filaments, and 10 μM of nocodazole and 5 mM ACR was used to disrupt microtubules and intermediate filaments, respectively. For untreated controls, DMSO that was diluted to identical levels was added to cells.

Plasmid constructs. To facilitate live cell imaging studies, plasmid constructs in which M-PMV Gag and Env were fused to GFP and the red fluorescent protein mCherry, respectively, were co-transfected into CMMT cells. Briefly, pSARM-GagGFP-M100A is a proviral construct containing a Kozak-optimized ribosomal start site, an M100A amino acid substitution, and a *gag-egfp* fusion replacing the *pro* and *pol* genes. The plasmid pTML-Env-mCherry is a derivative of the pTMO construct [37], and contains the M-PMV *env* gene under transcriptional control

of the myoproliferative sarcoma virus LTR, with mCherry fused to the cytotail of Env via a 6 amino acid linker. A second Env-mCherry fusion construct, pSARMX-EnvCherry, was generated by PCR cloning of PPQISPP-mcherry-PPSIQPP into the *env* gene of the plasmid pSARMX, just upstream the membrane-spanning domain of Env. This second construct behaves and localizes comparably to the pTML-Env-mCherry plasmid used in this manuscript, and is incorporated into virions, which was confirmed by sucrose density gradient analysis (manuscript in preparation).

Antibodies and staining reagents. In pulse-chase assays, M-PMV Gag was immunoprecipitated with polyclonal rabbit anti-p27CA antibody (1:1000). For detection of Env and Gag, goat anti-M-PMV polyclonal antibody (1:1000) was utilized as previously described [8]. For immunostaining of cytoskeleton networks in fixed CMMT cells, rhodamine phalloidin and anti-alpha tubulin mouse monoclonal antibody (Invitrogen, Carlsbad, CA), were utilized to detect actin filaments and microtubules, respectively. To detect intermediate filaments, cells were immunostained with FITC-conjugated anti-vimentin monoclonal antibody (eBioscience, San Diego, CA).

Immunofluorescence microscopy. CMMT cells expressing M-PMV provirus were grown as monolayers on 22-mm glass coverslips and immunostained 15 hours after seeding. For immunostaining of actin and intermediate filaments, cells were fixed with 4% paraformaldehyde for 20 min, permeabilized using 0.1% Triton X-100 for 10 min and blocked with Dako blocking reagent (Dako,

Carpinteria, CA) for 10 min, all at room temperature. Dyes and/or antibodies specific for these cytoskeletal networks were diluted in Dako antibody diluent and added to cells according to manufacturer's protocols. Immunostaining of microtubules was performed in similar manner, with the exception of CMMT cells being fixed with a mixed solution of 3.75% PFA and 0.25% gluteraldehyde. After washing twice with 1X PBS, coverslips were mounted in ProLong antifade reagent (Invitrogen) containing DAPI for nuclei staining. Cells were visualized using a 60X oil objective on a Deltavision deconvolution fluorescence microscope (Applied Precision Inc., Issaquah, WA). Images were acquired and processed using Deltavision SoftWoRx software (Applied Precision Inc., Issaquah, WA).

Metabolic labeling and immunoprecipitation of M-PMV proteins. CMMT cells were pulse-labeled as described previously [8]. Briefly, cells were starved for 15 min in methionine- and cysteine-deficient DMEM and then pulse-labeled for 30 min with 100 μCi of [^{35}S]methionine-[^{35}S]cysteine protein-labeling mix (Perkin-Elmer NEN, Boston, MA). Cells were then washed and chased in complete DMEM media for 2, 3 or 4 hrs. Where indicated, cytochalasin D, nocodazole or ACR was added to cells immediately at the beginning of the chase (4 hr treatment). Pulse and chase cell lysates and chase culture media were collected and processed as described previously [8]. Viral proteins were immunoprecipitated from cell lysates and culture media samples using polyclonal rabbit anti-p27CA antibody and then separated by SDS-polyacrylamide gel electrophoresis. SDS-PAGE gels were dried and exposed to phosphor screens, and then visualized and quantified using the Packard CycloneTM phosphor

imaging software OptiQuant (Perkin-Elmer, Shelton, CT). Further quantification to determine the molar percentage or molar ratios of Gag precursor Pr78 and p27 capsid at each time point were calculated as described previously [8]. For optimal detection of M-PMV Env, a similar assay was performed with the exception that cells were pulse-labeled with [^{3}H]-leucine and lysed using 1% Triton X-100 lysis buffer (1% Triton X-100, 0.05M NaCl, 0.025M Tris, pH 8.0) instead of 1% SDS. Viral proteins in cell lysates and culture media from this assay were immunoprecipitated with polyclonal goat anti-M-PMV antibody. SDS-PAGE gels were treated with En3hance as per manufacturer's protocol (Perkin-Elmer, Waltham MA) and then exposed to autoradiography films for at least 5 days at -70^{o}C before development.

Live cell imaging. CMMT cells transfected with pSARM-GagGFP-M100A were visualized in real time at 6-8 hrs post-transfection using the Deltavision deconvolution microscope. Cells co-transfected with pSARM-GagGFP-M100A and pTML-Env-mCherry were imaged at 15-18 hrs post-transfection due to delayed expression of the Env-mCherry signal. For imaging capsid movement along microtubules, CMMT cells were co-transected with pSARM-GagGFP-M100A and p-mCherry-tubulin, and imaged 15-18 hrs post-transfection. To image capsids and actin filaments, cells were transduced with CellLight® actin-RFP (Life Technologies, Carlsbad, CA) followed by transfection with pSARM-GagGFP-M100A and imaged 6-8 hrs post-transfection. During imaging, live cells were kept in a CO_2-permeable microchamber maintained at a temperature of 37^{o}C. Videos were acquired for untreated CMMT cells and for those treated with

nocodazole for 2 hrs and 4 hrs. Similar imaging was performed for cells treated with cytochalasin D or ACR for 4 hrs. For each video, images were acquired across 5 z-stacks every 5s over a total 2 min time period. The quick projection feature of the Deltavision SoftWorx software was utilized to process all videos to generate identical output frame speeds of 5 frames per second.

Video analysis. Particle tracking and velocity measurements were performed using the ImageJ (http://rsbweb.nih.gov/ij/) software plug-in MTrackJ (E. Meijering, Biomedical Imaging Group Rotterdam, Netherlands). Statistical analysis of velocity measurements was performed using the Mann-Whitney non-parametric t-test. A p value of less than 0.005 was considered to be statistically significant. To determine mean squared displacement, trajectories were generated for multiple randomly selected Gag-GFP particles in untreated CMMT cells and those treated with nocodazole for 4 hrs, using the ImageJ plug-in Particle Detector and Tracker [38]. The trajectories were filtered to only include those that contained at least 12 time points. The x/y coordinates of a particle at each time point within the trajectory were applied in the formula $[1/N\ {}_N\Sigma_{i=0}\ (\ r_i(t) - r_i(0)\ )^2]$ to calculate mean squared displacement (MSD). This formula takes into account the vector distance, $r_i(t)$-$r_i(0)$, that is traveled by particle *i* over a time interval of length *t*, and the squared magnitude of this vector is averaged over many such time intervals. This quantity was further averaged for all particles considered (N=20 for each group of untreated and nocodazole-treated cells), summing *i* from 1 to N and dividing by N. A plot of MSD as a function of time interval was then separated into different phases based on

changes in the trend of the graph [33]. Transformation of this graph to log-log scale, and subsequent calculation of the slope of the line of each phase yielded a numerical value that provides information about the type of particle movement. Slopes equal to 1, >1 or <1 represent Brownian motion, directed or hindered movement, respectively [33].

Results

Microtubule disruption causes a significant decrease in the kinetics of M-PMV production from CMMT cells.

To evaluate the role of microtubules, actin filaments and IF in intracellular transport of M-PMV, pulse-chase assays were performed to determine how the disruption of one or more of these cytoskeletal networks influences the kinetics of M-PMV transport and release. An advantage of pulse-chase time course assays is that Gag proteins can be tracked from the stages of synthesis and assembly to the point of release. Furthermore, since M-PMV capsid movement can be bidirectional, which we have detailed by live imaging (Clark et al., submitted), pulse-chase assays ensure that the net direction of intracellular M-PMV capsid transport being studied is indeed anterograde. As indicated by the experimental outline in Figure 1A, CMMT cells, chronically infected with M-PMV, were pulse-labeled for 30 min with [^{35}S]-methionine and then chased in radiolabel-free media for 0, 2, 3, and 4 hrs. Cytoskeletal inhibitors were added to CMMT cells at the beginning of the chase, with 10 μM nocodazole, 2.5 μM cytochalasin D, or 5 mM acrylamide (ACR), being used to disrupt microtubules, actin filaments, and IF, respectively. Immunostaining of fixed CMMT cells with rhodamine phalloidin and Alexa 488-conjugated anti-alpha tubulin confirmed the disruptive effects of cytochalasin D and nocodazole, with complete depolymerization of actin (Figure 1B, left panel) and microtubules (Figure 1B, middle panel) being evident after 4 hrs of treatment with these drugs. Immunostaining with FITC-conjugated anti-vimentin (Figure 1B, right panel) revealed major alterations in IF organization

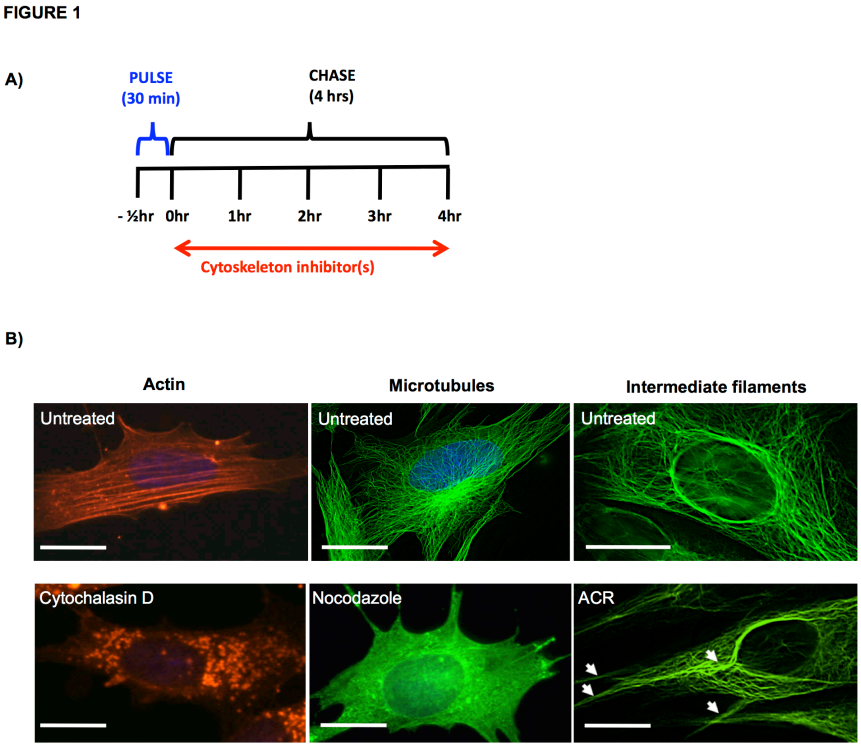

Figure 1. Cytoskeleton disruption in CMMT cells.
(A) Schematic of pulse-chase assay (quantitated in Figure 2) illustrating the timing of treatment with cytoskeleton-disrupting drugs during the chase. (B) Immunofluorescence microscopy confirming disruption of actin filaments (left panel), microtubules (middle panel) and IF (right panel) after 4 hrs of treatment with 2.5 μM cytochalasin D, 10 μM nocodazole, or 5% ACR, respectively. Bar = 15 μm.

after 4 hrs of ACR treatment, which has been reported before [23-25]. Treatment with ACR caused a collapse of vimentin fibers, leading to fiber bundling and a less extensive IF network, as well as cell shrinkage and the formation of cell retraction fibers (white arrows, Figure 1B, right panel). Importantly, ACR treatment was also found to depolymerize actin filaments in CMMT cells, which likely contributed to cell retraction (data not shown). Similar effects were noted when cells were treated with 1% ββ′-iminodipropionitrile (IDPN), which is also commonly used to disrupt IF (data not shown).

Cell lysates and culture media were collected from these drug-treated cells and untreated controls at the indicated time points during the chase. M-PMV Gag gene products from the collected samples were immunoprecipitated as described in Materials and Methods, subjected to SDS-PAGE and imaged using a phosphor screen. The kinetics of Gag precursor processing was determined by acquiring band intensities for Gag (Pr78), Gag-Pro (Pr95), Gag-Pro-Pol (Pr180) and capsid (p27) and then calculating the percentage of Pr78 and p27 relative to the sum of these proteins at each time point (Figure 2A, left panel). Data for untreated cells are represented by the black line, while the blue, green and red lines represent results for treatment with nocodazole, cytochalasin D or ACR, respectively. Dual treatment with nocodazole and ACR is indicated by the grey line. A comparison of virus release at 2 hrs and 4 hrs during the chase was also performed by calculating the ratio of Gag precursor proteins from pulse-labeled cells that were shed as capsid protein (p27) (Figure 2A, right panel). As shown in the left panel of Figure 2A, the half-life of Gag precursor processing of Pr78 to p27 in untreated

CMMT cells was 1.5 hrs. When CMMT cells were treated with nocodazole after the pulse, a delay of approximately 1 hr was noted for the half-life, as compared to the untreated control. A statistically significant decrease ($p=0.0027$) in virion release was also noted after 2 hrs of nocodazole treatment (Figure 2A, right panel). Despite this initial delay, the absolute levels of p27 continued to increase (Figure 2A) and at later time points during nocodazole treatment, were eventually found to reach levels near those observed for untreated cells.

In contrast to what was observed for nocodazole-treated cells, treatment with cytochalasin D had a negligible effect on the kinetics of Gag processing. The effects of ACR treatment, which disrupt both IF and actin filaments, were also minimal but a 30 min delay in Gag precursor processing was noted when compared to untreated and cytochalasin D-treated CMMT cells (Figure 2A). Differences in the levels of virion release are also evident in the autoradiographs in Figure 2B which illustrates p27 protein immunoprecipitated from chase culture media and cell lysates during treatment with the indicated cytoskeletal inhibitors. For purposes of clarity, only p27 bands from each set of untreated or treated CMMT cells are shown, and these were digitally re-assembled without modification to better indicate p27 levels at specific time points. It is important to note that while levels of both cell-associated (cell lysates) and cell-free (culture media) capsid protein are shown here, the sum of these p27 levels is used in quantitative analyses as a more accurate indicator of capsid release, since previous studies have shown that cleavage of Gag requires particle budding and release from the cell. Interestingly, when all three cytoskeleton networks were

simultaneously compromised using a combination of nocodazole and ACR (or IDPN), Gag processing and virion release from CMMT cells still occurred at the reduced rates observed for CMMT cells treated with nocodazole alone (Figure 2A and 2B). Of note, similar results were obtained from pulse-chase assays utilizing the alternative cytoskeleton inhibitors, taxol and latrunculin B, which stabilizes microtubules and depolymerizes actin filaments, respectively (data not shown), confirming that our observations are the result of disruptive effects on these specific cytoskeletal components. A leaky release of virions from the cytoplasm due to possible side effects of these drug treatments on the integrity of the plasma membrane is unlikely, since as described above efficient Gag precursor processing to p27 by the viral protease can only occur when the capsid undergoes completion of the budding process [26,27]. Thus, in summary, the most pronounced effects on Gag processing and virus output involved microtubule disruption, although virus release still occurred, albeit at a delayed rate, in the absence of three major functional cytoskeletal networks.

FIGURE 2

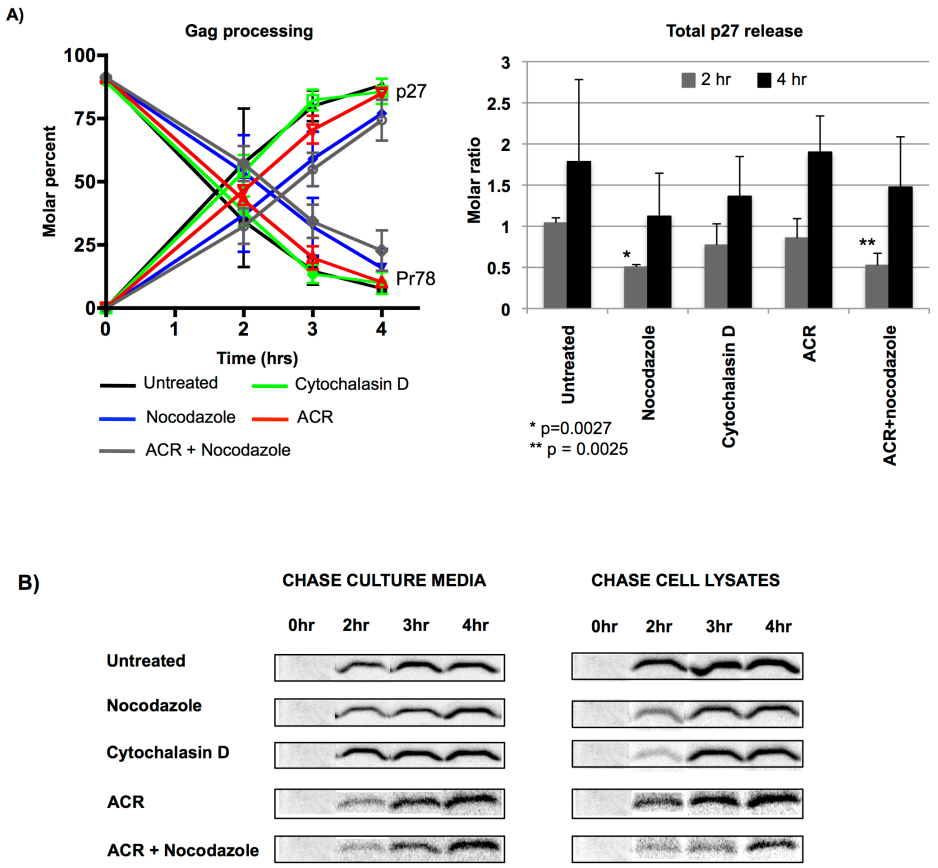

Figure 2. Effect of microtubule, actin or IF disruption on the kinetics of Gag precursor processing and virion release.
CMMT cells were metabolically labeled with [^{35}S]methionine and then chased for 0, 2, 3, and 4 hrs in the absence or presence of indicated drugs. (A) Data shown illustrates the molar percent of Pr78 and p27 at each time point (left panel) from untreated cells (black lines) or those treated with cytochalasin D (green lines), nocodazole (blue lines), ACR (red lines) or nocodazole and ACR (grey lines), which were added at the beginning of the chase. The right panel indicates the molar ratio of p27 that was released at 2 hrs (grey bars) and 4 hrs (black bars) after the indicated drug treatments. The stars indicate a significant statistical difference of $p<0.05$ (paired t-test) when compared to the untreated control. (B) Time-course autoradiographs illustrating p27 capsid protein released from untreated cells or those treated with indicated drugs. Data shown is representative of five independent assays.

M-PMV virions released from nocodazole-treated CMMT cells lack Env.

Since the most pronounced effect on M-PMV Gag release was observed following microtubule disruption, a pulse-chase assay was also performed to determine the effects on Env after nocodazole treatment. Since Env precursor Pr86 and its processed protein products gp70, gp22 and gp20 all have relatively low methionine content, [^{3}H]-leucine was utilized for efficient radiolabeling of these proteins. M-PMV Gag and Env proteins were then immunoprecipitated from pulse cell lysates, 5 hr chase cell lysates and chase culture media with a goat anti-M-PMV polyclonal antibody as described in Materials and Methods. As shown in Figure 3, the level of the Env protein products gp70 and gp20 in virions released from nocodazole-treated cells is significantly reduced when compared to the level of Env in virions released from the untreated control. The band, with a molecular mass of 78kDa that is observed in the chase media from nocodazole-treated cells is residual Gag Pr78, which is also detected in COS-1 cells expressing an *env*-gene deleted M-PMV provirus (Figure 3, right panel). Quantitation of the radioactivity associated with the region of the gel encompassing gp70 demonstrated a more than 60% reduction in area under the curve for virions from nocodazole treated cells, although again the sharpness of the peak is consistent with this residual radiolabel being in Pr78 (Supplementary Figure 1). Analysis of the levels of Env precursor Pr86 in the CMMT chase cell lysates, showed increased intensity in this band in treated cells, consistent with a two- to three-fold decrease in Env processing in the presence of nocodazole. In addition, a small increase in the intensity of gp70 and gp22 was observed in treated cells (figure 3, chase lysates),

suggesting that whatever precursor was cleaved remained cell associated. The disruption of actin or intermediate filaments had negligible effects on Env processing and release (data not shown).

FIGURE 3

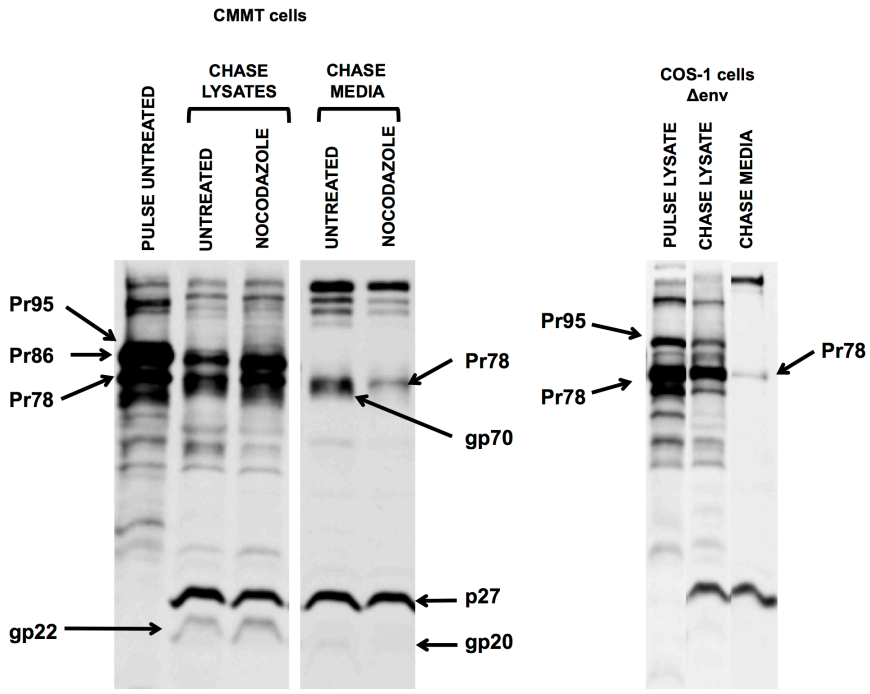

Figure 3. Microtubule disruption leads to a deficiency in Env incorporation in released virions.
Autoradiography of CMMT cells that were metabolically labeled with [^{35}H]leucine for 30 min and chased in non-radioactive media for 5 hrs with or without nocodazole. Indicated are the major Gag precursors Pr78 and Pr95 and the processed product p27, and the Env precursor Pr86 and its processed products gp70, gp22 and gp20. To better illustrate Pr86, lysates of COS-1 cells that were transfected with a ΔEnv plasmid construct are also shown. Data shown is representative of three independent experiments.

Live cell imaging of nocodazole-treated CMMT cells reveals a loss in linear movement of M-PMV Gag and Env.

Although results from the pulse-chase assays provide strong evidence for a predominant, but non-essential, role for microtubules in M-PMV capsid release, this approach does not define the actual effect on intracellular capsid transport over the course of nocodazole treatment. In addition, it provides no indication of whether virion release is the result of co-transport or independent trafficking of Gag and Env. Live cell microscopy experiments were therefore performed to gain a real time perspective of capsid and Env movements before and during nocodazole treatment. Using live-cell microscopy, M-PMV-producing CMMT cells were visualized in real time approximately 7 hours post-transfection with a plasmid construct expressing codon-optimized M-PMV Gag-GFP (pSARM-GagGFP-M100A; Clark et al., submitted). Analysis at this early time point allows for a balance between the level of detectable GFP signal and the number of Gag-GFP particles that is statistically relevant for velocity measurements. Visualization at this time point also increases the likelihood that the observed fluorescent capsids are newly synthesized and are not endocytosed particles. M-PMV capsids containing Gag-GFP were observed as dynamic green fluorescent puncta, with many exhibiting plus-ended movement towards the cell periphery (Movie S1). In cells that were co-transfected with plasmids expressing Gag-GFP, and mCherry fused to the microtubule subunit tubulin, a few distinct Gag-GFP particles were observed to move linearly along microtubules that were visible as red dynamic tubular structures (Movie S1, Supplementary Figure 2). As we described previously (Clark et al., submitted), bidirectional movement and

occasional stalling of Gag-GFP particles was often noted, which is typical for microtubule motor-based movement given that switching of cargo between minus- and plus-ended motors tends to occur [28-30]. These data are thus consistent with the pulse-chase experiments suggesting a role for microtubules in capsid transport. In contrast, live imaging of CMMT cells stained with actin-RFP and transfected with the plasmid expressing Gag-GFP revealed a lack of linear movements along actin filaments, suggesting limited utilization of this cytoskeletal network for long range transport (Movie S2), which is also in agreement with results from the pulse-chase experiments.

Imaging was then performed on CMMT cells co-transfected with plasmids expressing Gag-GFP and Env-mCherry before and during nocodazole treatment. Cells were imaged every 5 seconds for a total of 2 minutes. As shown in Movie S3, in addition to the green Gag-GFP and red Env-mCherry particles that were observed to exhibit movement independent of each other, a large fraction of yellow, co-localized Gag-Env puncta were observed, illustrating, for the first time, intracellular co-transport of Gag and Env. To assess the pattern of the path taken by these particles, their movement in untreated CMMT cells was tracked using the ImageJ plug-in MTrackJ, which allows for individual particle tracking. Only particles that exhibited movement towards or near the plasma membrane were considered. In general, the Env-containing vesicles with associated Gag (yellow) exhibited long, linear trajectories, while the individual Gag-GFP (green) and Env-mCherry (red) puncta, exhibited similar but shorter trajectories (Movie S3 and Figure 4A, left panel). The movement of some of each type of particle was also

observed to be bi-directional.

When cells were monitored 2 hrs after nocodazole treatment, a dramatic effect on intracellular movement was observed and linear tracks were essentially absent for all particles (Movie S4 and Figure 4A, middle panel). Thus, an intact microtubule network is critical for intracellular trafficking at this time after initiation of nocodazole treatment. Surprisingly, after 4 hrs of nocodazole treatment, movement of a majority of Gag-GFP particles was again evident, as shown by the green tracks (Movie S5 and Figure 4A, right panel). The movement of these Gag-GFP particles was non-linear and was found to occur throughout the cell, including the periphery. In sharp contrast, this was not the case for Env-mCherry and co-localized Gag-Env vesicles, which remained static at this later time point. Given that Env-containing vesicles would be predicted to move linearly exclusively on microtubules, this observation confirms microscopic evidence that microtubules remained depolymerized at this time.

To further characterize particle movement, the velocity of Gag-GFP, Env-mCherry and Gag-Env vesicles in untreated cells (n=5) and cells treated with nocodazole for 2 hrs (n=5) and 4 hrs (n=5) was calculated, also using MTrackJ. As shown in Figure 4B, Gag-GFP particles in untreated cells exhibited a median maximum velocity of approximately 0.5 μm/s, which is within the range of what has been previously described for microtubule-based movement [17,31,32]. While this velocity decreased substantially (at least five-fold) to less than 0.1 μm/s in cells treated with nocodazole for 2 hrs, a significant ($p<0.0001$) three-fold

recovery to a median velocity of approximately 0.3 μm/s was observed in cells after 4 hrs of nocodazole treatment. This recovered movement, however, has a significantly lower ($p<0.0001$) median velocity in the 4-hour nocodazole-treated cells compared to what is observed in untreated cells. In contrast, Env-mCherry particles and co-localized Gag-Env particles in untreated CMMT cells initially demonstrated median maximum velocities of 0.5 μm/s and 0.6 μm/s, respectively, that was reduced to <0.1 μm/s upon nocodazole treatment, but did not exhibit any recovery in velocity after nocodazole treatment at the 4 hr time point, which is consistent with the particle track patterns visualized by live imaging. To account for cell-to-cell variability, single cell analysis was also performed in which Gag-GFP particle movement in the same cell was monitored pre- and post-treatment with nocodazole. Results obtained were similar to those observed for the multi-cell analysis described above (data not shown), and importantly the observed changes in the velocity and track patterns of Gag-GFP, Env-mCherry and Gag-Env particles during nocodazole treatment are in agreement with results acquired from the pulse-chase assays described above, which demonstrated a delay in Gag release and also a lack of Env incorporation in released M-PMV capsids. Similar imaging experiments performed for cytochalasin D-treated cells and ACR-treated cells revealed no significant changes in capsid velocities, though it should be noted that treatment with these drugs distorted cell morphology substantially, therefore making it difficult to accurately monitor capsid movement in live cells (data not shown).

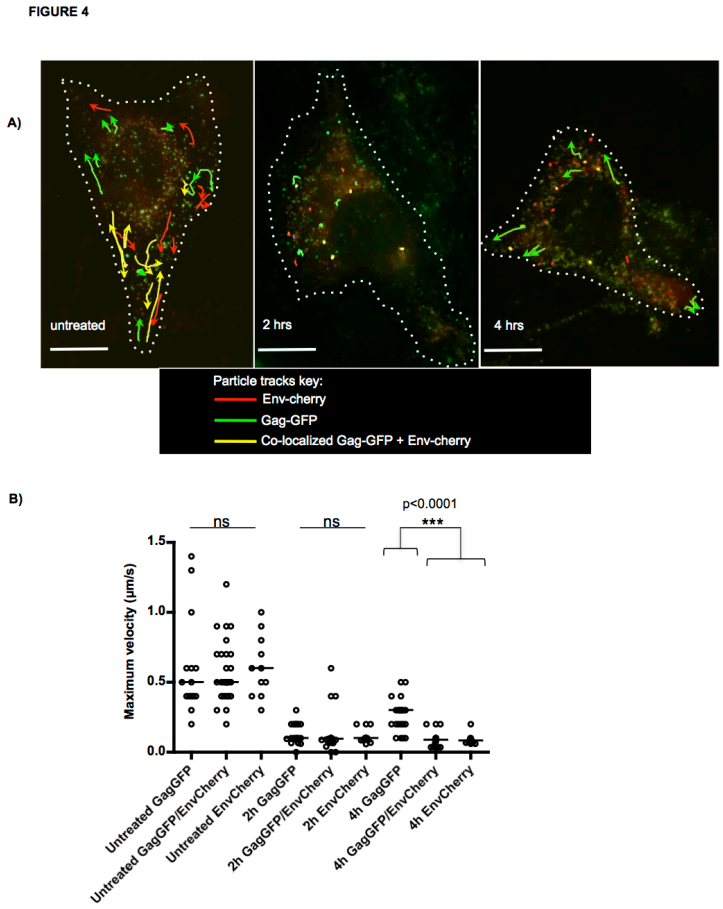

Figure 4. Nocodazole treatment leads to a transient decrease in linear movement of intracellular capsids.
CMMT cells were co-transfected with pSARM-GagGFP-M100A and pTML-Env-mCherry and visualized in real time with a Deltavision deconvolution microscope. Live imaging of untreated cells and those treated with nocodazole for 2 hrs and 4 hrs was performed. Videos were recorded over a 2 minute time period, with each video having an identical frame rate of 5 frames per second. (A) Illustration of tracks for Gag-GFP (green), Env-mCherry (red) and co-localized Gag-Env particles (yellow) in untreated and nocodazole-treated cells. Tracks shown are for particles moving towards or near the plasma membrane, with arrow heads indicating direction of movement. Data shown is representative of at least five independent imaging experiments. Bars = 15 µm. See accompanying Movies S2-S4 for real time visualization of particle tracking. (B) Maximum velocity measurements of Gag-GFP particles (n≥15), Env-mCherry particles (n≥10) and co-localized Gag-Env particles (n≥23) in untreated cells and nocodazole-treated cells after 2 hrs and 4 hrs of drug treatment. A minimum of 5 cells was analyzed at each time point. Bars indicate median values. Statistical significance is denoted by p value or ns (not significant).

M-PMV capsid movement in 4 hr nocodazole-treated CMMT cells appears to utilize a directed mode of transport.

Since our results demonstrated a clear, albeit staggered and short-range movement of M-PMV capsids containing Gag-GFP after 4 hrs of nocodazole treatment, it was important to define whether this motion was random diffusion in the cytoplasm or directed transport. A property of particle movement that is commonly utilized for this purpose is mean squared displacement (MSD), which is the average distance a given particle travels in a defined period of time. Importantly, it takes into account the distance that is traveled relative to the particle's starting position, thereby helping to distinguish between random and productive movement. To obtain MSD values, particle trajectories were first generated using the ImageJ plug-in Particle Detector and Tracker, which allows for the automated and simultaneous selection of multiple fluorescent particles in live cells, based on user-defined parameters, as described in Materials and Methods. Trajectories were generated for randomly selected particles (n=20) for each group of untreated CMMT cells (n=4) and 4 hr nocodazole-treated cells (n=5), and the MSD for each time interval (Δt) within the trajectory was calculated (see Materials and Methods). Using these values, curves relating MSD to time were generated for each of the 40 total particle trajectories. A typical particle trajectory and corresponding graph is illustrated in Figure 5A. Separation of the curve into phases indicates a change in the type of movement over the course of the trajectory. Once converted to a log-log scale (Figure 5B), the slope of each phase confers a numerical value to the type of movement, with values of 1

representing Brownian motion, and values >1 or <1 indicating directed and obstructed movement, respectively. Typically, values within a window of 0.9-1.1 are considered to exhibit Brownian motion, with values greater than 1.1 suggesting active transport [33]. By utilizing this method, the collective analyses of trajectory phases of particles (n=20) in 4 hr nocodazole-treated cells revealed that the movement of the majority (~60%) of Gag-GFP labeled capsids involved a directed mode of transport, which was similar to what was observed for particle trajectories (n=20) in untreated CMMT cells (Figure 5C). The median MSD of Gag-GFP particles in 4 hr nocodazole-treated cells is not statistically significant from the upper MSD value that denotes Brownian motion, and so this form of movement cannot be entirely ruled out. However, as evidenced by the particle tracks in Figure 4A and Movie S4, the pattern of Gag-GFP movement in nocodazole-treated cells after 2 hrs is distinctly different from the patterns observed after 4 hrs of nocodazole treatment (Figure 4A and Movies S4 and S5), despite the fact that Brownian motion would occur at both time points. These observations together with the MSD analyses, collectively suggest that the movement of Gag-GFP particles after 4 hrs of nocodazole treatment is directed to some degree.

FIGURE 5

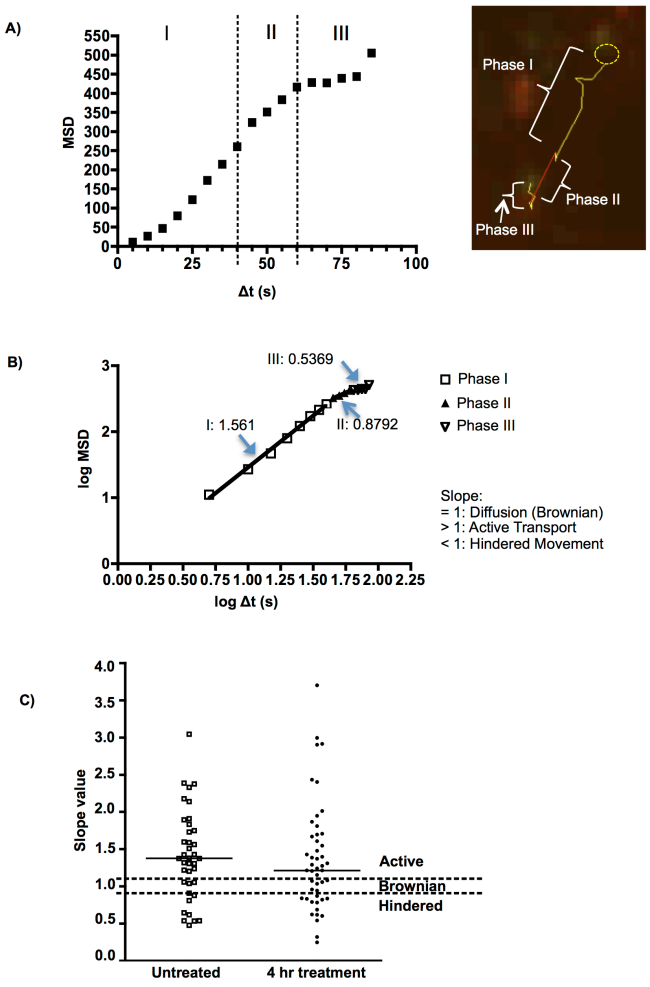

Figure 5. MSD analysis of intracellular capsid movement after long-term nocodazole treatment.
(A) Representative particle trajectory and accompanying MSD graph with separated phases I-III indicated. Conversion of this graph to a log-log scale is shown in (B), with calculated slope values indicating a different mode of movement for each phase of the trajectory. (C) Analysis of MSD of Gag-GFP trajectories (n=20 per group) in untreated cells (n=4) and cells treated with nocodazole (n=4) for 4 hrs. Solid bars indicate median slope values for each group of cells, with dotted lines relating slope values to the type of particle movement.

Discussion

The aim of current study was to elucidate whether previously reported pericentriolar interactions between M-PMV Gag and Env-containing recycling vesicles are maintained as stable co-transported entities towards the plasma membrane or if these interactions simply facilitate the transfer of Gag to an anterograde trafficking system. It was also necessary to elucidate whether this (co-)transport occurs via a cytoskeleton-dependent network. This study involved a real time approach using time-course pulse-chase assays and live-cell imaging experiments, to monitor the kinetics of M-PMV capsid transport over extended periods of time. Doing so provided insight into dynamic M-PMV-host interactions, by helping to identify cytoskeletal factors involved in anterograde intracellular transport, and shedding light on the extent to which these factors are required by M-PMV.

For the first time, live cell imaging provides direct evidence that the interactions between Gag and Env are not short-lived, with clear co-localization and sustained anterograde co-transport of Gag-Env particles being observed in CMMT cells. A benefit of utilizing CMMT cells for these studies is that endogenous Gag or Env that is constitutively produced by the cells allows for normal assembly of GFP-labeled capsids and mixed trimers [34] of wild-type and mCherry-labeled Env. Thus, it is possible that a fraction of fluorescent-tagged Gag particles are associated with endogenous Env, and vice versa. Indeed, the similar median velocities of Gag-GFP, Gag-Env and Env-mCherry particles in untreated CMMT cells may reflect this. However, there was a significant difference between the

velocities and patterns of movement of Gag-GFP versus Gag-Env or Env-mCherry particles after 4 hours of nocodazole treatment, and the overall consistency of the live imaging and pulse-chase results lend validity to the differential transport and release patterns observed for Gag and Env.

The data collectively demonstrate that the intracellular transport of Env and Gag-Env co-localized vesicles, and subsequent release of Env are critically dependent on the presence of microtubules. While efficient intracellular transport of Gag also primarily depends on this cytoskeletal network, a unique and unexpected finding from our results was that the effect of microtubule disruption on capsid transport was only temporary, with nocodazole-treated cells exhibiting an initial two-fold reduction in Gag processing and release but later showing levels of Gag release that were near those observed for untreated cells. However, released virions lacked Env and these observations were strongly supported by accompanying live imaging results.

The observed movement and release of Gag in the absence of microtubules is likely to include a combination of factors that are secondary to the disruption of the MTOC by nocodazole. While a role for alternate cytoskeletal pathways in nocodazole-treated cells could not be confirmed by live imaging due to the shrinking morphological effects of CytD and ACR, biochemical pulse-chase assays suggest that actin and/or intermediate filaments play a minimal role in facilitating the release of Gag in the absence of microtubules. Furthermore, live imaging of untreated CMMT cells stained with actin-RFP and transfected with a

plasmid expressing Gag-GFP failed to demonstrate linear movement of Gag-GFP particles on actin filaments (data not shown). This is in sharp contrast to the distinct linear tracks observed for Gag-GFP on mCherry-labeled microtubules. However, these findings do not rule out a role for the dense cortical actin network, which may facilitate short-range movement of capsids when proximal to the plasma membrane.

The movement of Gag-GFP particles that was observed in nocodazole-treated cells after 4 hrs appeared to be distributed throughout the cell, and was typically short-range and staggered in nature, as demonstrated by particle tracking. In sharp contrast, Env-mCherry vesicles and Gag-Env co-localized vesicles were visibly static throughout these treated cells. This is further highlighted by the difference in velocity of Gag-GFP particles when compared to Gag-Env and Env-mCherry particles after 4 hrs of nocodazole treatment (p value<0.0001). As illustrated by the model in Figure 6, the loss in spatial proximity of nascent or pre-existing Env or Env-mCherry with recycling endosomal vesicular compartments due to MTOC disruption, and a cessation in vesicular trafficking due to microtubule depolymerization likely contributed to the stagnant nature of Env-mCherry and Gag-Env particles in nocodazole-treated cells. These data, together with the pulse-chase assay results showing a lack of Env in released particles, strongly suggest an absolute dependence of Env-containing recycling vesicles on microtubules, and by extension, an inability of Env to utilize other secretory or vesicular trafficking pathways that are microtubule-independent.

Collectively, the differential effects on Gag and Env transport following microtubule depolymerization also argue against the regeneration and/or presence of nocodazole-resistant microtubules. While nocodazole-resistant microtubules composed of detyrosinated tubulin have been reported, their stability persists for only short term nocodazole-treatment, with treatments greater than 1-2 hrs leading to their complete depolymerization [35]. Indeed, immunostaining with an antibody targeting detyrosinated tubulin in CMMT cells demonstrated a complete loss of these microtubules after 4 hrs of nocodazole treatment (data not shown).

The observed albeit inefficient movement of Gag-GFP particles after long-term nocodazole treatment was likely a combination of existing Gag-particles, and nascent Gag-GFP synthesized from dispersed polysomes (Figure 6). However, results from the pulse-chase experiments, which track the fate of radiolabeled proteins, suggest that Gag that was synthesized prior to the addition of nocodazole was eventually released 4 hours after microtubule depolymerization. The fact that Gag-GFP particles exhibited some degree of movement, unlike the static nature of both Env-mCherry and Gag-Env vesicles as shown by live imaging, suggest that the motile Gag/Gag-GFP particles at the 4 hr time point were not associated with Env vesicles.

The staggered movement of Gag-GFP particles over limited distances may have been the result of stochastic unstable interactions with microtubule-independent trafficking components, or reflective of Brownian motion. The median MSD of

Gag-GFP particles in 4 hr nocodazole-treated cells suggested that the movement was active in nature, and given that a notable level of virion release was observed at this time point, it was likely the result of directed motion. However, the MSD value was not statistically significant from the range that denotes Brownian motion and so it is not improbable that both forms of movement are occurring to some degree. These irregular movements and/or transient interactions, particularly in the cell periphery, may have been sufficient to facilitate capsid release.

The possibility of capsid assembly occurring directly at the plasma membrane also cannot be discounted. Random molecular interactions and inefficient staggered movements of Gag may occur even in the presence of microtubules, and a minimal release of non-viable Env-deficient capsids from untreated cells is not implausible. Indeed, it should be noted that while short non-linear particle tracks were exhibited by the majority of Gag-GFP particles in nocodazole-treated cells, a similar pattern was also observed for a minor population of Gag-GFP particles in untreated cells. However, it is clear that although microtubules are not critical for Gag transport and release, the alternative pathway(s) that is utilized does not yield functional Env-containing virions, highlighting the importance of the interdependent relationship between Gag and Env.

The sustained co-localization of Gag-GFP and Env-mCherry that was observed as highly motile or stagnant particles in untreated and nocodazole-treated cells, respectively, suggests that Env is important for mediating a stable interaction

between Gag and the Env-containing recycling vesicles. It is currently unclear if this is solely a direct Env-Gag interaction, or if interactions with Env trigger conformational changes in Gag that allow it to dock on to the recycling vesicle. Further support for an Env-mediated interaction is derived from previous studies in which cells expressing M-PMV provirus with an *env* deletion exhibited a 7-fold decrease in Gag release, despite the presence of microtubules and a functional recycling vesicular trafficking network.

Interestingly, the results from the pulse-chase experiments demonstrated continued release of M-PMV Gag even when all three cytoskeleton components were compromised. In addition, earlier studies involving the PLA2 inhibitor ONO-RS-082 prompted the suggestion of a membrane tubule-vesicular means of transport [3,12,13]. These observations prompted an evaluation of a cytoskeleton-independent, membrane tubule-based transport network. However, live imaging experiments of untreated cells, nocodazole-treated cells, and cells treated with BFA which induces membrane tubule formation, all failed to show productive linear movement of Gag-GFP along or on these membrane tubular structures, with only transient interactions being observed (data not shown). Furthermore, live imaging of CMMT cells treated with ONO-RS-082, which inhibits tubule formation, revealed that despite a dose-dependent block in virion release, intracellular movement of Gag-GFP was still evident (data not shown), suggesting differential effects of this compound on transport and release. This is not entirely surprising given that the PLA2 superfamily of enzymes, which are also involved in the generation of membrane curvature, are likely to influence the

formation and release of budding vesicles. Thus, intracellular (co-)transport of Gag and Env is unlikely to be cytoskeletal-independent. This is further supported by studies that have demonstrated that the elongation and/or movement of membrane tubule structures also require a functional cytoskeletal network.

In summary, live cell imaging has for the first time definitively demonstrated intracellular anterograde co-transport of M-PMV Gag and Env in real time. Results have further shown that the co-localization of Gag and Env vesicles is stable and sustained during transport, and that this interaction is primarily mediated by Env, which is consistent with previous findings [3,12,13]. Importantly, the novel differential effects on Gag and Env transport and release following microtubule depolymerization, as shown by live imaging and biochemical pulse chase assays, highlight an absolute dependence of Env-containing vesicles, and by extension the associated Gag, on microtubule-based transport. It will be of interest to map the molecular and structural determinants that shape the specificity of Env for recycling vesicles and its interaction with Gag. It is important to note that while microtubules appear to be partially dispensable for Gag transport and capsid release, the alternative pathway(s) is not viable for the production of Env-containing virions (Figure 6). Nonetheless, identifying and characterizing trafficking factors that facilitate short-range Gag transport, in the presence and absence of microtubules, will help define distinct genres of intracellular trafficking pathways and may reveal a broader scope of interactions between Gag and host cell transport factors.

FIGURE 6

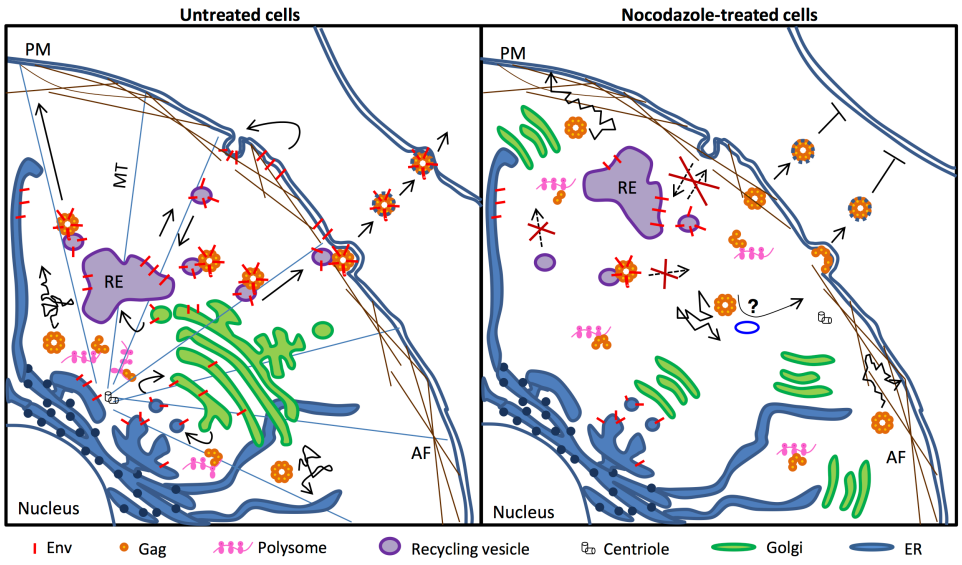

Figure 6. Model illustrating anterograde co-transport of M-PMV Env and Gag on recycling vesicles.
In the presence of microtubules (MT) and the microtubule organizing center (MTOC), capsid assembly from Gag-translating polysomes occurs at the pericentriolar region. Env, which traffics through the recycling endosome (RE), mediates a stable interaction between pre-assembled capsids and RE-derived vesicles to facilitate anterograde linear transport on MT to the plasma membrane (PM). Nocodazole treatment results in a loss of MT and a dispersal of MTOC organelles, resulting in Gag synthesis and capsid assembly throughout the cell, including the periphery. The recycling, transport and release of Env, which rely on vesicular transport, cease due to a dependence of recycling vesicles on MT. Capsid release continues to occur at an inefficient rate due to stochastic movements and/or interactions of Gag with cortical actin filaments (AF) or microtubule-independent transport/secretory vesicles. Capsid assembly may also occur directly at the PM, leading to the release of non-infectious Env-deficient virions.

Supporting Figures

Available in electronic version of this dissertation

Movie S1
Live imaging of untreated CMMT cells that are co-transfected with pSARM-GagGFP-M100A and the mCherry-tubulin plasmid construct to demonstrate movement of GFP-tagged M-PMV capsids along microtubules.

Available in electronic version of this dissertation

Movie S2
Live imaging of CMMT cells transfected with pSARM-GagGFP-M100A and subsequently transduced with actin-RFP to observe GFP-tagged M-PMV capsid association with actin filaments.

Available in electronic version of this dissertation

Movies S3a-S4a
Supporting movies for Figure 4A. Videos (5 frames per second) of CMMT cells (illustrated in Figure 4A) with particle tracking to demonstrate the movement of GFP-tagged M-PMV capsids in untreated cells and at indicated times after nocodazole treatment.

Available in electronic version of this dissertation

Movies S3b-S4b
Supporting movies for Figure 4A. Videos (5 frames per second) of CMMT cells (illustrated in Figure 4A) without particle tracking to demonstrate the movement of GFP-tagged M-PMV capsids in untreated cells and at indicated times after nocodazole treatment.

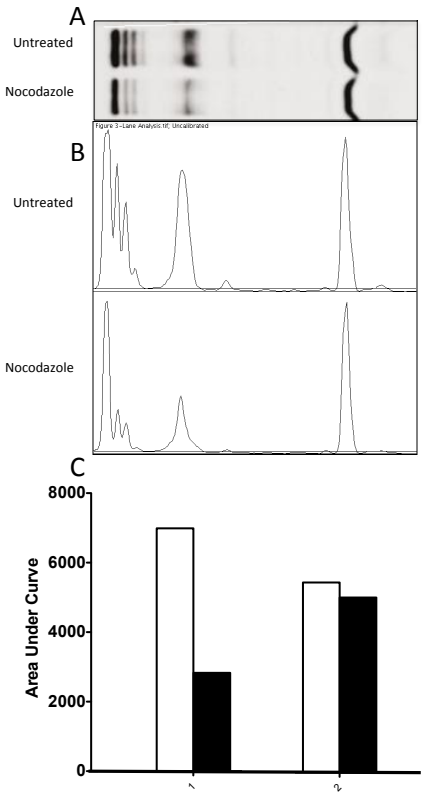

Figure S1
(A) Lanes adapted from Figure 3, Chase Media, of untreated (top) and nocodazole treated (bottom) CMMT cells. (B) Histogram of band intensities from the gel for untreated (top) and nocodazole treated (bottom) CMMT cells. Peaks corresponding to a band on the gel are located directly underneath the respective band. (C) Bar graph of area under the curve of the band intensity derived from histograms in (B). White bars represent the band intensity of untreated CMMT cells, while black bars represent the band intensity of nocodazole-trated CMMT cells. Area under the curve was measured only for the bands corresponding to Pr78/gp70, Pr78 (group 1) and p27 (group 2) (as depicted in Figure 3).

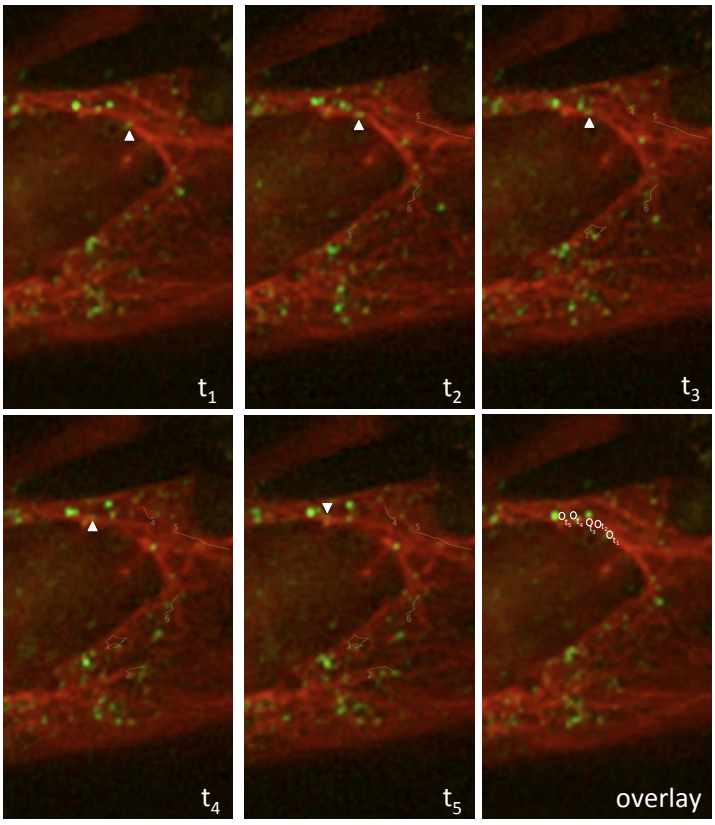

Figure S2
Frame by frame depiction of Movie S1 to demonstrate movement and displacement of a GFP-tagged M-PMV capsid along a microtubule. Images were not collected from consecutive frames. Each image (t_1 - t_5) was derived from the 0:01, 0:04, 0:07, 0:08, and 0:09 timepoint of the video, respectively.

Acknowledgements

This work was supported by NIH grant CA-27834 from the National Cancer Institute and Czech Ministry of Education grant MSM 6046137305 and by Czech Science Foundation grant P302/12/1895. J. Clark was the recipient of an American Society for Microbiology Robert D. Watkins Fellowship. We thank the James B. Pendleton Charitable Trust for the contribution of advanced imaging equipment utilized in the experiments in this manuscript. We thank Dr. Jan Lipov, Dr. Greg Melikian, and Dr. Joseph Roland for helpful discussions. We also thank Pavel Ulbrich (Institute of Chemical Technology, Prague, Czech Republic) and Eileen Breding (Yerkes National Primate Research Center, Atlanta GA) for excellent advice and assistance with transmission electron microscopy, and the Robert P. Apkarian Integrated Electron Microscopy Core of Emory University for sample preparations.

Literature Cited

1. Choi G, Park S, Choi B, Hong S, Lee J, et al. (1999) Identification of a cytoplasmic targeting retention signal in a retroviral Gag polyprotein. J Virol 73: 5431-5437.

2. Sakalian M, Hunter E (1999) Separate assembly and transport domains within the gag precursor of Mason-Pfizer monkey virus. J Virol 73: 8073-8082.

3. Sfakianos JN, LaCasse RA, Hunter E (2003) The M-PMV cytoplasmic targeting-retention signal directs mascent gag polypeptides to a pericentriolar region of the cell. Traffic 4: 660-670.

4. Vlach J, Lipov J, Rumlova M, Veverka V, Lang J, et al. (2008) D-retrovirus morphogenetic switch driven by the targeting signal accessibility to Tctex-1 of dynein. Proc Natl Acad Sci USA 105: 10565-10570.

5. Rhee SS, Hunter E (1990) A single amino acid substitution within the matrix protein of a type D retrovirus converts its morphogenesis to that of a type C retrovirus. Cell 63: 77-86.

6. Rhee SS, Hunter E (1990) Structural role of the matrix protein of type D retroviruses in gag polyprotein stability and capsid assembly. J Virol 64: 4383-4389.

7. Rhee SS, Hunter E (1991) Amino acid substitutions within the matrix domain of type D retroviruses affect assembly, transport and membrane association of a capsid. EMBO J 10: 535-546.

8. Stansell E, Apkarian R, Haubova S, Diehl WE, Tytler EM, et al. (2007) Basic residues in the Mason-Pfizer monkey virus gag matrix domain regulate intracellular trafficking and capsid-membrane interactions. J Virol 81: 8977-8988.

9. Stansell E, Tytler E, Walter MR, Hunter E (2004) An early stage of Mason-Pfizer monkey virus budding is regulated by the hydrophobicity of the gag matrix domain core. J Virol 78: 5023-5031.

10. Hong S, Choi G, Park S, Chung A-S, Hunter E, et al. (2001) Type D retrovirus Gag polyprotein interacts with the cytosolic chaperonin TRiC. J Virol 75: 2526-2534.

11. Brown CR, Doxsey SJ, Hong-Brown LQ, Martin RL, Welch WJ (1996) Molecular chaperones and the centrosome. A role for TCP-1 in microtubule nucleation. J Biol Chem 271: 824-832.

12. Sfakianos JN, Hunter E (2003) M-PMV capsid transport is mediated by Env/Gag interactions at the pericentriolar recycling endosome. Traffic 4: 671-680.

13. Ullrich O, Reinsch S, Urbe S, Zerial M, Parton RG (1996) Rab11 regulates recycling through the pericentriolar recycling endosome. J Cell Biol 135: 913-924.

14. Martinez NW, Xue X, Berro RG, Kreitzer G, Resh MD (2008) Kinesin KIF4 regulates intracellular trafficking and stability of the human immunideficiency virus Type 1 Gag polyprotein. J Virol 82: 9937-9950.

15. Hollinshead M, Rodger G, Eijl HV, Law M, Hollinshead R, et al. (2001) Vaccinia virus utilizes microtubules for movement to the cell surface. J Cell Biol 154: 389-402.

16. Suomalainen M, Nakano MY, Keller S, Boucke K, Stidwill RP, et al. (1999) Microtubule-dependent plus- and minus-end-directed motilities are competing processes for nuclear targeting of adenovirus. J Cell Bio 144.

17. Lee GE, Murray JW, Wolkoff AW, Wilson DW (2006) Reconstitution of herpes simplex virus microtubule-dependent trafficking in vitro. J Virol 80: 4264-4275.

18. Miranda-Saksena M, Armati P, Boadle RA, Holland DJ, Cunningham AL (2000) Anterograde transport of herpes simplex virus type 1 in cultured, dissociated human and rat dorsal root ganglion neurons. J Virol 74: 1827-1839.

19. Jouvenet N, Monaghan P, Way M, Wileman T (2004) Transport of African swine fever virus from assembly sites to the plasma membrane is dependent on microtubules and conventional kinesin. J Virol 78: 7990-8001.

20. Sathish N, Zhu FX, Yuan Y (2009) Kaposi's sarcoma-associated herpesvirus ORF45 interacts with kinesin-2 transporting viral capsid-tegument complexes along microtubules. . PLos Pathog 5: e1000332.

21. Glotzer JB, Michou A-I, Baker A, Saltik M, Cotten M (2001) Microtubule-independent motility and nuclear targeting of adenovirus with fluorescently labeled genomes. J Virol 75: 2421-2434.

22. Yea C, Dembowy J, Pacione L, Brown M (2007) Microtubule-mediated and microtubule-independent transport of adenovirus Type 5 in HEK293 cells. J Virol 81: 6899-6908.

23. Durham HD (1986) The effect of beta, beta'-iminidipropionitrile (IDPN) on cytoskeletal organization in cultured human skin fibroblasts. Cell Biol Int Rep 10: 599-610.

24. Griffin JW, Fahnestock KE, Price DL, Cork LC (1983) Cytoskeletal disorganization induced by local application of beta, beta'-iminodiproprionitrile and 2,5-hexanedione. Ann Neurol 14: 55-61.

25. Kumar N, Robidoux J, Daniel KW, Guzman G, Floering LM, et al. (2007) Requirement of vimentin filament assembly for β_3-adrenergic receptor activation of ERK MAP kinase and lipolysis. . J Biol Chem 282: 9244-9250.

26. Parker SD, Hunter E (2001) Activation of the Mason-Pfizer monkey virus protease within immature capsids in vitro. PNAS 98: 14631-14636.

27. Yasudo J, Hunter E (1998) A proline-rich motif (PPPY) in the Gag polyprotein of Mason-Pfizer monkey virus plays a maturation-independent role in virion release. J Virol 72: 4095-4103.

28. Shah JV, Flanagan LA, Janmey PA, Leterrier J-F (2000) Bidirectional translocation of neurofilaments along microtubules mediated in part by dynein/dynactin. Mol Biol Cell 11: 3495-3508.

29. Hendricks AG, Perlson E, Ross JL, Schroeder HW, Tokito M, et al. (2010) Motor coordination via a tug-of-war mechanism drives bidirectional vesicle transport. Curr Biol 20: 697-702.

30. Ross JL, Shuman H, Holzbaur EL, Goldman YE (2008) Kinesin and dynein-dynactin at intersecting microtubules: motor density affects dynein function. Biophys J 94: 3115-3125.

31. Gazzola M, Burckhardt CJ, Bayati B, Engelke M, Greber UF, et al. (2009) A stochastic model for microtubule motors describes the in vivo cytoplasmic transport of human adenovirus. PLos Comput Biol 5: e1000623.

32. Bremner KH, Scherer J, Yi J, Vershinin M, Gross SP, et al. (2009) Adenovirus transport via direct interaction of cytoplasmic dynein with the viral capsid hexon subunit. Cell Host Microbe 6: 523-535.

33. Forest T, Barnard S, Baines JD (2005) Active intracellular movement of herpesvirus capsids. Nat Cell Biol 7: 429-431.

34. Salzwedel K, Berger E (2009) Complementation of diverse HIV-1 Env defects through cooperative subunit interactions: a general property of the functional trimer. Retrovirology 6:75.

35. Quinones GB, Danowski BA, Devaraj A, Singh V, Ligon LA (2011) The posttranslational modification of tubulin undergoes a switch from dyrosination to acetylation as epithelial cells become polarized. . Mol Biol Cell 22: 1045-1057.

36. Gluzman Y (1981) SV40-transformed simian cells support the replication of early SV40 mutants. Cell 23: 175-182.

37. Brody BA, Kimball MG, Hunter E (1994) Mutations within the transmembrane glycoprotein of Mason-Pfizer monkey virus: Loss of SU-TM association and effects on infectivity. Virology 202: 673-683.

38. Sbalzarini IF, Koumoutsakos. P (2005) Feature point tracking and trajectory analysis for video imaging in cell biology. . J Struct Biol 151: 182-195.

Discussion

The work presented in this dissertation provides valuable insight into the host cell machinery utilized by M-PMV Gag and Env for intracellular transport of immature capsids to the plasma membrane for budding. The first manuscript addresses the advantages of being able to study individual capsid movement in a real-time imaging system by creating a Gag-GFP fusion protein that can be tracked in live cells. Optimization followed by characterization of this construct showed strong evidence for use of microtubules for intracellular transport of fluorescently-labeled capsids. The second manuscript goes further by evaluating the M-PMV capsid utilization of three major cellular cytoskeletal proteins. Results from this manuscript showed that M-PMV Gag and Env cotransport along microtubules and that release of Env-containing virions is dependent on an intact microtubule system in the cell. These results also provided strong support for the current hypothesis that M-PMV capsids interact with Env-containing recycling vesicles, traveling along microtubules, destined for the plasma membrane.

Because of the separation of assembly and budding that is characteristic of D-type retroviruses, they make an excellent model for studying these processes. In this study, we employ the use of M-PMV, the prototypical D-type retrovirus. To add to the body of knowledge that is available through mutational studies using biochemical assays and fixed cell microscopy, we constructed a Gag-GFP fusion that could be used to study the intracellular behavior of individual capsids

in live cells. Fusion of eGFP to proteins for this purpose has been well documented in several viruses, but is not a trivial process. The addition of a 27 kD protein, GFP, to a protein could have negative effects on proper assembly, the ability of the protein to interact properly with other proteins, and proper sorting and localization of the protein. Several controls must be performed to ensure that fluorescently-tagged proteins behave similarly to that of the WT protein. In this work, we show that the expression of the Gag-GFP fusion required codon-optimization, strengthening of the Kozak consensus sequence, and substitution of an in-frame methionine in the MA domain of Gag to an alanine (M100A). We also showed that expressing the fusion protein alone, in the context of an M-PMV proviral construct, had detrimental effects on capsid morphology, the kinetics of capsid release, and resulted in very low levels of Env glycoprotein expression. The latter result appeared to reflect the loss of sequences necessary for lariat formation during RNA splicing as a consequence of Gag codon optimization. The defect in capsid assembly and release could be rescued by co-expression of the fusion protein with untagged Gag from proviral constructs. This also provided Env in trans to facilitate intracellular capsid transport. Western blot and sucrose gradient density fractionation confirmed that co-expression resulted in co-assembly of the GFP-tagged and untagged Gag.

Fixed cell localization studies confirmed that the localization of GFP-tagged and untagged Gag, localized comparably within the cell. This was also true for mutants of Gag, such as R55W and K16A that exhibit altered morphogenesis, with the former now accumulating at and budding from the plasma membrane and the latter budding into intracellular vesicles [59,69]. Additionally, a third

mutant, R22A, which appears to be blocked in transport at the cortical actin layer [69], was similarly blocked in the GFP-tagged form of Gag. Following confirmation that subcellular localization was equivalent to untagged protein, the Gag-GFP fusion was studied in live cell imaging experiments.

The initial observation of capsid transport in living cells was that capsid movement was not uniform. There were several different types of movement. Some of the capsids seemed arrested in place. Others seemed to be moving in a Brownian manner. And a third population of capsids observed, displayed what appeared to be a directed, active mode of transport with long-range displacement from start to finish. Further characterization of this third population of capsid showed that this movement occurred bi-directionally, with oscillating instantaneous velocities. These characteristics were consistent with this third population of capsids utilizing microtubules for long-range, lateral transport through the cell. When microtubules were labeled with the mCherry fluorescent protein in live cells, long-range transport was observed to occur along microtubular tracks. Along with this, a significant number of capsids were associated with the microtubules, but not moving at all. This is also a characteristic of using microtubules for transport, as cargo that transports along microtubules often undergo periods of halted movement as they wait for the correct motors to interact and transport them to the proper location in the cell [114]. This oscillation of instantaneous velocities and the bidirectional movement is consistent with what has been described for vesicular transport [115] and viruses utilizing microtubules for intracellular transport of viral components [101,116].

Kinesins are likely the molecular motors used in this process, although further studies must be employed to elucidate which kinesins may be involved in the intracellular transport of M-PMV. Studies of kinesins show that the motor is capable of propelling cargo along microtubules at velocities as high as 4 um/s. Kinesins are also responsible for stalling cargo during periods of complete cessation of movement [100,114-117]. The behavior of the M-PMV capsids is comparable to what has been seen in the extensively studied Vaccinia virus whereby long range movement of intracellular enveloped viruses (IEV) require kinesin-1 for transport from their site of replication to the cortical actin layer. Like M-PMV, analysis of live cell imaging of Vaccinia virus [101] using microtubules show IEV traveling bidirectionally, switching from one microtubule to another and have a wide range of instantaneous velocities.

The second manuscript adds to the preliminary findings that capsids are utilizing microtubules for transport by disrupting the microtubule network of the cell with nocodazole. Interestingly, although depolymerizing microtubules caused a delay in the capsid release from the cell, it did not completely block the ability of the capsids to be released from the cell, thus providing evidence that microtubules are utilized for efficient for intracellular transport of M-PMV capsids, but are not absolutely required. However, analysis of the virions released from nocodazole-treated cells showed that they were deficient in Env glycoproteins, providing strong evidence that although capsids can be transported through the cell in the absence of microtubules, these cytoskeletal elements are necessary for the Gag and Env interactions that lead to Env incorporation into the virus. Upon live-cell imaging of cells co-transfected with a

GagGFP and EnvCherry construct, we were able to visualize that Gag and Env were co-transported through the cell. Since previous studies have shown that this interaction does not occur at the point where Env is being exported from the TGN [63], and that Env incorporation is dependent on its endocytosis from the plasma membrane, we hypothesize that this co-transport must be occurring between assembled capsids and Env-containing recycling vesicles. Other studies showing co-localization of M-PMV Gag with Rab-11, the Rab GTPase associated with the early recycling compartment, as well as transferrin, another marker for the recycling pathway, in the pericentriolar region [56] of the cell coupled with a lack of evidence in TEM studies of WT M-PMV capsids budding into intracellular vesicles [69], also lend validity to the hypothesis that these capsids are interacting, directly or indirectly, with Env-containing vesicles trafficking along microtubules toward the plasma membrane.

Although the results from the second study in this dissertation provide compelling evidence that M-PMV uses microtubules for efficient intracellular movement, there are still several questions that remained to be answered. Specifically, while depolymerization of microtubules does not prevent capsids from being released from the cell, the alternate mechanism used by capsids for transport and release remains unknown. Surprisingly, biochemical data from cells treated with actin-disrupting drugs or microtubule- and actin-disrupting drugs, simultaneously, show that capsid release is not affected by the absence of actin filaments. Therefore, it appears as if these capsids are transported to the plasma membrane for budding in a microtubule- and actin- independent manner. This type of movement has also been described for minus-end directed

transport of adenovirus, where depolymerization of microtubules and actin filaments does not prevent nuclear targeting and subsequent gene expression of adenovirus [118]. We hypothesize that depolymerization of microtubules causes redistribution of polysomes, allowing the capsid assembly to occur at locations near the plasma membrane. These capsids can then interact stochastically with cellular components capable of transporting in a microtubule-independent manner. Another possibility is that the capsids are being assembled at the plasma membrane in a mechanism similar to C-type retroviruses. Establishment of this alternate mechanism, with the current, available resources, to date, remains elusive.

The availability of a Gag-GFP fusion has several other implications for contributing to M-PMV research. Although the main focus of the work presented in this dissertation focuses on methods used by the virus for intracellular transport, the ability to visualize capsid movement in live cells opens up the door for being able to study the effects mutations have on individual capsids, differentiating between blocks in steps in the viral life cycle versus delays or deferment to alternative mechanisms, and identifying viral and host cell interaction partners in a dynamic system. Specifically, further studies utilizing the Gag-GFP fusion can be used to elucidate the pathway used by Gag and Env to interact in order to produce infectious virions. Compartments in the cell, such as the recycling compartment, have been implicated in this pathway [63]. The fusion protein allows the study of capsid use of this compartment by labeling the compartment with a second fluorescent protein with minimal spectral overlap, such as mCherry or cyan fluorescent protein (CFP) and performing colocalization

studies. Further information can be learned by triple labeling experiments, whereby a Gag-GFP, Env-mCherry, and the endosomal compartment of interest are visualized in live cells, and analyzed for colocalization, as well as single particle tracking of the Gag and Env proteins into and out of the labeled compartment. Other experiments for which the Gag-GFP fusion would be beneficial include studying the intracellular transport and cellular localization of M-PMV Gag mutants, or studying how expressing certain Env mutants affect trafficking and sorting of capsids.

One major caveat to many of these experiments performed here is that the total time of the live cell imagining is relatively short. Most of the imaging experiments in this dissertation extended for a total of only two minutes, with five seconds between each image capture. Although this was sufficient for visualizing and characterizing capsid movement, and for characterizing the use of the cellular cytoskeleton for transport, conclusions about the entire journey a capsid takes from just after assembly to just before budding are difficult to make. According to pulse-chase data presented in this dissertation, it takes approximately 2.5 hours for 50% of assembled capsids to be released into the extracellular space. The two-minute window for which we acquired the images in this dissertation therefore only represents 1% of this time it takes for assembled particles to be transported, bud, and be released. The ability to image over longer periods of time, however, require longer lapses in time between capturing images in order to reduce or prevent the effects of photobleaching, wherein fluorophores lose their ability to fluoresce due to photon-induced chemical damage. To increase the time between image captures, however, has a negative effect on the

ability to do single particle tracking. In order to do long-term imaging, the eGFP should be replaced with a photoactivatable GFP (paGFP). Using a paGFP, a laser can be used to activate only a small population of fluorescently labeled capsids from a specific location in the cell. This would allow a microscopy-based pulse-chase experiment whereby, specific capsids can be activated by the laser (pulse) and then be followed over longer periods of time, with longer time laspes (chase). With fewer particles to track, single particle tracking software or manual particle tracking may be easier to deconvolute compared to tracking several hundred to thousands of particles at unknown stages in their viral life cycle.

Another caveat, specific to single particle tracking, was the availability of single particle tracking software capable of efficiently detecting and tracking the fluorescent particles over time, and then taking the data collected from this tracking, usually a table of x-, y-, and z- coordinates for each particle at each time point, and measuring specific parameters such as mean squared displacement (MSD) and instantaneous velocity. These parameters, as seen in this dissertation, can be used to determine the type of movement (hindered, active, Brownian) of a particle as well as implicate certain host cell proteins involved in capsid transport, such as the cellular cytoskeleton. In an attempt to integrate single particle tracking and trajectory analysis, we have collaborated with Caterina Strambia at the University of Massachusetts, on the development of a novel open-microscopy-based software known as OMEGA. Although this software was not specifically used in this dissertation, the implications for this software are large. In essence, the software uses the algorithms from Sblazarini et al. that are used in the MOSAIC Particle Tracker 3D program [119] to detect and track individual

particles, and directly links these trajectories with trajectory analysis. Although in its beta stages of development, this software has the potential to facilitate the field of single particle tracking analysis.

Summary

Earlier studies of assembly, transport, and budding of M-PMV, the prototypic D-type retrovirus, have provided invaluable clues as to the viral and host cell proteins that are involved in these processes. These studies have relied on biochemical and fixed-cell imaging to show an essential role for the cellular vesicular transport system as well the viral Env glycoprotein. In this dissertation, we set out to further identify and elucidate the role of viral proteins and the host cell components, by constructing an M-PMV Gag-GFP fusion vector that could be used for real time-time visualization of individual capsids. After constructing a codon- optimized, Kozak consensus sequence-optimized Gag-GFP fusion expressed in a proviral backbone, pSARM-GagGFP-M100A, we confirmed by a series of controls that, with co-expression with WT M-PMV, this GFP-tagged Gag behaved comparably to untagged Gag. Based on the velocity and characterization of the movement of capsids containing the Gag-GFP, real-time imaging showed preliminary evidence for the use microtubules for M-PMV capsid transport. Employing the use of cytoskeletal inhibitors, a role for microtubules in the intracellular transport, as well as the incorporation of Env into virions, was confirmed. A surprising result, however, showed that even though microtubules are indispensable for the intracellular transport of Env-containing vesicles, and

capsids associated with these vesicles, capsid movement can be seen after long-term microtubule disruption. The mechanism used by the capsids to move through the cell and be released from the cell has yet to be elucidated, although mean-squared displacement and pulse-chase analysis suggests that it is an active process. Along with studying the intracellular transport of M-PMV capsids, the availability of a Gag-GFP fusion could prove to be instrumental in studying individual capsids in a dynamic, real-time system.

Literature Cited (Introduction and Discussion)

1. Rous P (1911) A sarcoma of the fowl transmissible by an agent separable from the tumor cells. J Exp Med 13: 397-411.

2. Crawford LV, Crawford EM (1961) The properties of Rous sarcoma virus purified by density gradient centrifugation. Virology 13: 227-232.

3. Poiesz BJ, Ruscetti FW, Gazdar AF, Bunn PA, Minna JD, et al. (1980) Detection and isolation of type C retrovirus particles from fresh and cultured lymphocytes of a patient with cutaneous T-cell lymphoma. Proc Natl Acad Sci U S A 77: 7415-7419.

4. Yoshida M, Miyoshi I, Hinuma Y (1982) Isolation and characterization of retrovirus from cell lines of human adult T-cell leukemia and its implication in the disease. Proc Natl Acad Sci U S A 79: 2031-2035.

5. Baltimore D (1970) RNA-dependent DNA polymerase in virions of RNA tumour viruses. Nature 226: 1209-1211.

6. Temin HM, Mizutani S (1970) Viral RNA-dependent DNA Polymerase: RNA-dependent DNA Polymerase in Virions of Rous Sarcoma Virus. Nature 226: 1211-1213.

7. Bernhard W (1958) Electron microscopy of tumor cells and tumor viruses; a review. Cancer Res 18: 491-509.

8. Levin JG, Hu SC, Rein A, Messer LI, Gerwin BI (1984) Murine leukemia virus mutant with a frameshift in the reverse transcriptase coding region: implications for pol gene structure. J Virol 51: 470-478.

9. Kramer RA, Schaber MD, Skalka AM, Ganguly K, Wong-Staal F, et al. (1986) HTLV-III gag protein is processed in yeast cells by the virus pol-protease. Science 231: 1580-1584.

10. Crawford S, Goff SP (1985) A deletion mutation in the 5' part of the pol gene of Moloney murine leukemia virus blocks proteolytic processing of the gag and pol polyproteins. J Virol 53: 899-907.

11. Dunn BM, Goodenow MM, Gustchina A, Wlodawer A (2002) Retroviral proteases. Genome Biol 3: REVIEWS3006.

12. Toh H, Kikuno R, Hayashida H, Miyata T, Kugimiya W, et al. (1985) Close structural resemblance between putative polymerase of a Drosophila transposable genetic element 17.6 and pol gene product of Moloney murine leukaemia virus. EMBO J 4: 1267-1272.

13. Jacks T, Madhani HD, Masiarz FR, Varmus HE (1988) Signals for ribosomal frameshifting in the Rous sarcoma virus gag-pol region. Cell 55: 447-458.

14. Jacks T, Power MD, Masiarz FR, Luciw PA, Barr PJ, et al. (1988) Characterization of ribosomal frameshifting in HIV-1 gag-pol expression. Nature 331: 280-283.

15. Jacks T, Townsley K, Varmus HE, Majors J (1987) Two efficient ribosomal frameshifting events are required for synthesis of mouse mammary tumor virus gag-related polyproteins. Proc Natl Acad Sci U S A 84: 4298-4302.

16. Jacks T, Varmus HE (1985) Expression of the Rous sarcoma virus pol gene by ribosomal frameshifting. Science 230: 1237-1242.

17. Bernstein HB, Tucker SP, Hunter E, Schutzbach JS, Compans RW (1994) Human immunodeficiency virus type 1 envelope glycoprotein is modified by O-linked oligosaccharides. J Virol 68: 463-468.

18. Leonard CK, Spellman MW, Riddle L, Harris RJ, Thomas JN, et al. (1990) Assignment of intrachain disulfide bonds and characterization of potential glycosylation sites of the type 1 recombinant human immunodeficiency virus envelope glycoprotein (gp120) expressed in Chinese hamster ovary cells. J Biol Chem 265: 10373-10382.

19. Pinter A, Honnen WJ (1988) O-linked glycosylation of retroviral envelope gene products. J Virol 62: 1016-1021.

20. Einfeld D, Hunter E (1988) Oligomeric structure of a prototype retrovirus glycoprotein. Proc Natl Acad Sci U S A 85: 8688-8692.

21. Stein BS, Engleman EG (1990) Intracellular processing of the gp160 HIV-1 envelope precursor. Endoproteolytic cleavage occurs in a cis or medial compartment of the Golgi complex. J Biol Chem 265: 2640-2649.

22. Bedgood RM, Stallcup MR (1992) A novel intermediate in processing of murine leukemia virus envelope glycoproteins. Proteolytic cleavage in the late Golgi region. J Biol Chem 267: 7060-7065.

23. Hallenberger S, Bosch V, Angliker H, Shaw E, Klenk HD, et al. (1992) Inhibition of furin-mediated cleavage activation of HIV-1 glycoprotein gp160. Nature 360: 358-361.

24. Geiselhart V, Bastone P, Kempf T, Schnolzer M, Lochelt M (2004) Furin-mediated cleavage of the feline foamy virus Env leader protein. J Virol 78: 13573-13581.

25. Chopra HC, Mason MM (1970) A New Virus in a Spontaneous Mammary Tumor of a Rhesus Monkey. Cancer Res 30: 2081-2086.

26. Mason MM, Bogden AE, Ilievski V, Esber HJ, Baker JR, et al. (1972) History of a rhesus monkey adenocarcinoma containing virus particles resembling oncogenic RNA viruses. J Natl Cancer Inst 48: 1323-1331.

27. Jensen EM, Zelljadt I, Chopra HC, Mason MM (1970) Isolation and propagation of a virus from a spontaneous mammary carcinoma of a rhesus monkey. Cancer Res 30: 2388-2393.

28. Bittner JJ (1942) The Milk-Influence of Breast Tumors in Mice. Science 95: 462-463.

29. Fine DL, Peinta RJ, Malan LB, Kubicek MT, Bennett DG, et al. (1974) Biologic characteristics of transformed rhesus foreskin cells infected with Mason-Pfizer monkey virus. J Natl Cancer Inst 52: 1135-1142.

30. Pienta RJ, Fine DL, Hurt T, Smith CK, Landon JC, et al. (1972) Transformation of rhesus foreskin cells by Mason-Pfizer monkey virus. J Natl Cancer Inst 48: 1913-1917.

31. Fine DL, Landon JC, Pienta RJ, Kubicek MT, Valerio MG, et al. (1975) Responses of infant rhesus monkeys to inoculation with Mason-Pfizer monkey virus materials. J Natl Cancer Inst 54: 651-658.

32. Bryant ML, Gardner MB, Marx PA, Maul DH, Lerche NW, et al. (1986) Immunodeficiency in rhesus monkeys associated with the original Mason-Pfizer monkey virus. J Natl Cancer Inst 77: 957-965.

33. Sonigo P, Barker C, Hunter E, Wain-Hobson S (1986) Nucleotide sequence of Mason-Pfizer monkey virus: an immunosuppressive D-type retrovirus. Cell 45: 375-385.

34. Henrickson RV, Maul DH, Osborn KG, Sever JL, Madden DL, et al. (1983) Epidemic of acquired immunodeficiency in rhesus monkeys. Lancet 1: 388-390.

35. Letvin NL, Eaton KA, Aldrich WR, Sehgal PK, Blake BJ, et al. (1983) Acquired immunodeficiency syndrome in a colony of macaque monkeys. Proc Natl Acad Sci U S A 80: 2718-2722.

36. Lerche NW, Marx PA, Osborn KG, Maul DH, Lowenstine LJ, et al. (1987) Natural history of endemic type D retrovirus infection and acquired immune deficiency syndrome in group-housed rhesus monkeys. J Natl Cancer Inst 79: 847-854.

37. Barker CS, Wills JW, Bradac JA, Hunter E (1985) Molecular cloning of the Mason-Pfizer monkey virus genome: characterization and cloning of subgenomic fragments. Virology 142: 223-240.

38. Bradac J, Hunter E (1984) Polypeptides of Mason-Pfizer monkey virus. I. Synthesis and processing of the gag-gene products. Virology 138: 260-275.

39. Chatterjee S, Bradac J, Hunter E (1985) A rapid screening procedure for the isolation of nonconditional replication mutants of Mason-Pfizer monkey virus: identification of a mutant defective in pol. Virology 141: 65-76.

40. Overbaugh J, Miller AD, Eiden MV (2001) Receptors and entry cofactors for retroviruses include single and multiple transmembrane-spanning proteins as well as newly described glycophosphatidylinositol-anchored

and secreted proteins. Microbiol Mol Biol Rev 65: 371-389, table of contents.

41. Rasko JE, Battini JL, Gottschalk RJ, Mazo I, Miller AD (1999) The RD114/simian type D retrovirus receptor is a neutral amino acid transporter. Proc Natl Acad Sci U S A 96: 2129-2134.

42. Tailor CS, Nouri A, Zhao Y, Takeuchi Y, Kabat D (1999) A sodium-dependent neutral-amino-acid transporter mediates infections of feline and baboon endogenous retroviruses and simian type D retroviruses. J Virol 73: 4470-4474.

43. Chen SS, Lee SF, Hao HJ, Chuang CK (1998) Mutations in the leucine zipper-like heptad repeat sequence of human immunodeficiency virus type 1 gp41 dominantly interfere with wild-type virus infectivity. J Virol 72: 4765-4774.

44. Dubay JW, Roberts SJ, Brody B, Hunter E (1992) Mutations in the leucine zipper of the human immunodeficiency virus type 1 transmembrane glycoprotein affect fusion and infectivity. J Virol 66: 4748-4756.

45. Ghosh JK, Shai Y (1999) Direct evidence that the N-terminal heptad repeat of Sendai virus fusion protein participates in membrane fusion. J Mol Biol 292: 531-546.

46. Luo Z, Matthews AM, Weiss SR (1999) Amino acid substitutions within the leucine zipper domain of the murine coronavirus spike protein cause defects in oligomerization and the ability to induce cell-to-cell fusion. J Virol 73: 8152-8159.

47. Song C, Hunter E (2003) Variable sensitivity to substitutions in the N-terminal heptad repeat of Mason-Pfizer monkey virus transmembrane protein. J Virol 77: 7779-7785.

48. Song C, Micoli K, Hunter E (2005) Activity of the Mason-Pfizer monkey virus fusion protein is modulated by single amino acids in the cytoplasmic tail. J Virol 79: 11569-11579.

49. Brody BA, Rhee SS, Hunter E (1994) Postassembly cleavage of a retroviral glycoprotein cytoplasmic domain removes a necessary incorporation signal and activates fusion activity. J Virol 68: 4620-4627.

50. Felber BK, Hadzopoulou-Cladaras M, Cladaras C, Copeland T, Pavlakis GN (1989) rev protein of human immunodeficiency virus type 1 affects the stability and transport of the viral mRNA. Proc Natl Acad Sci U S A 86: 1495-1499.

51. Pollard VW, Malim MH (1998) The HIV-1 Rev protein. Annu Rev Microbiol 52: 491-532.

52. Ernst RK, Bray M, Rekosh D, Hammarskjold ML (1997) Secondary structure and mutational analysis of the Mason-Pfizer monkey virus RNA constitutive transport element. RNA 3: 210-222.

53. Bray M, Prasad S, Dubay JW, Hunter E, Jeang KT, et al. (1994) A small element from the Mason-Pfizer monkey virus genome makes human immunodeficiency virus type 1 expression and replication Rev-independent. Proc Natl Acad Sci U S A 91: 1256-1260.

54. Rizvi TA, Lew KA, Murphy EC, Jr., Schmidt RD (1996) Role of Mason-Pfizer monkey virus (MPMV) constitutive transport element (CTE) in the

propagation of MPMV vectors by genetic complementation using homologous/heterologous env genes. Virology 224: 517-532.

55. Rizvi TA, Schmidt RD, Lew KA (1997) Mason-Pfizer monkey virus (MPMV) constitutive transport element (CTE) functions in a position-dependent manner. Virology 236: 118-129.

56. Sfakianos JN, LaCasse RA, Hunter E (2003) The M-PMV cytoplasmic targeting-retention signal directs nascent Gag polypeptides to a pericentriolar region of the cell. Traffic 4: 660-670.

57. Rhee SS, Hunter E (1991) Amino acid substitutions within the matrix protein of type D retroviruses affect assembly, transport and membrane association of a capsid. EMBO J 10: 535-546.

58. Choi G, Park S, Choi B, Hong S, Lee J, et al. (1999) Identification of a cytoplasmic targeting/retention signal in a retroviral Gag polyprotein. J Virol 73: 5431-5437.

59. Rhee SS, Hunter E (1990) A single amino acid substitution within the matrix protein of a type D retrovirus converts its morphogenesis to that of a type C retrovirus. Cell 63: 77-86.

60. Vlach J, Lipov J, Rumlova M, Veverka V, Lang J, et al. (2008) D-retrovirus morphogenetic switch driven by the targeting signal accessibility to Tctex-1 of dynein. Proc Natl Acad Sci U S A 105: 10565-10570.

61. Weldon RA, Jr., Parker WB, Sakalian M, Hunter E (1998) Type D retrovirus capsid assembly and release are active events requiring ATP. J Virol 72: 3098-3106.

62. Punnonen EL, Ryhanen K, Marjomaki VS (1998) At reduced temperature, endocytic membrane traffic is blocked in multivesicular carrier endosomes in rat cardiac myocytes. Eur J Cell Biol 75: 344-352.

63. Sfakianos JN, Hunter E (2003) M-PMV capsid transport is mediated by Env/Gag interactions at the pericentriolar recycling endosome. Traffic 4: 671-680.

64. Song C, Dubay SR, Hunter E (2003) A tyrosine motif in the cytoplasmic domain of mason-pfizer monkey virus is essential for the incorporation of glycoprotein into virions. J Virol 77: 5192-5200.

65. Rhee SS, Hunter E (1987) Myristylation is required for intracellular transport but not for assembly of D-type retrovirus capsids. J Virol 61: 1045-1053.

66. Conte MR, Klikova M, Hunter E, Ruml T, Matthews S (1997) The three-dimensional solution structure of the matrix protein from the type D retrovirus, the Mason-Pfizer monkey virus, and implications for the morphology of retroviral assembly. EMBO J 16: 5819-5826.

67. Prchal J, Srb P, Hunter E, Ruml T, Hrabal R (2012) The structure of myristoylated Mason-Pfizer monkey virus matrix protein and the role of phosphatidylinositol-(4,5)-bisphosphate in its membrane binding. J Mol Biol 423: 427-438.

68. Stansell E, Tytler E, Walter MR, Hunter E (2004) An early stage of Mason-Pfizer monkey virus budding is regulated by the hydrophobicity of the Gag matrix domain core. J Virol 78: 5023-5031.

69. Stansell E, Apkarian R, Haubova S, Diehl WE, Tytler EM, et al. (2007) Basic residues in the Mason-Pfizer monkey virus gag matrix domain regulate

intracellular trafficking and capsid-membrane interactions. J Virol 81: 8977-8988.

70. Hong W (1998) Protein transport from the endoplasmic reticulum to the Golgi apparatus. J Cell Sci 111 (Pt 19): 2831-2839.

71. Burgess TL, Kelly RB (1987) Constitutive and regulated secretion of proteins. Annu Rev Cell Biol 3: 243-293.

72. Maxfield FR, McGraw TE (2004) Endocytic recycling. Nat Rev Mol Cell Biol 5: 121-132.

73. Hopkins CR (1983) Intracellular routing of transferrin and transferrin receptors in epidermoid carcinoma A431 cells. Cell 35: 321-330.

74. Goldstein JL, Brown MS, Anderson RG, Russell DW, Schneider WJ (1985) Receptor-mediated endocytosis: concepts emerging from the LDL receptor system. Annu Rev Cell Biol 1: 1-39.

75. Reaves B, Horn M, Banting G (1993) TGN38/41 recycles between the cell surface and the TGN: brefeldin A affects its rate of return to the TGN. Mol Biol Cell 4: 93-105.

76. Mallet WG, Maxfield FR (1999) Chimeric forms of furin and TGN38 are transported with the plasma membrane in the trans-Golgi network via distinct endosomal pathways. J Cell Biol 146: 345-359.

77. Hutagalung AH, Novick PJ (2011) Role of Rab GTPases in membrane traffic and cell physiology. Physiol Rev 91: 119-149.

78. Stenmark H (2009) Rab GTPases as coordinators of vesicle traffic. Nat Rev Mol Cell Biol 10: 513-525.

79. Carroll KS, Hanna J, Simon I, Krise J, Barbero P, et al. (2001) Role of Rab9 GTPase in facilitating receptor recruitment by TIP47. Science 292: 1373-1376.

80. Semerdjieva S, Shortt B, Maxwell E, Singh S, Fonarev P, et al. (2008) Coordinated regulation of AP2 uncoating from clathrin-coated vesicles by rab5 and hRME-6. J Cell Biol 183: 499-511.

81. Christoforidis S, Miaczynska M, Ashman K, Wilm M, Zhao L, et al. (1999) Phosphatidylinositol-3-OH kinases are Rab5 effectors. Nat Cell Biol 1: 249-252.

82. Shin HW, Hayashi M, Christoforidis S, Lacas-Gervais S, Hoepfner S, et al. (2005) An enzymatic cascade of Rab5 effectors regulates phosphoinositide turnover in the endocytic pathway. J Cell Biol 170: 607-618.

83. Wu XS, Rao K, Zhang H, Wang F, Sellers JR, et al. (2002) Identification of an organelle receptor for myosin-Va. Nat Cell Biol 4: 271-278.

84. Hume AN, Collinson LM, Rapak A, Gomes AQ, Hopkins CR, et al. (2001) Rab27a regulates the peripheral distribution of melanosomes in melanocytes. J Cell Biol 152: 795-808.

85. Hales CM, Vaerman JP, Goldenring JR (2002) Rab11 family interacting protein 2 associates with Myosin Vb and regulates plasma membrane recycling. J Biol Chem 277: 50415-50421.

86. Hoepfner S, Severin F, Cabezas A, Habermann B, Runge A, et al. (2005) Modulation of receptor recycling and degradation by the endosomal kinesin KIF16B. Cell 121: 437-450.

87. Matanis T, Akhmanova A, Wulf P, Del Nery E, Weide T, et al. (2002) Bicaudal-D regulates COPI-independent Golgi-ER transport by recruiting the dynein-dynactin motor complex. Nat Cell Biol 4: 986-992.

88. Vale RD (1987) Intracellular transport using microtubule-based motors. Annu Rev Cell Biol 3: 347-378.

89. Atkinson SJ, Doberstein SK, Pollard TD (1992) Moving off the beaten track. Curr Biol 2: 326-328.

90. Schuh M (2011) An actin-dependent mechanism for long-range vesicle transport. Nat Cell Biol 13: 1431-1436.

91. Wu X, Bowers B, Rao K, Wei Q, Hammer JA, 3rd (1998) Visualization of melanosome dynamics within wild-type and dilute melanocytes suggests a paradigm for myosin V function In vivo. J Cell Biol 143: 1899-1918.

92. Kuznetsov SA, Langford GM, Weiss DG (1992) Actin-dependent organelle movement in squid axoplasm. Nature 356: 722-725.

93. Waterman-Storer CM, Karki S, Holzbaur EL (1995) The p150Glued component of the dynactin complex binds to both microtubules and the actin-related protein centractin (Arp-1). Proc Natl Acad Sci U S A 92: 1634-1638.

94. Ali MY, Krementsova EB, Kennedy GG, Mahaffy R, Pollard TD, et al. (2007) Myosin Va maneuvers through actin intersections and diffuses along microtubules. Proc Natl Acad Sci U S A 104: 4332-4336.

95. Cao TT, Chang W, Masters SE, Mooseker MS (2004) Myosin-Va binds to and mechanochemically couples microtubules to actin filaments. Mol Biol Cell 15: 151-161.

96. Douglas MW, Diefenbach RJ, Homa FL, Miranda-Saksena M, Rixon FJ, et al. (2004) Herpes simplex virus type 1 capsid protein VP26 interacts with dynein light chains RP3 and Tctex1 and plays a role in retrograde cellular transport. J Biol Chem 279: 28522-28530.

97. Suomalainen M, Nakano MY, Keller S, Boucke K, Stidwill RP, et al. (1999) Microtubule-dependent plus- and minus end-directed motilities are competing processes for nuclear targeting of adenovirus. J Cell Biol 144: 657-672.

98. Lanier LM, Volkman LE (1998) Actin binding and nucleation by Autographa california M nucleopolyhedrovirus. Virology 243: 167-177.

99. Sanderson CM, Hollinshead M, Smith GL (2000) The vaccinia virus A27L protein is needed for the microtubule-dependent transport of intracellular mature virus particles. J Gen Virol 81: 47-58.

100. Rietdorf J, Ploubidou A, Reckmann I, Holmstrom A, Frischknecht F, et al. (2001) Kinesin-dependent movement on microtubules precedes actin-based motility of vaccinia virus. Nat Cell Biol 3: 992-1000.

101. Hollinshead M, Rodger G, Van Eijl H, Law M, Hollinshead R, et al. (2001) Vaccinia virus utilizes microtubules for movement to the cell surface. J Cell Biol 154: 389-402.

102. Tang Y, Winkler U, Freed EO, Torrey TA, Kim W, et al. (1999) Cellular motor protein KIF-4 associates with retroviral Gag. J Virol 73: 10508-10513.

103. Martinez NW, Xue X, Berro RG, Kreitzer G, Resh MD (2008) Kinesin KIF4 regulates intracellular trafficking and stability of the human immunodeficiency virus type 1 Gag polyprotein. J Virol 82: 9937-9950.

104. Ono A, Freed EO (2004) Cell-type-dependent targeting of human immunodeficiency virus type 1 assembly to the plasma membrane and the multivesicular body. J Virol 78: 1552-1563.

105. Dong X, Li H, Derdowski A, Ding L, Burnett A, et al. (2005) AP-3 directs the intracellular trafficking of HIV-1 Gag and plays a key role in particle assembly. Cell 120: 663-674.

106. Welsch S, Keppler OT, Habermann A, Allespach I, Krijnse-Locker J, et al. (2007) HIV-1 buds predominantly at the plasma membrane of primary human macrophages. PLoS Pathog 3: e36.

107. Deneka M, Pelchen-Matthews A, Byland R, Ruiz-Mateos E, Marsh M (2007) In macrophages, HIV-1 assembles into an intracellular plasma membrane domain containing the tetraspanins CD81, CD9, and CD53. J Cell Biol 177: 329-341.

108. Bennett AE, Narayan K, Shi D, Hartnell LM, Gousset K, et al. (2009) Ion-abrasion scanning electron microscopy reveals surface-connected tubular conduits in HIV-infected macrophages. PLoS Pathog 5: e1000591.

109. Chu H, Wang JJ, Qi M, Yoon JJ, Wen X, et al. (2012) The intracellular virus-containing compartments in primary human macrophages are largely inaccessible to antibodies and small molecules. PLoS One 7: e35297.

110. Campbell EM, Hope TJ (2008) Live cell imaging of the HIV-1 life cycle. Trends Microbiol 16: 580-587.

111. Desai P, Person S (1998) Incorporation of the green fluorescent protein into the herpes simplex virus type 1 capsid. J Virol 72: 7563-7568.

112. Muller B, Daecke J, Fackler OT, Dittmar MT, Zentgraf H, et al. (2004) Construction and characterization of a fluorescently labeled infectious human immunodeficiency virus type 1 derivative. J Virol 78: 10803-10813.

113. Lux K, Goerlitz N, Schlemminger S, Perabo L, Goldnau D, et al. (2005) Green fluorescent protein-tagged adeno-associated virus particles allow the study of cytosolic and nuclear trafficking. J Virol 79: 11776-11787.

114. Dohner K, Nagel CH, Sodeik B (2005) Viral stop-and-go along microtubules: taking a ride with dynein and kinesins. Trends Microbiol 13: 320-327.

115. Murray JW, Bananis E, Wolkoff AW (2000) Reconstitution of ATP-dependent movement of endocytic vesicles along microtubules in vitro: an oscillatory bidirectional process. Mol Biol Cell 11: 419-433.

116. Amorim MJ, Bruce EA, Read EK, Foeglein A, Mahen R, et al. (2011) A Rab11- and microtubule-dependent mechanism for cytoplasmic transport of influenza A virus viral RNA. J Virol 85: 4143-4156.

117. Chambers R, Takimoto T (2010) Trafficking of Sendai virus nucleocapsids is mediated by intracellular vesicles. PLoS One 5: e10994.

118. Glotzer JB, Michou AI, Baker A, Saltik M, Cotten M (2001) Microtubule-independent motility and nuclear targeting of adenoviruses with fluorescently labeled genomes. J Virol 75: 2421-2434.

119. Sbalzarini IF, Koumoutsakos P (2005) Feature point tracking and trajectory analysis for video imaging in cell biology. Journal of Structural Biology 151: 182-195.